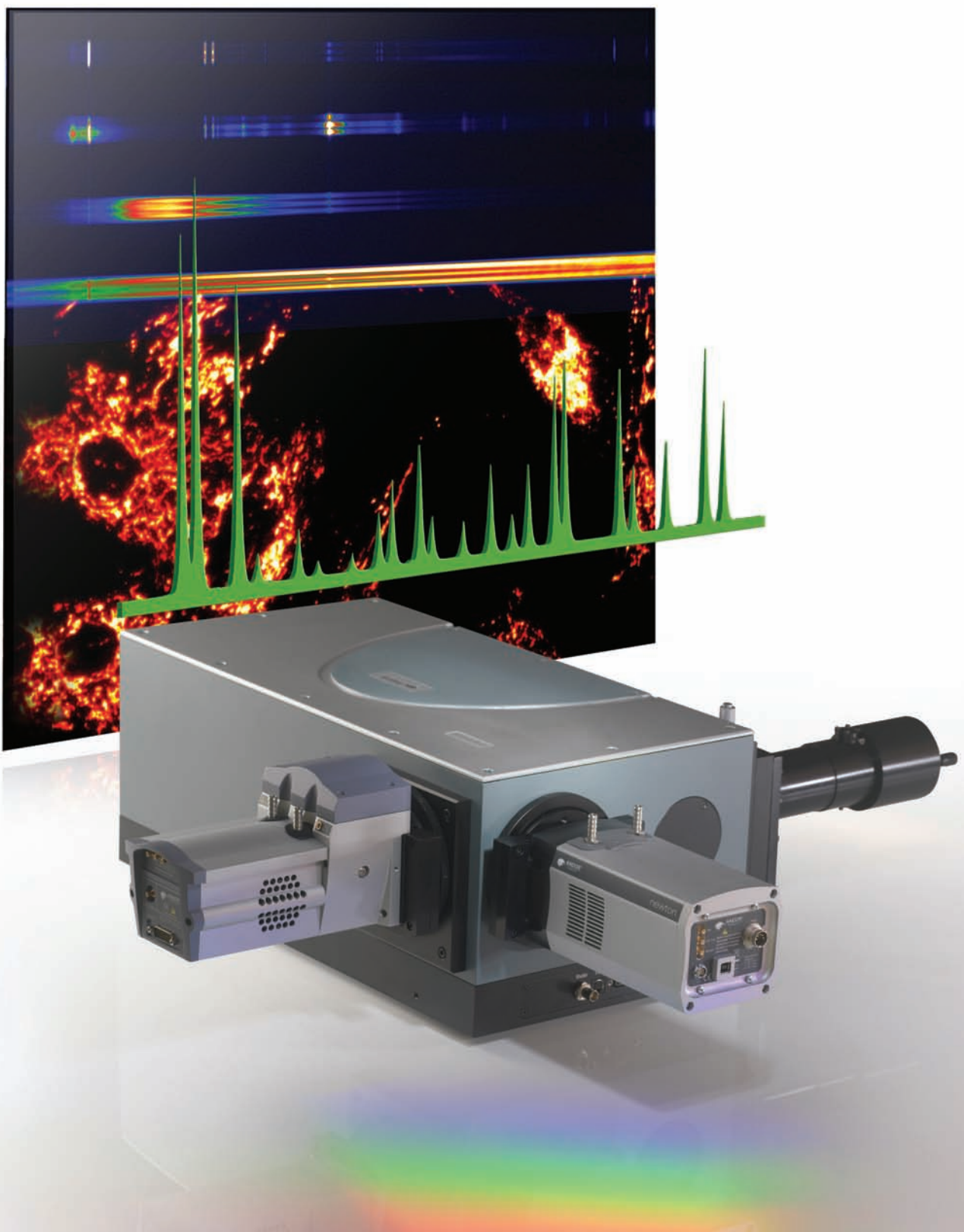




# Spectroscopy Solutions

**"A Modular Approach"**



# Andor Spectroscopy Product Portfolio

Engineered from the outset with “ease-of-use” in mind, every Andor Spectroscopy system features a combination of market leading detectors and spectral instruments, seamlessly controlled through Andor’s dedicated and intuitive Solis software platform. From configuration of these pre-aligned, pre-calibrated instruments to integration into each unique laboratory set-up, Andor Spectroscopy solutions allow researchers around the world to focus quickly on their own challenges: achieving high quality results and breakthrough discoveries.



## Software - Page 6 - 7

Solis Spectroscopy and Solis Scanning offer interactive and dedicated graphical interfaces for simultaneous multi-channel or single point detector data acquisition, spectrographs and motorized accessories control.

## Cameras - Page 8 - 19

Market leading CCDs, InGaAs PDAs, Intensified CCDs and Electron-Multiplying CCDs for VUV to NIR Spectroscopy. Unsurpassed combination of cutting-edge Thermo-Electric cooling, proprietary vacuum technology and ultra-low-noise electronics to extract the very best performance from every Andor camera.

## Scanning Accessories - Page 36 - 37

Extending Spectroscopy from UV into Short and Long-Wave IR through a range of single point detectors including a PMTs, Si photodiode, InGaAs, PbS, InSb and MCT. Software-controlled data acquisition unit synchronizes simultaneously detectors, monochromators and motorised accessories.

## Spectrographs - Page 20 - 27

Complete family of rugged, pre-aligned and pre-calibrated Czerny-Turner & echelle spectrographs, for applications ranging from high-resolution UV plasma studies to NIR photoluminescence. The ideal partner for Andor’s high-performance detectors and accessories for ultimate low-light detection.

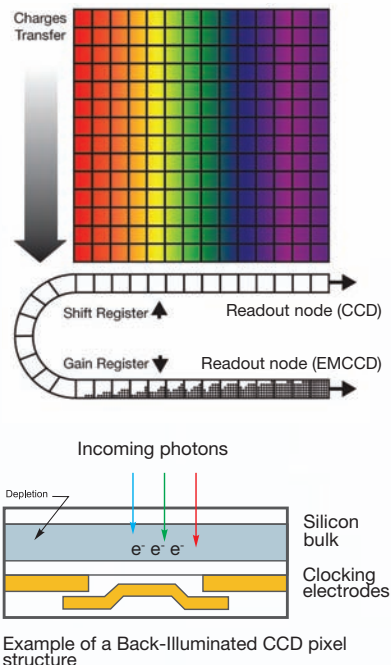
## Accessories - Page 28 - 35

From gratings to fibre optics, sample chamber, filter wheel and microscope coupling interfaces, each accessory allows seamless optimization of Andor detection system performance and easy integration into researchers complex experimental setups.

## Application and Technical Notes - Page 40 - 55

Our experience has enabled us to bring together the latest cutting-edge technology in the fields of sensors, electronics, optics, vacuum technology and software to deliver world-class, market-leading scientific Spectroscopy detection systems.

Andor's experience in manufacturing high-performance Spectroscopy systems spans over 20 years, with thousands of detectors in the field and a proud history of remarkable advances in a wide variety of research areas, truly helping scientists all over the world to "Discover new ways of seeing".



## CCD basics

A Charge Coupled Device, or CCD, is a 2D matrix of silicon diode photo-sensors referred to as "pixels". Incident photons with sufficient energy are absorbed in the silicon bulk and liberate an electron which can be stored and detected as part of a readout sequence. Photons with wavelength  $\lambda > 1.1\mu\text{m}$  do not have enough energy to create a free electron and therefore set the upper detection limit of silicon CCDs.

The probability of detecting a photon at a particular wavelength is known as Quantum Efficiency (QE). QE will vary with Depletion depth of the silicon, quality of the CCD structural layers and clocking electrodes "transparency".

At the end of an exposure, the CCD pixel charges are transferred sequentially under a masked area known as the shift register. This serial register connects to an amplifier that digitizes the signal and allows a quantitative readout of the amount of electrons per pixel.

The principal types of high performance CCD-based digital cameras include :

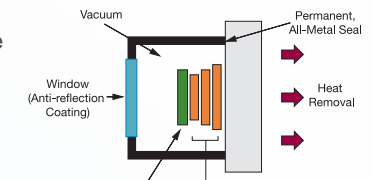
- The Charge-Coupled-Device (CCD)
- The Electron-Multiplying CCD (EMCCD) - with on-chip gain for sensitivity down to single photon
- The Intensified CCD (ICCD) - Image Intensifier provides fast optical shuttering and signal amplification

## Ultravac™ – Market-leading vacuum and cooling technology

Cooling sensors reduces thermally generated noise that would otherwise interfere with the useful signal, hence making it a prerequisite for high sensitivity measurements. The sensor must be operated in a vacuum in order to :

1. Guarantee access to the best cooling performance, hence lowest dark current
2. Increase sensor lifetime by avoiding condensation and sensor degradation

Outgassing is a natural process occurring in any permanent vacuum system, whereby remanent impurities contained in the chamber will be slowly released and potentially affect cooling performance over time. Over 20 years experience in vacuum technology ensures that Andor cameras come with an un-matched warranty on vacuum integrity, guaranteeing cooling performance year after year. Combined with Andor's highly efficient Thermo-Electric cooling interface, temperatures as low as  $-100^\circ\text{C}$  will be achieved without the inconvenient use of Liquid Nitrogen ( $\text{LN}_2$ ), see SNR discussion in the technical notes section. Andor's industry-leading vacuum seal design also means that only one window is required in front of the sensor enabling maximum photon throughput, which is especially suited for photon-starved applications.



## Making sense of sensitivity – signal-to-noise ratio considerations

A camera Signal-to-Noise Ratio (commonly abbreviated to S/N or SNR) is the true comparison basis between detectors and detector technologies. It takes into account both photon capture capability of the detector and different noise sources along the detection path that can impact on the integrity of the useful signal. The sources of this noise are the following :

- **Readout noise** - inherent sensor electron-to-voltage conversion and amplification noise
- **Thermal noise** - originating from sensor, blackbody radiation (SWIR region) or image intensifier photocathode
- **Photon noise / Shot noise** - statistical incoming photon variation
- **Spurious Charge / Clocking Induced Charge (CIC)** - result of impact ionization during charge transfer

$$\text{Noise}_{\text{total}} = \sqrt{N_{\text{readout}}^2 + F^2 \cdot G^2 \cdot (N_{\text{darknoise}}^2 + N_{\text{photon}}^2 + N_{\text{CIC}}^2)}$$

**CCD** sensitivity is shot noise and readout noise limited - typically used at slow digitization speeds  
**EMCCD** sensitivity is shot noise and CIC limited – typically used for photon-starved and ultrafast Spectroscopy  
**ICCD** sensitivity is shot noise and photocathode thermal noise (EBI) limited – typically used for ns time-resolution



## Software

"Discover new ways of seeing" takes its true meaning when the most sensitive Spectroscopy detection solutions on the market combine with Andor's comprehensive software capabilities. From seamless configuration of spectrographs and cameras to actual data acquisition optimization, Andor Solis software and Software Development Kit offer a truly powerful, yet user-friendly modular approach to Spectroscopy.



### Solis for Spectroscopy

Modular Raman Spectroscopy, Laser Induced Breakdown Spectroscopy (LIBS) and Plasma diagnostics are only a few examples of applications where Andor Solis Spectroscopy allows researchers to truly focus on their own experimental challenges. With its unique interactive real-time control interface, users can optimize system optical performance through wavelength, gratings and entrance/exit slits selection at the touch of a button, while accessing all key detectors acquisition parameters to optimise the quality of the signal. Solis also features a comprehensive range of acquisition options including ultrafast kinetic series and "Crop mode" operation, simultaneous multi-track recording, photon-counting mode, and time-resolved series capture for lifetime fluorescence studies.

### Solis for Scanning

With detection capabilities ranging from UV to the Long Wave IR (LWIR) region through a comprehensive range of single point detectors - including PMTs, PbS and MCT, Solis Scanning offers a dedicated platform for scanning applications. Spectrograph/monochromators, detectors, data acquisition unit, lock-in amplifier / chopper and motorised accessories can all be conveniently synchronised through a series of intuitive interfaces. A single software package features a comprehensive step-by-step experiment building interface for parametrizing and synchronizing all components of the detection chain. Complex scanning sequences involving multiple gratings, filters and up to 2 monochromators for fluorescence measurements - including a tuneable light source setup - can be seamlessly captured prior to acquisition start and executed without further intervention of the user. Solis Scanning can also handle multiple detectors control and data display for Absorption - Transmission - Reflection Spectroscopy, while offering post-acquisition mathematical data processing ranging from simple ratios and lifetime measurements to fast phenomena analysis.

### Software Development Kit (SDK)

Andor SDK features a comprehensive library of camera and spectrograph controls, ideally suited for complex experiments integration including third party hardware control and SDK - i.e. microscope motorised stage or light sources – and user specific data analysis protocols. Available as 32 and 64-bit libraries for Windows (XP, Vista and 7) and Linux, the SDK provides a suite of functions that allow configuration of the data acquisition process in a number of different ways. The dynamic link library can be used with a wide range of programming environments including C/C++, C#, Delphi, VB6, VB.NET, Labview and Matlab.

## Spectroscopy cameras

Andor has been taking pride in helping researchers around the world achieve breakthrough discoveries for the last 20 years. By keeping at the forefront of detector technology, Andor is able to offer a range of market leading high-performance, ultra sensitive Spectroscopy detectors. Our CCDs, ICCDs, EMCCDs and InGaAs arrays can operate from the VUV to Near-Infrared spectral regions with a unique combination of high sensitivity (down to single photon in the case of EMCCD technology) and ultrafast acquisition speeds.

### CCD

A 2 dimensional silicon-based semiconductor matrix of photo-sensors, with sensitivity ranging from soft X-Ray to NIR (1.1 μm). Spectroscopy CCDs are traditionally a rectangular format with a maximum width of 28 mm and a height up to 13 mm, i.e. matching the focal plane size of the vast majority of high-end spectrographs.

### Intensified CCD (ICCD)

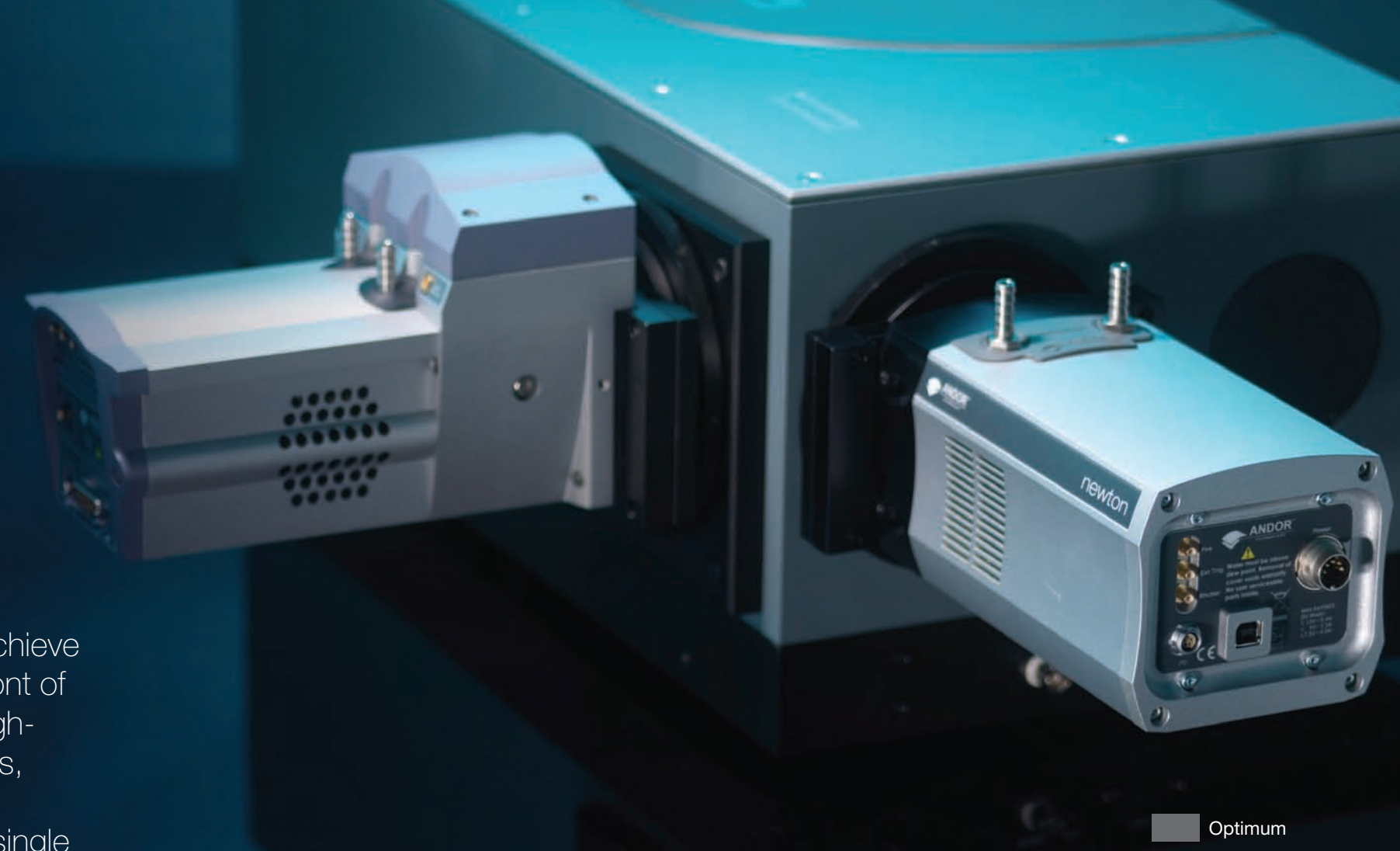
Combination of a CCD matrix with a fibre coupled Image Intensifier, which provides optical shuttering capabilities and time-resolution down to the nanosecond regime while also offering a signal amplification up to x1000.

### InGaAs

Indium Gallium Arsenide (InGaAs) is a photo-sensitive material used for detection up to 2.2 μm. The typical sensor architecture for Spectroscopy applications is a single row array of up to 25.6 mm.

### Electron Multiplying CCD (EMCCD)

Identical architecture to standard CCD sensors, with the addition of an on-chip amplification channel prior to the digitization node, designed to overcome the readout noise limitation of slow-scan CCDs. This revolutionary technology opens the door to ultra-sensitive and ultra-fast Spectroscopy.



Applications	Newton	Newton <sup>EM</sup>	iXon <sup>EM+</sup>	iDus	InGaAs	iStar
Absorption - Transmission - Reflection	UV-NIR	UV-Vis	UV-NIR	UV-NIR	NIR-SWIR	UV-Vis
Photoluminescence - Fluorescence	UV-NIR	UV-Vis	UV-NIR	UV-NIR	NIR-SWIR	UV-Vis
Raman (SERS, SORS, CARS, Stimulated)	244-830 nm	244-633 nm	244-830 nm	244-830 nm	1064 nm	244-633 nm
Micro-Raman and Micro-Fluorescence	UV-NIR	UV-Vis	UV-NIR	UV-NIR	NIR-SWIR	UV-Vis
Photon Counting	-	UV-Vis	UV-Vis	-	-	UV-Vis
Single Molecule Spectroscopy	-	UV-Vis	UV-Vis	-	-	UV-Vis
Hyper-Spectral Imaging	-	UV-Vis	UV-Vis	-	-	-
LIBS	-	-	UV-NIR (885 model)	-	-	UV-NIR
Plasma Studies	UV-NIR	UV-Vis	UV-NIR	UV-NIR	NIR-SWIR	UV-NIR

Sensor type	Description
BR-DD	Back-Illuminated, Deep Depletion CCD with fringe suppression
BU	Back-Illuminated CCD, UV-Enhanced, 350 nm optimized
BU2	Back-Illuminated CCD, UV-Enhanced, 250 nm optimized
BV	Back-Illuminated CCD, VIS optimized
FI	Front-Illuminated CCD
OE	Open-Electrode CCD
UV	Front-Illuminated CCD with UV coating
UVB	Back-Illuminated CCD with UV coating
VP	Virtual Phase CCD (Proprietary technology from Texas Instrument)

# iDus CCD cameras

## Workhorse Spectroscopy Cameras

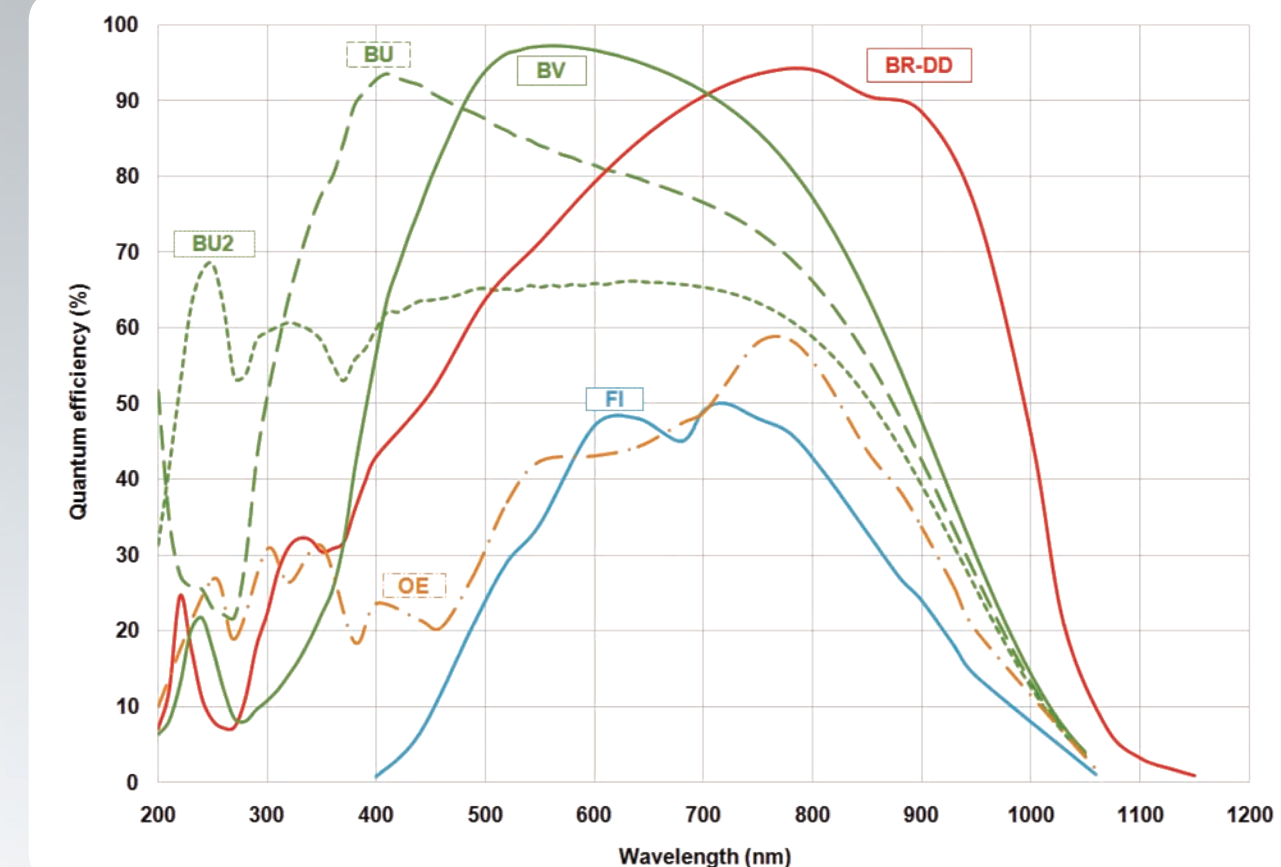
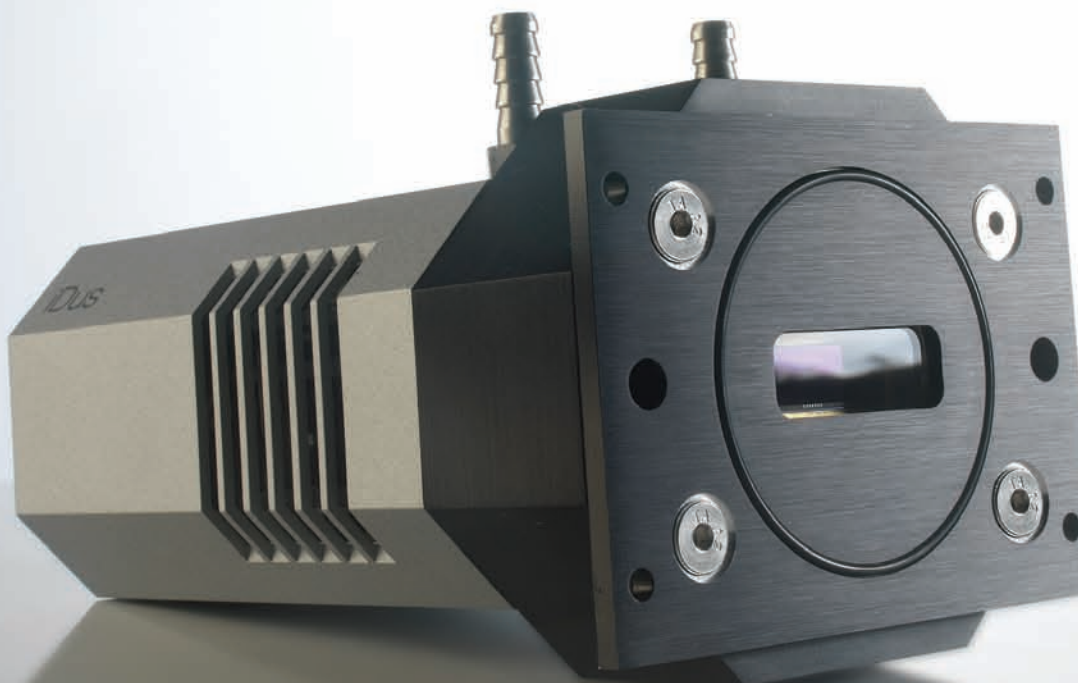
The iDus is Andor's most popular platform for the Spectroscopy research and OEM communities. Boasting sensor QE up to 95%, state-of-the-art Ultravac™, cooling down to -100°C and a range of 1024 x 127 and 1024 x 256 CCD matrix with UV to NIR optimised options. The iDus series is the camera of choice for everyday Spectroscopy measurements, as well as more advanced, low light detection applications.

### Key applications

- Absorption - Transmission - Reflection
- Raman (244, 532, 785 and 833 nm)
- Fluorescence - Luminescence
- Plasma studies

View our cameras online  
[www.andor.com](http://www.andor.com)

360° Rotate



### Features

Peak QE of 95%	High detector sensitivity options both in VIS and NIR regions
TE cooling to -100°C	Negligible dark current without the inconvenience of LN <sub>2</sub>
Ultravac™ – Guaranteed hermetic vacuum seal	Permanent vacuum integrity, critical for deep cooling and best sensor performance
Fringe suppression technology for back-thinned option	As standard for 401 sensor – virtually eliminates etalonning effect above 650 nm
Deep-Depletion (BR-DD) sensor option	High NIR QE with zero etalonning – ideal for NIR Raman
Simple USB 2.0 connection	User friendly plug-and-play connection directly to the back of the camera

### Benefits

Model	Active pixels (µm)	Pixel size (µm)	Deepest cooling	Sensor options
DU401	1024 x 127	26 x 26	-100°C	BV, FI
DU401-BR-DD	1024 x 128	26 x 26	-100°C	BR-DD
DU420	1024 x 255	26 x 26	-100°C	BU, BU2, BV, OE
DU420-BR-DD	1024 x 256	26 x 26	-100°C	BR-DD
DV401	1024 x 127	26 x 26	-70°C	BV, FI
DV420	1024 x 255	26 x 26	-70°C	BU, BU2, BV, OE

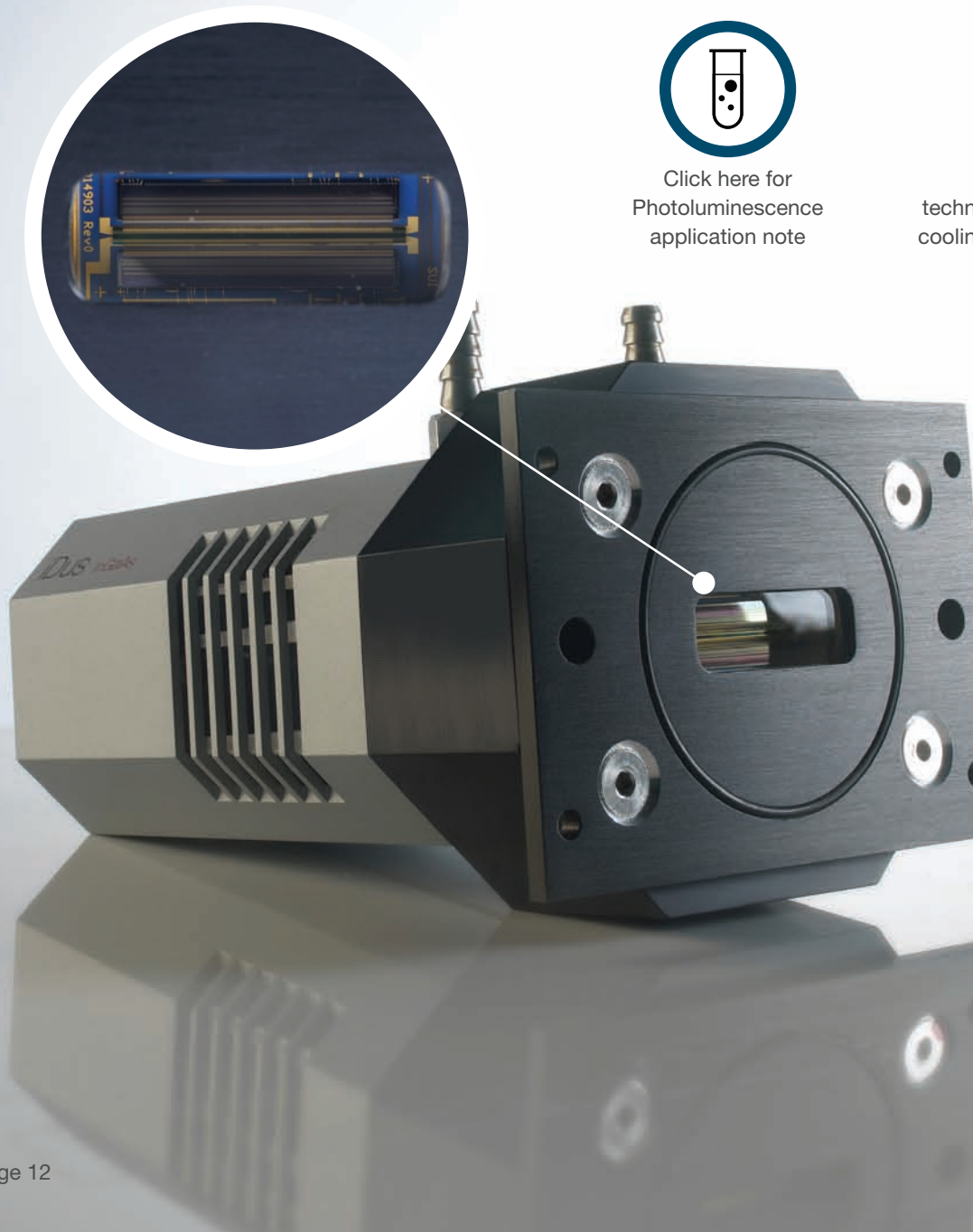


Click here for  
technical note – LN<sub>2</sub> vs TE  
cooling for BR-DD sensors

# iDus InGaAs

## Andor's iDus InGaAs detector array for Spectroscopy

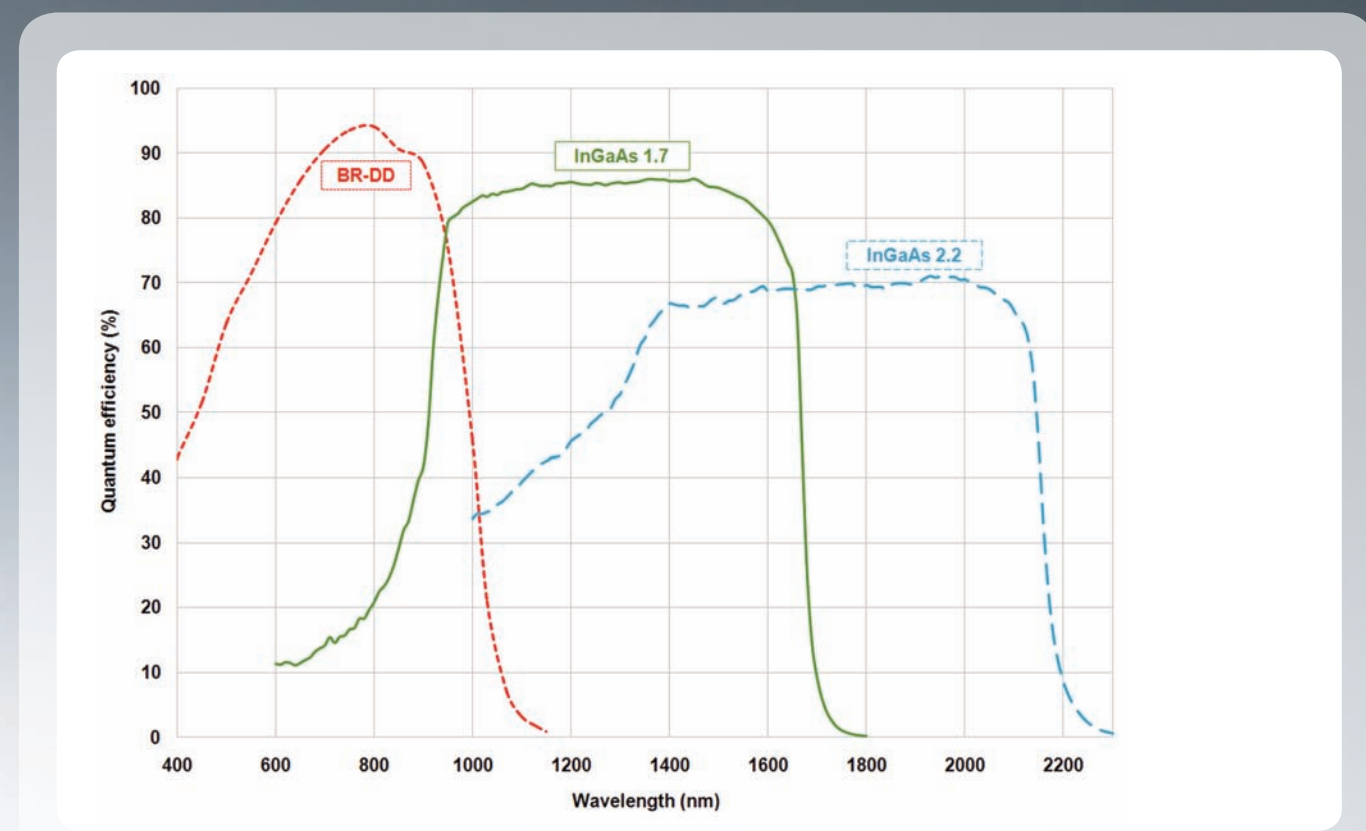
Andor iDus InGaAs 1.7 and 2.2 array series provide the most compact and optimized research-grade platform for Spectroscopy applications up to either 1.7 or 2.2  $\mu\text{m}$ . The Thermo-Electrically cooled, in-vacuum sensors reach cooling temperatures of -90°C where the best signal-to-noise ratio can be achieved for the majority of the applications in this spectral region. Beyond this cooling point blackbody radiation from any elements facing the sensor will dominate the dark signal, and since Quantum Efficiency will be impacted with decreasing cooling temperature, TE cooling will allow access to optimum SNR performance.



Click here for  
Photoluminescence  
application note



Click here for  
technical note – LN<sub>2</sub> vs TE  
cooling for InGaAs sensors



### Features

High Quantum Efficiency  
Peak QE >80% for 1.7  $\mu\text{m}$  cut-off  
Peak QE >70% for 2.2  $\mu\text{m}$  cut-off

Typically attainable TE cooling to -90°C

UltraVac™

Minimum exposure time of 1.4  $\mu\text{sec}$

25  $\mu\text{m}$  pixel width option

25.6 mm wide arrays options

Software selectable output amplifiers

Simple opto-mechanical coupling interface

Simple USB 2.0 connection

### Benefits

Maximum sensitivity in the NIR

Minimise dark current efficiently without the inconvenience of LN<sub>2</sub>

Ensures best sensor performance and protection in time

Allows study of fast transient phenomena

Optimised for high dynamic range and high resolution

Optimised for Czerny-Turner spectrograph focal plane size

Choice of High Dynamic Range (HDR) or High Sensitivity (HS)

Readily integrate with Andor Shamrock spectrograph series

User-friendly plug-and-play connection directly to the back of the camera

Model	Array size (mm)	Array size (pixels)	Pixel size (W x H, $\mu\text{m}$ )	Upper cut-off wavelength ( $\mu\text{m}$ )
DU490A-1.7	12.8	512 x 1	25 x 500	1.7
DU490A-2.2	12.8	512 x 1	25 x 250	2.2
DU491A-1.7	25.6	1024 x 1	25 x 500	1.7
DU491A-2.2	25.6	1024 x 1	25 x 250	2.2
DU492A-1.7	25.6	512 x 1	50 x 500	1.7
DU492A-2.2	25.6	512 x 1	50 x 250	2.2

### Key applications

- NIR and SWIR Absorption - Transmission - Reflection
- Raman (1064 nm)
- NIR Photoluminescence

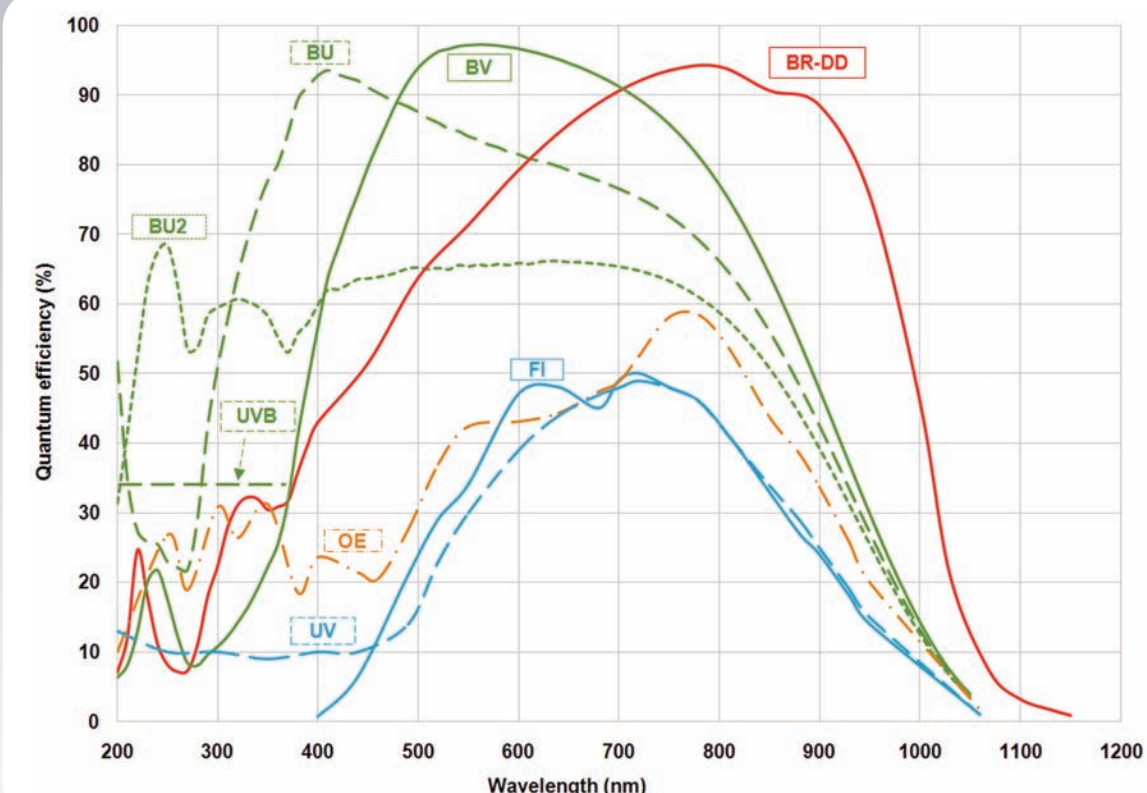
# Newton CCD

## The World's fastest Spectroscopy CCD

When it comes to the best in Spectroscopy detection, the Newton CCD cameras always come first. With a wide range of sensors boasting up to 95% QE, pixels as small as 13.5 µm and the Andor state-of-the-art Ultravac™ platform for everlasting cooling performance to -100°C, the Newton series offers no compromise when it comes to high sensitivity. Its low-noise, multi-MHz electronics platform enables spectral collection faster than 1600 spectra per second, ideal for transient phenomena studies.

### Key applications

- Absorption - Transmission - Reflection
- Raman (244, 532, 785 and 833 nm)
- Fluorescence - Luminescence
- Plasma studies
- Fast Transient phenomena study



### Features

Multi-megahertz readout

### Benefits

High repetition rates achievable with low noise electronics - ideal for transient phenomena study

TE cooling to -100°C

Negligible dark current without the inconvenience of LN<sub>2</sub>

UltraVac™ - guaranteed hermetic vacuum seal technology

Permanent vacuum integrity, critical for deep cooling & best sensor performance access

Down to 13.5 x 13.5 µm pixel size

Optimised pixel size for achievement of high resolution Spectroscopy

Crop mode operation

Achieve the highest possible spectral rates of over 1600 spectra per second

Deep-depletion sensor option

High NIR QE with zero etalonning - ideal for NIR Raman

Software-selectable output amplifiers (DU940)

Choice of High Dynamic Range (HDR) or High Sensitivity (HS)

Simple opto-mechanical coupling interface

Readily integrate with Andor Shamrock spectrograph series

Simple USB 2.0 connection

User friendly plug-and-play connection directly to the back of the camera

Model	Active pixels (µm)	Pixel size (µm)	Sensor options
DU920	1024 x 255	26 x 26	BU, BU2, BV, OE, UVB
DU920-BR-DD	1024 x 256	26 x 26	BR-DD
DU940	2048 x 512	13.5 x 13.5	BU, BU2, BV, FI, UV

# iXon<sup>EM+</sup> and Newton<sup>EM</sup>

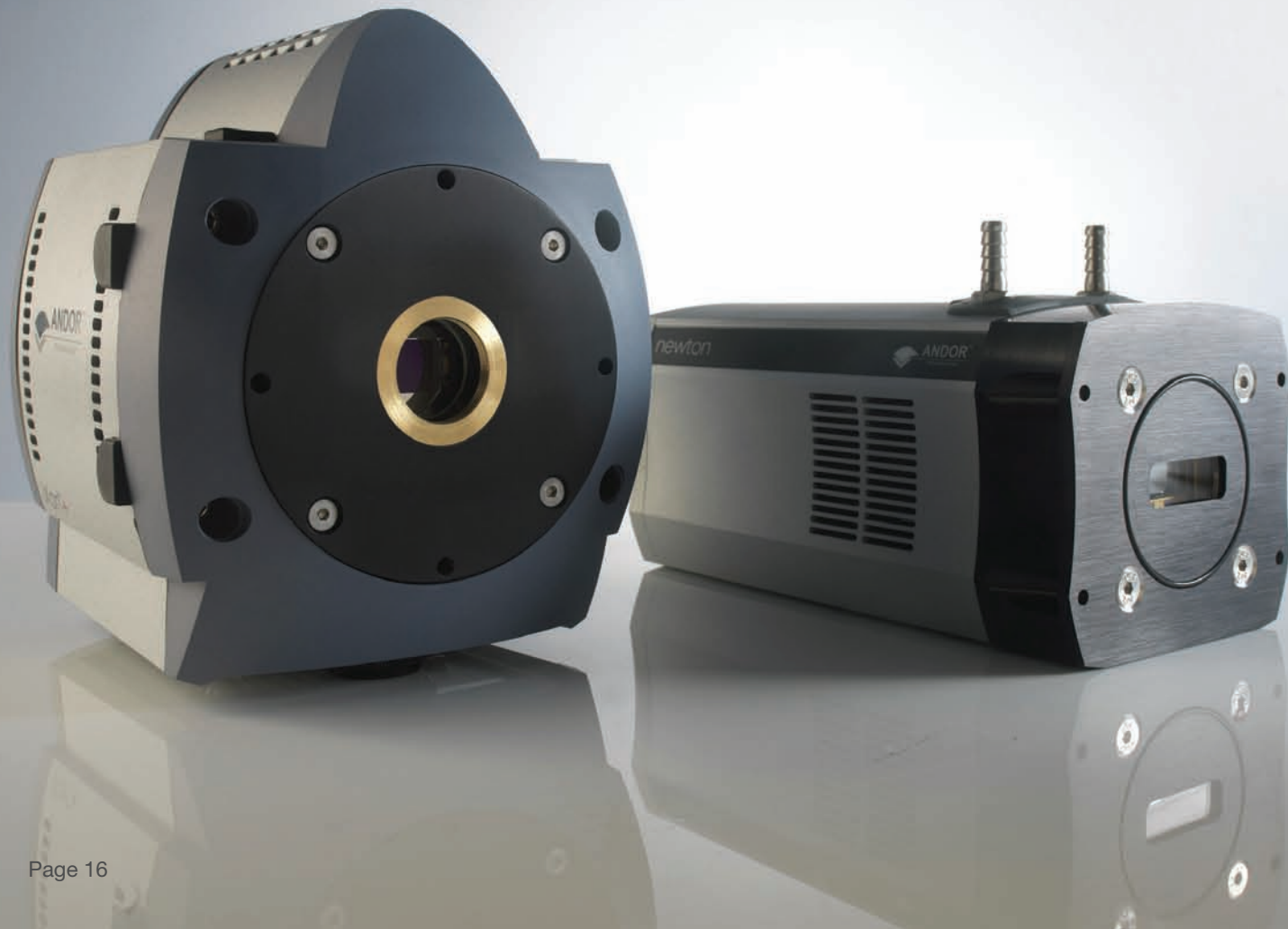
## Speed and Sensitivity with NO compromise

From the pioneers of EMCCD technology the iXon<sup>EM+</sup> and Newton<sup>EM</sup> series have brought low-light Spectroscopy to a new level of performance. Featuring Andor's market leading TE cooling to -100°C, Ultravac™ vacuum technology, Quantum Efficiency up to 95% and sub-electron read noise with on-chip Electron-Multiplying amplification, Newton<sup>EM</sup> and iXon<sup>EM+</sup> cameras offer the absolute combination of sensitivity and acquisition speed.



Professor Michael Morris  
Professor of Chemistry  
University of Michigan

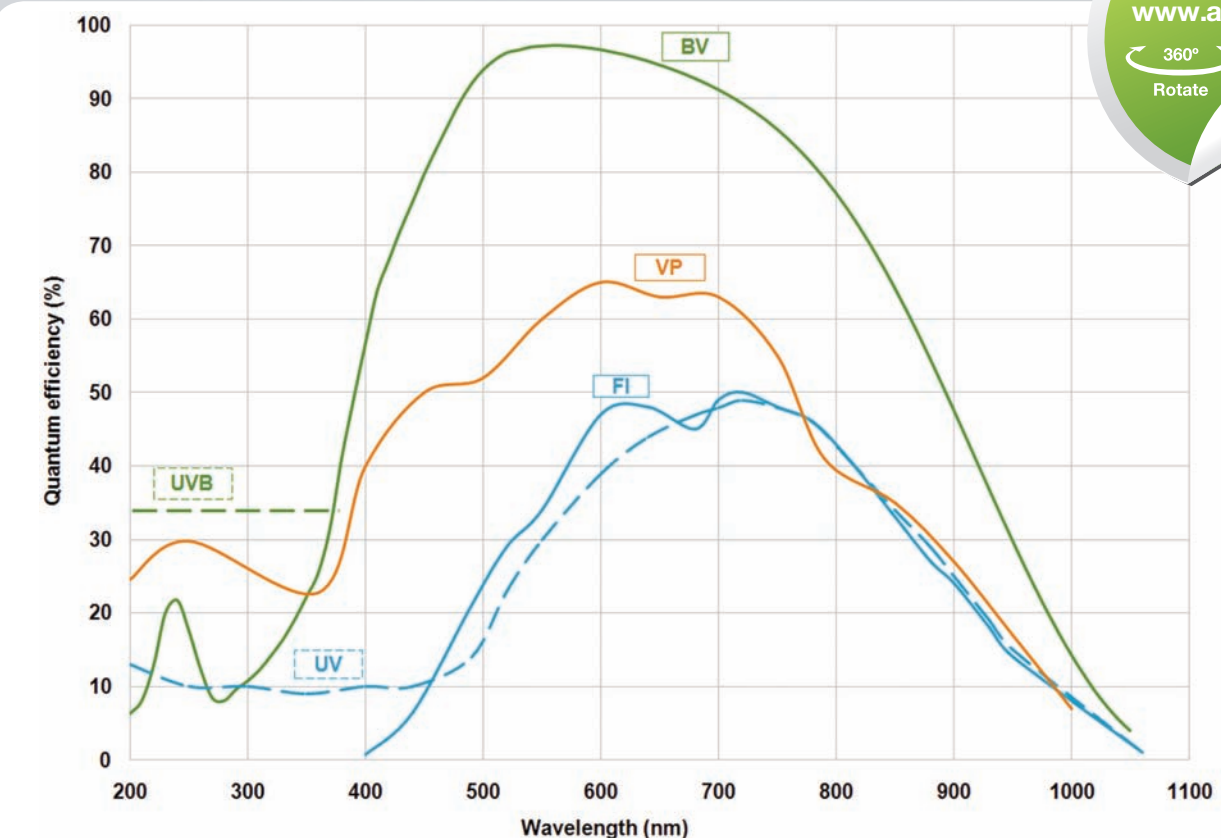
"In our lab the Andor Newton<sup>EM</sup> EMCCD has enabled millisecond Raman Spectroscopy and Hyper-spectral Raman imaging in times as short as a minute or two. And the 1600 x 400 format is just right for Spectroscopy".



[Click here for Raman EMCCD application notes](#)



[Click here for EMCCD for Spectroscopy technical note](#)



### Features

<1 e<sup>-</sup> readout noise and up to 95% QE

Industry benchmark for fast frame and spectral rate

Cropped mode option

Ultravac™ technology and TE cooling down to -100°C

True 16-bits digitization

Software-selectable output amplifiers

Spectroscopy and Imaging sensor formats available

Seamless integration with Andor spectrographs

### Benefits

'Silent' noise floor, perfectly complements high QE performance for extremely low-light detection

Full vertical binning up to 650 spectra per second or imaging frame rate up to 35 full-frames per second

Boosts spectral rate of Newton cameras up to 1515 spectra per second

Permanent vacuum integrity, critical for deep cooling and best sensor performance access

Lowest internal noise and highest linearity from scientific-grade A/D converters

Choice of High Sensitivity (low light applications) or Electron Multiplication (ultra-low light applications down to single photon)

25 mm wide option for maximum spectral information collection, or up to 13 mm tall option for larger vertical field of view, ideally suited for Micro-Spectroscopy

Simple opto-mechanical coupling to Andor Shamrock spectrograph series, with all-integrated dedicated software control

Model	Active pixel matrix	Pixel size (μm)	Fastest spectral rate *	Data transfer interface	Sensor options
Newton 970	1600 X 200	16 X 16	1515 sps	USB 2.0	BV, FI, UV, UVB
Newton 971	1600 X 400	16 X 16	1515 sps	USB 2.0	BV, FI, UV, UVB
iXon 885	1004 X 1002	8 X 8	14493 sps	PCI	VP
iXon 888	1024 X 1024	13 X 13	4170 sps	PCI	BV, UVB
iXon 897	512 X 512	16 X 16	8237 sps	PCI	BV, UVB

\* sps = spectra per second



# iStar ICCD

## Fast optical shuttering for low-light time-resolved Spectroscopy

Andor's iStar intensified CCD camera series is designed to offer the ultimate integrated detection solution for rapid, nanosecond scale Imaging and Spectroscopy. The iStar is the most compact intensified CCD platform on the market, with a software-controlled, on-board Digital Delay Generator (DDG™), for seamless integration of complex experiments. The iStar also offers a wide range of Gen II & Gen III image intensifiers, relay phosphors and input windows.



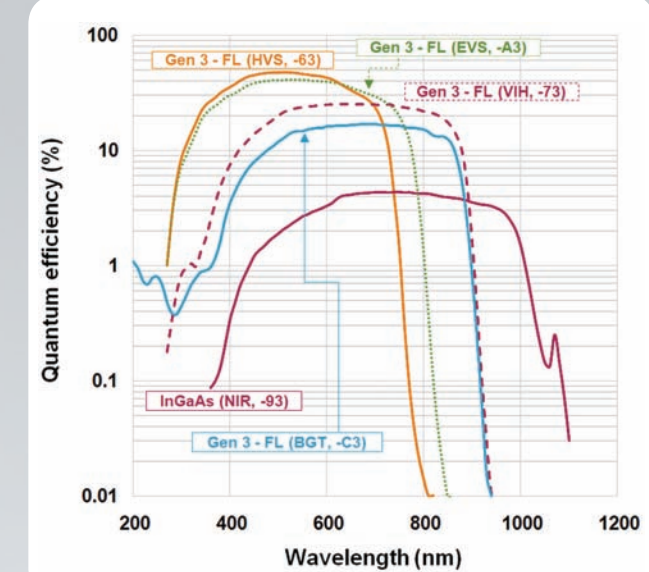
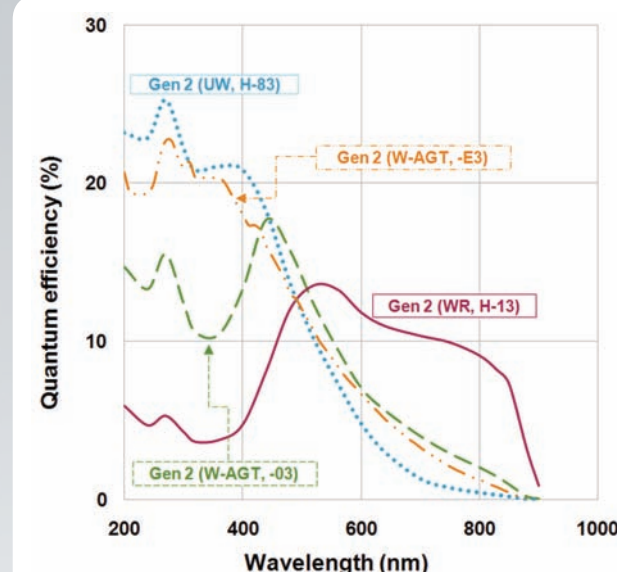
Professor JJ Laserna  
Professor of Chemistry  
University of Malaga

"The Andor iStar ICCD detectors played a vital role in allowing us to develop this new mobile standoff detection system since their sensitivity allowed us to work with exceedingly low light levels. Furthermore, their refresh rates meant we could analyze spectral information at rates in excess of 10 Hz and, therefore, perform simultaneous Raman and LIBS Spectroscopy in real time".



### Key applications

- Laser Induced Breakdown Spectroscopy (LIBS)
- Time-Resolved Raman and Resonance Raman Spectroscopy (TR<sup>3</sup>)
- Time-resolved Fluorescence - Luminescence
- Plasma studies
- Laser flash photolysis
- Single molecule Spectroscopy



### Features

Integrated digital delay generator DDG™

Ultra compact design

Close-coupled gating

IntelliGate™

High resolution Gen 2 and 3 intensifiers

Thermo-Electric cooling down to -40°C

Real-time control

True optical gate setting

### Benefits

Built into the camera head for lowest available propagation delay for the entire system - no other delays to be considered. Compact, efficient system for ultimate gating performance and accurate gating control. Comprehensive software-controlled functionalities and multi-outputs control.

Rugged and integration-friendly design with no external controller. Fibre-optic coupling for highest optical throughput without vignetting.

Gating as short as 1.2 ns - the ultimate temporal resolution for both Imaging and Spectroscopy applications.

Optional intelligent MCP gating for on/off ratios >10<sup>8</sup>:1 in the UV

Highest available intensifier resolution with QE > 50% and sensitivity up to 1090 nm

Negligible dark current, suitable for photon counting

Intuitive Windows user interface for rapid CCD, DDG™ and spectrograph real-time acquisition setup

Ensures access to the accurate optical shuttering performance of the photocathode

Photo-cathode	Type	Minimum gating speed	Peak QE (typical)	Models	Active pixel matrix	Effective pixel size (μm)	Image intensifier choice [fibre optic taper]
-03	Gen 2 broadband	<2 ns	18%	DH720	1024 x 256	26 x 26	Ø18 mm [1:1] Ø25 mm [1:1]
-13	Gen 2 NIR-enhanced	<50 ns	13.5%	DH734	1024 x 1024	13 x 13	Ø18 mm [1:1] Ø25 mm [1.5:1]
-63	Gen 3 VIS-enhanced	<2 ns	47.5%	DH740	2048 x 512	13.5 x 13.5	Ø18 mm [1:1] Ø25 mm [1:1]
-73	Gen 3 NIR-enhanced	<2 ns	25.5%				
-83	Gen 2 UV-enhanced	<100 ns	25%				
-93	Gen 3 InGaAs	<2 ns	4%				
-A3	Gen 3 VIS & NIR enhanced	<2 ns	40%				
-C3	Gen 3 VIS & NIR-enhanced with UV phosphor	<2 ns	17%				
-E3	Gen 2 UV-enhanced	<2 ns	22%				



Click here for stand-off LIBS application note

# Spectrographs

Andor technical know-how extends far beyond market-leading performance detectors, with a comprehensive range of high-end Spectrographs. At the heart of this portfolio is the Shamrock family, which offers ultimate flexibility and performance with its “out-of-the-box”, pre-aligned and pre-calibrated approach and seamless combination with Andor’s highly sensitive Spectroscopy cameras. The Mechelle 5000 is Andor’s dedicated detection solution for LIBS, offering a unique combination of 750 nm band-pass with high optical resolution in one single acquisition.

## Shamrock 163

Rugged, compact 163 mm focal length manual spectrograph, highly configurable for general, everyday lab Spectroscopy.

## Shamrock 303i

Laboratory workhorse platform, with plug-and-play USB interface, fully motorised grating turret, slits and filter wheel and imaging-optimized optics for multi-track spectral acquisition.

## Shamrock 500i

Ideal combination of high spectral resolution, imaging capabilities for multi-track acquisitions and monochromator capabilities with single point detector use for detection up to 12 µm. With the convenience of a USB controlled, fully motorized platform and accessory range.

## Shamrock 750

Delivers the highest spectral resolution of the Shamrock range while also featuring monochromator capabilities and plug-and-play, fully motorised interface.

## Mechelle 5000

Patented optical echelle design with band-pass ranging from 200 nm to 975 nm and resolution power  $\lambda/\Delta\lambda$  of 5000 across the full wavelength range, all accessible in a single acquisition without the need for moving components.



Optimum

Applications	Shamrock 163	Shamrock 303i	Shamrock 500i	Shamrock 750	Mechelle
Absorption - Transmission - Reflection	✓	✓	✓	✓	
Photoluminescence - Fluorescence	✓	✓	✓	✓	
Raman (SERS, SORS, CARS, Stimulated)	✓	✓	✓	✓	
Micro-Raman and Micro-Fluorescence	✓	✓	✓	✓	
Photon Counting	✓	✓	✓	✓	
Single Molecule Spectroscopy	✓	✓	✓	✓	
LIBS	✓	✓	✓	✓	✓
Plasma Studies	✓	✓	✓	✓	✓
Multi-track Spectroscopy	✓	✓	✓	✓	

# Shamrock 163

## Versatile compact benchtop spectrograph

The Shamrock 163 is the most compact research-grade Czerny-Turner spectrograph on the market. Its 163 mm focal length, high F/3.6 aperture and wide range of seamlessly interchangeable gratings, slits and light coupling accessories make it the ideal tool for general benchtop Spectroscopy measurements.



### Key applications

- Absorption - Transmission - Reflection
- Fluorescence - Luminescence
- Micro-Fluorescence
- Photon counting
- Single molecule Spectroscopy
- Plasma studies
- Radiometry



Click here for  
accessory tree



Resolution calculator  
[www.andor.com/calculators](http://www.andor.com/calculators)

### Features

Compact & rugged design with horizontal and vertical mounting positions

Imaging-configurable platform

Wide range of interchangeable gratings for optimisation of wavelength range and resolution

Variety of fixed slits for optimisation of resolution

Large choice of light coupling interfaces

Calibrated micrometer drive for wavelength tuning

### Benefits

Portability & ease of integration

Lens-based accessories enable multi-track Spectroscopy

Simple precision locking mechanism for seamless upgradability

Interchangeable laser-cut precision slits from 10 to 200 µm

Includes fibre-optics and C-mount microscope couplers

Simple & rapid wavelength adjustment

### Spectrograph specifications

Aperture ratio (F/#)	F/3.6
Focal length (mm)	163
Reciprocal dispersion	4.34 nm/mm
Resolution	0.29 nm <sup>†</sup>
Band pass	120 nm <sup>†</sup>
Mechanical range	0 - 1400 nm
Gratings	Single, interchangeable
Slit sizes	Fixed: 10, 25, 50, 75, 100, 200 µm Adjustable (Manual): 10 µm to 3 mm
Size L x W x H	198 x 216 x 96 mm 7.8 x 8.5 x 3.8 in.
Weight kg [lb]	3.5 [7.71]

<sup>†</sup> = Nominal values using 1200 l/mm grating, 13.5 µm pixel and 27.6 mm wide sensor, 435.8 nm central wavelength.

# Shamrock 303i, 500i and 750

## Research grade high performance spectrographs

The Shamrock 303i, 500i and 750 imaging spectrographs are research-grade, high performance and rugged platforms designed for working with demanding low-light applications, but equally suited to routine measurements. The Shamrock series boasts a range of highly versatile accessories and are seamlessly configurable.

These instruments can be integrated with Andor's world-class range of CCDs, Electron-Multiplying CCDs and Intensified CCDs to offer versatile, yet most sensitive modular solutions on the market. Andor Solis software offers the most user-friendly and state-of-the-art real-time control of detectors, spectrograph and motorized accessories at the touch of a button.



## Features

Pre-aligned, pre-calibrated detector & spectrograph systems

Image astigmatism correction with toroidal optics (303i & 500i)

USB 2.0 interface

Triple exchangeable grating turret

Double detector outputs

Wide range of accessories available

Monochromator capabilities (500i and 750)

Gold and silver optics coating options

## Benefits

Motorised, individually factory-calibrated systems – out of the box operation and seamless integration to experimental set-ups

Maximum light throughput and optimised multi-track capabilities

"Plug and play" connectivity, ideal for laptop operation alongside multi USB camera control

Interchangeable in the field

For extended wavelength coverage when combining Andor UV-VIS CCD and InGaAs cameras

The ultimate in modular set-up and in-field upgradability, including:

- Motorized slits & filter wheel
- Microscope interfaces
- Shutters
- Fiber-optic & lens couplers
- Multi-way fiber-optic bundles
- Light sources and optics

Extract best optical resolution while allowing use of single point detectors with sensitivity up to 12 µm

Most efficient for NIR detection when used in conjunction with Andor InGaAs cameras and single point detectors



Resolution calculator  
[www.andor.com/calculators](http://www.andor.com/calculators)



Click here for  
accessory tree

## Key applications

- Absorption - Transmission - Reflection (UV-NIR and SWIR)
- Raman (244, 532, 785, 833 and 1064 nm)
- Fluorescence - Luminescence (UV-NIR and SWIR)
- Micro-Raman and Micro-Fluorescence
- Photon counting
- Single molecule Spectroscopy
- Plasma studies
- Laser Induced Breakdown Spectroscopy (LIBS)

## Spectrograph specifications comparison\*

	303i	500i	750
Aperture (F/#)	F/4	F/6.5	F/9.8
Focal length (mm)	303	500	750
Reciprocal dispersion (nm/mm)	2.38	1.65	1.10
Wavelength resolution (nm)	0.16	0.11	0.074
Bandpass (nm)	65	45	30
Mechanical range (nm)	0 - 1400	0 - 1415	0 - 1430
Multi-track capability	Y	Y	Y

\* = Specifications given for a 1200 l/mm grating at 435.8 nm, 10 µm slit and 13.5 µm pixel size, 27.6 mm wide CCD ; resolution figures assume FWHM of 5x 13.5 µm pixels.

# Mechelle

## High band pass echelle spectrograph

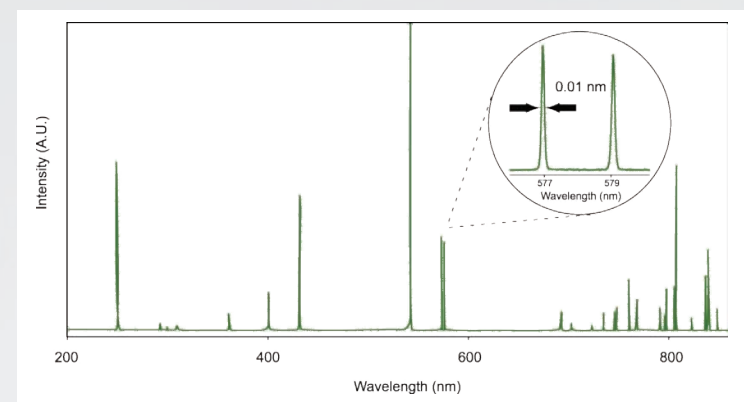
Andor's Mechelle 5000 spectrograph has been designed to provide simultaneous recording of a wide wavelength range (200 - 975 nm) in one acquisition. It has no moving components and is available in a pre-aligned detector/spectrograph format. Based on the echelle grating principle, its patented optical design provides extremely low crosstalk and maximum resolution compared with other spectrographs. It is designed to operate with both Andor's iKon CCD camera and the iStar 734 intensified camera in applications such as LIBS and plasma studies.

### Key applications

- Laser Induced Breakdown Spectroscopy (LIBS)
- Plasma studies



Echellogramme



Example of Mercury-Argon spectrum

### Features

Compact and robust design with no moving components

Patented optical design

Auto-temperature correction

N<sub>2</sub> purged

Pre-aligned detector/spectrograph solution

Low F-number

Wide range of accessories available

Peak labelling with NIST table

### Benefits

Ideal for non-lab based applications

Ensures maximum resolution and extremely low cross-talk

Corrects for the variation of prisms optical refractive index with temperature

Enables maximum throughput in the UV region

Enables fast, efficient experimental set-up

Highly efficient light collection

Including fibre optics, slits, aiming laser, collector/collimator and calibration lamps

Easy tagging of known atomic species at the press of a button



Click to view user publications  
[www.andor.com/publications](http://www.andor.com/publications)

### Spectrograph specifications

Wavelength range (nm)	200 - 975
Focal length (mm)	195
Aperture	F/7
Spectral resolution ( $\lambda/\Delta\lambda$ ) (corresponding to 3 pixels FWHM)	5000
Wavelength accuracy	Better than $\pm 0.05$ nm
Optical adjacent order cross talk	Better than $1 \times 10^{-2}$
Stray light	Better than $1.5 \times 10^{-4}$
Horizontal magnification	0.81
Vertical magnification	1.66

## Accessories and systems

"Modularity" is Andor's ethos when it comes to Spectroscopy systems, because every researcher's requirements are unique. This translates into the need for an extensive range of state-of-the-art accessories, from light collection to signal analysis and detection. Andor combines over 20 years of expertise in the fields of optics, mechanics and electronics, from designing complex interfaces to extract the very best of its market leading detectors and spectrographs, to working alongside key leading suppliers worldwide.

The result is Andor's ability to offer a comprehensive range of high performance dedicated or extremely versatile accessories, ranging from multi-cord fibre optics to sample chamber, light sources, gratings, slits and third party instruments interfaces including microscope and VUV monochromators.

### Spectral information tailoring

Selection of low and high density gratings with blazing from UV to NIR, interchangeable fixed, manual and motorised slits, mechanical shutters and filter wheel that accommodate neutral density, Raman edge and long/short pass types.

### Signal input coupling interfaces

Range of opto-mechanical couplers including fibre optics X-Y adjusters, F-number matchers, sample chamber and UV to NIR-optimized lenses. Andor's portfolio for modular Micro-Spectroscopy includes C-mount compatible flanges, wide-aperture slit, modular cage systems and a range of microscope feet for optical height matching.

### Fibre optic

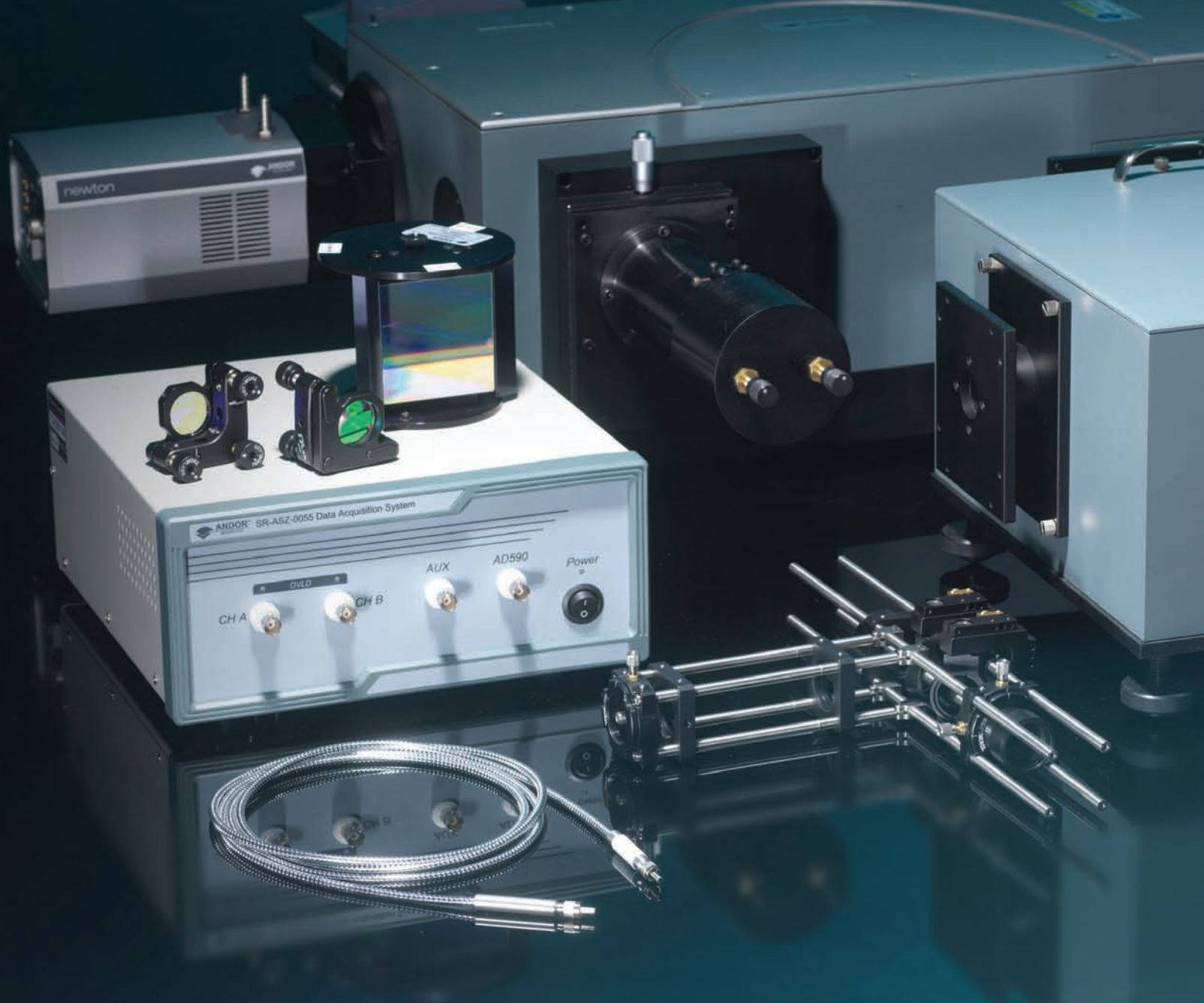
Multi-leg fibre ferrules "round-to-line" configurations, for maximum light collection along spectrograph entrance slit and multi-channels simultaneous acquisition with imaging-optimised spectral instruments.

### Spectrograph/monochromator accessories

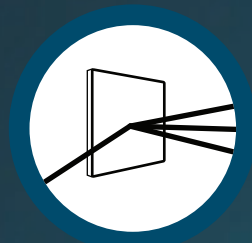
Family of single point detectors used in conjunction with Andor Shamrock 500i and 750 for acquisition from UV with PMTs and silicon photodiode to LWIR (up to 12 µm) region with InSb and MCT sensors.

### Light sources

Spectral calibration lamps including "pen-ray" style Mercury, Argon, Neon or Xenon lamps, and Deuterium and Xenon arc lamps for radiometric calibration or absorption measurements.



[Click here for accessory trees](#)



[Click here for grating selection](#)



[Click here for fibre optics](#)



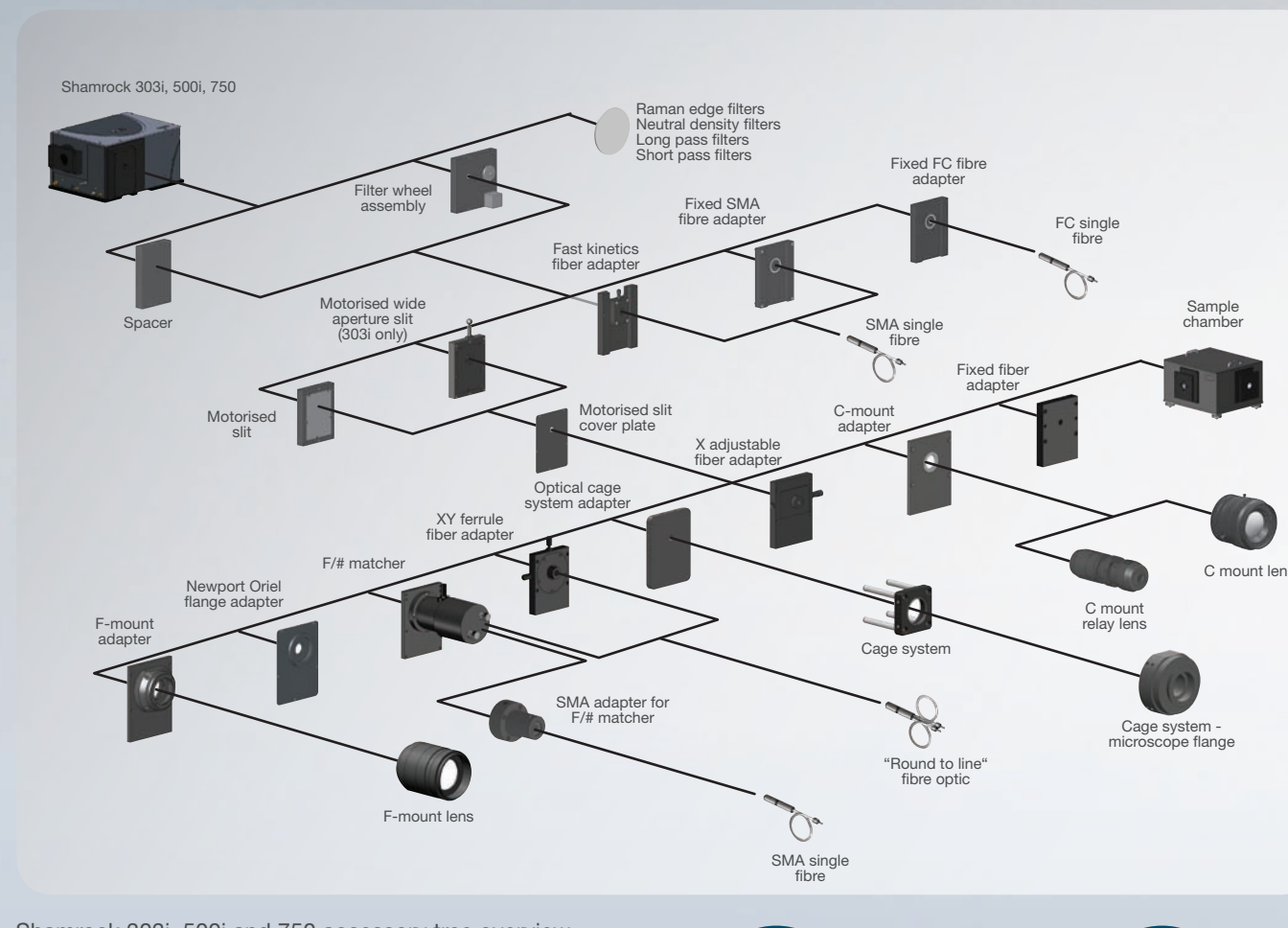
[Click here for MicroSpectroscopy](#)

# Spectrograph accessories configurations

Access to an unlimited range of detection system configurations is the basis of Andor's modular approach to Spectroscopy. That is why Andor is continuously and dynamically expanding its range of field-upgradable accessories to meet the ever-growing demand from researchers. Now including enhanced options for combining Microscopy & Spectroscopy.

Looking for light coupling interfaces to Andor spectrographs? Have an instant view of all standard accessories and just follow the configuration trees for compatibility check.

Can't see exactly what you are looking for? Want a grating with different groove density or different blaze angle, FC connection instead of SMA or custom light coupling between microscope an spectrograph? Andor's experienced and dedicated Customer Special Request (CSR) team will be eager to discuss these specific needs.



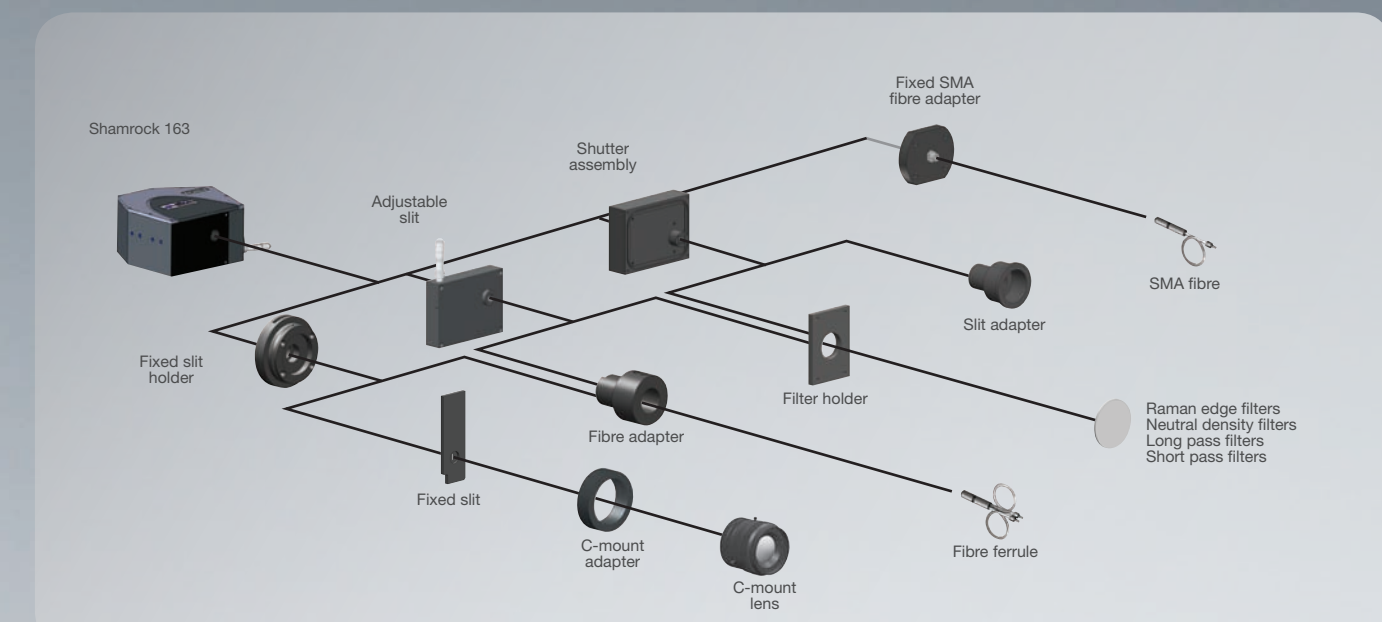
Shamrock 303i, 500i and 750 accessory tree overview



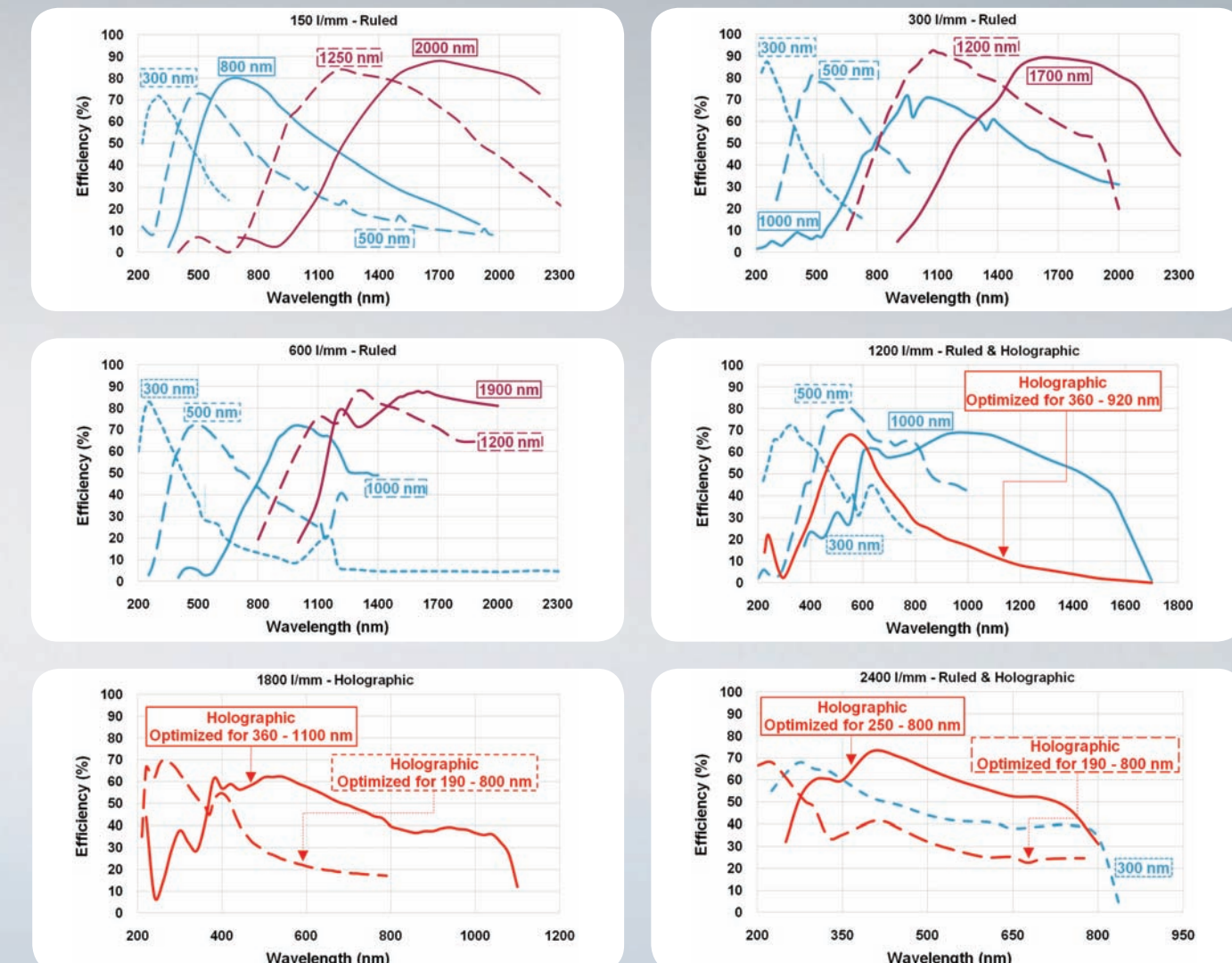
Specification sheets  
[www.andor.com/Spectroscopy](http://www.andor.com/Spectroscopy)



Resolution calculator  
[www.andor.com/calculators](http://www.andor.com/calculators)



Shamrock 163 accessory tree overview

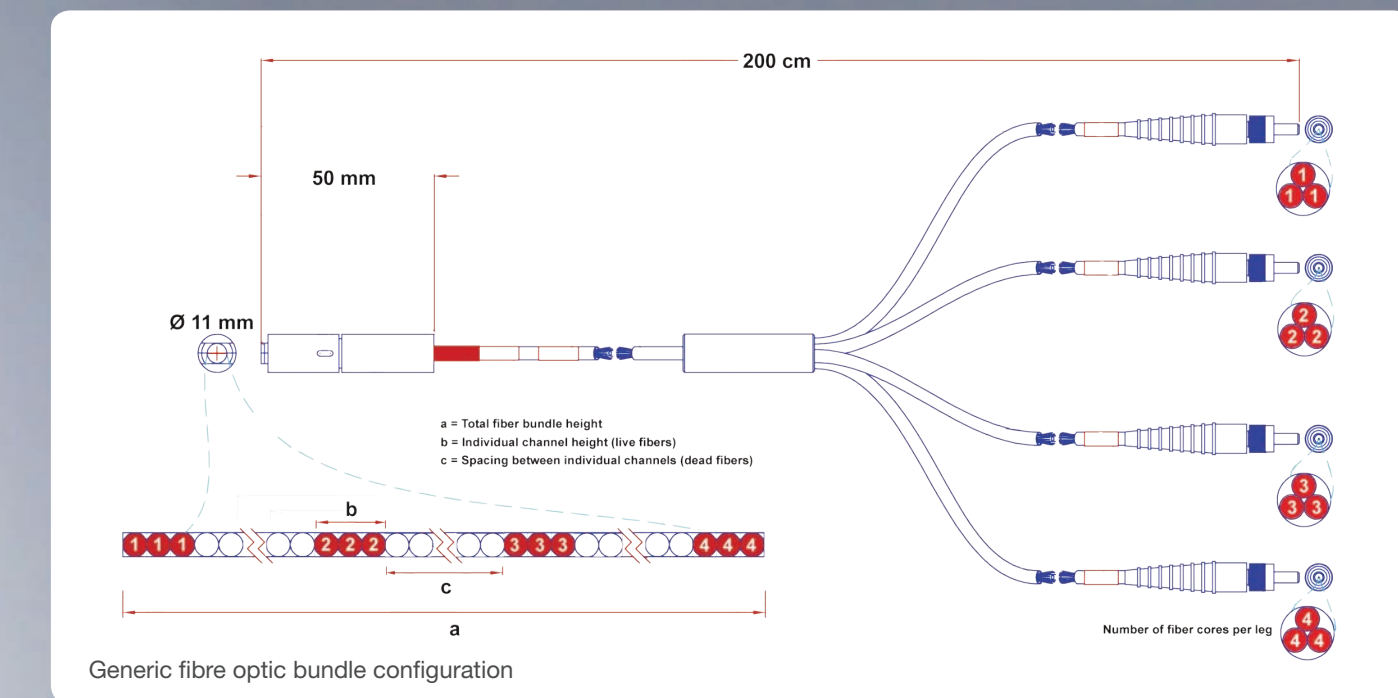


Have you found what you are looking for?

Andor offers a large variety of additional grating options, i.e. groove density and blaze. Please contact your local representative to discuss your specific needs.

## Fibre optics solutions

Fibre optic is one of the most convenient ways to collect and transport light from an experimental set-up to a spectrograph-based detection solution. Andor's series of "round-to-line", multi-core fibre optic bundles maximises the signal collection by positioning the multiple cores alongside the spectrograph entrance slit. Andor works with industry leading manufacturers to deliver solutions meeting any user requirements.



Fibre reference	Number of legs	Fibre core diameter	Optimised wavelength region	Number of fibre cores per leg	a (mm)	b (mm)	c (mm)
SR-OPT-8002	1 way	100 µm	VIS-NIR (LOH)	19	2.38	2.38	-
SR-OPT-8007	2 way	100 µm	VIS-NIR (LOH)	7	2.95	0.875	1.2
SR-OPT-8008	4 way	100 µm	VIS-NIR (LOH)	3	5.625	0.375	1.375
SR-OPT-8009	5 way	100 µm	VIS-NIR (LOH)	3	5.375	0.375	0.875
SR-OPT-8013	3 way	100 µm	VIS-NIR (LOH)	7	5.625	0.875	1.50
SR-OPT-8014	1 way	100 µm	UV-VIS (HOH)	19	2.38	2.38	-
SR-OPT-8015	2 way	100 µm	UV-VIS (HOH)	7	2.35	0.875	1.2
SR-OPT-8016	3 way	100 µm	UV-VIS (HOH)	3	5.625	0.875	1.5
SR-OPT-8017	4 way	100 µm	UV-VIS (HOH)	3	5.625	0.375	1.375
SR-OPT-8018	5 way	100 µm	UV-VIS (HOH)	3	5.375	0.375	0.875
SR-OPT-8019	1 way	200 µm	VIS-NIR (LOH)	19	4.66	4.66	-
SR-OPT-8020	2 way	200 µm	VIS-NIR (LOH)	7	5.43	1.745	2.0
SR-OPT-8021	3 way	200 µm	VIS-NIR (LOH)	3	5.635	0.735	1.715
SR-OPT-8022	4 way	200 µm	VIS-NIR (LOH)	3	5.88	0.735	1.715
SR-OPT-8024	1 way	200 µm	UV-VIS (HOH)	19	4.66	4.66	-
SR-OPT-8025	2 way	200 µm	UV-VIS (HOH)	7	5.43	1.715	2.0
SR-OPT-8026	3 way	200 µm	UV-VIS (HOH)	3	5.635	0.735	1.715
SR-OPT-8027	4 way	200 µm	UV-VIS (HOH)	3	5.88	0.735	1.715

a = Total fibre optic bundle height    b = Individual channel height (live fibres)  
 c = Spacing between individual channels (dead fibres)

### Features

- UV-Vis and Vis-NIR optimized options
- Numerical Aperture = 0.22
- 100 and 200 µm fibre core options
- From 1 to 5 leg options as standard
- Standard SMA connectors to Ø 11 mm Andor ferrule
- 2 m overall length – setup convenience and minimum transmission losses
- Re-enforced shield and ruggedised connectors
- Compatible with Andor Shamrock F/number matchers and X-Y adjusters

Have you found what you are looking for?

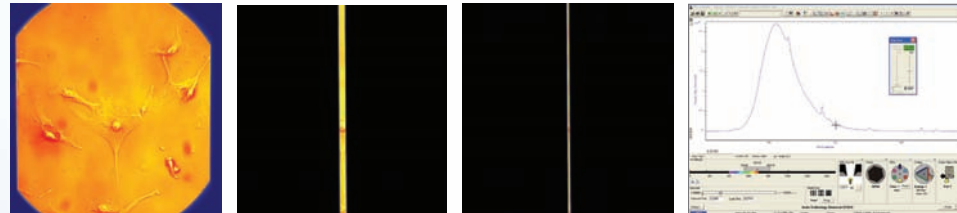
Need a different fibre core size? A longer overall cable? FC connectors? Additional channels / legs? Please contact your local Andor representative to discuss your specific needs



# MicroSpectroscopy

## Modular approach to combined Microscopy and Spectroscopy

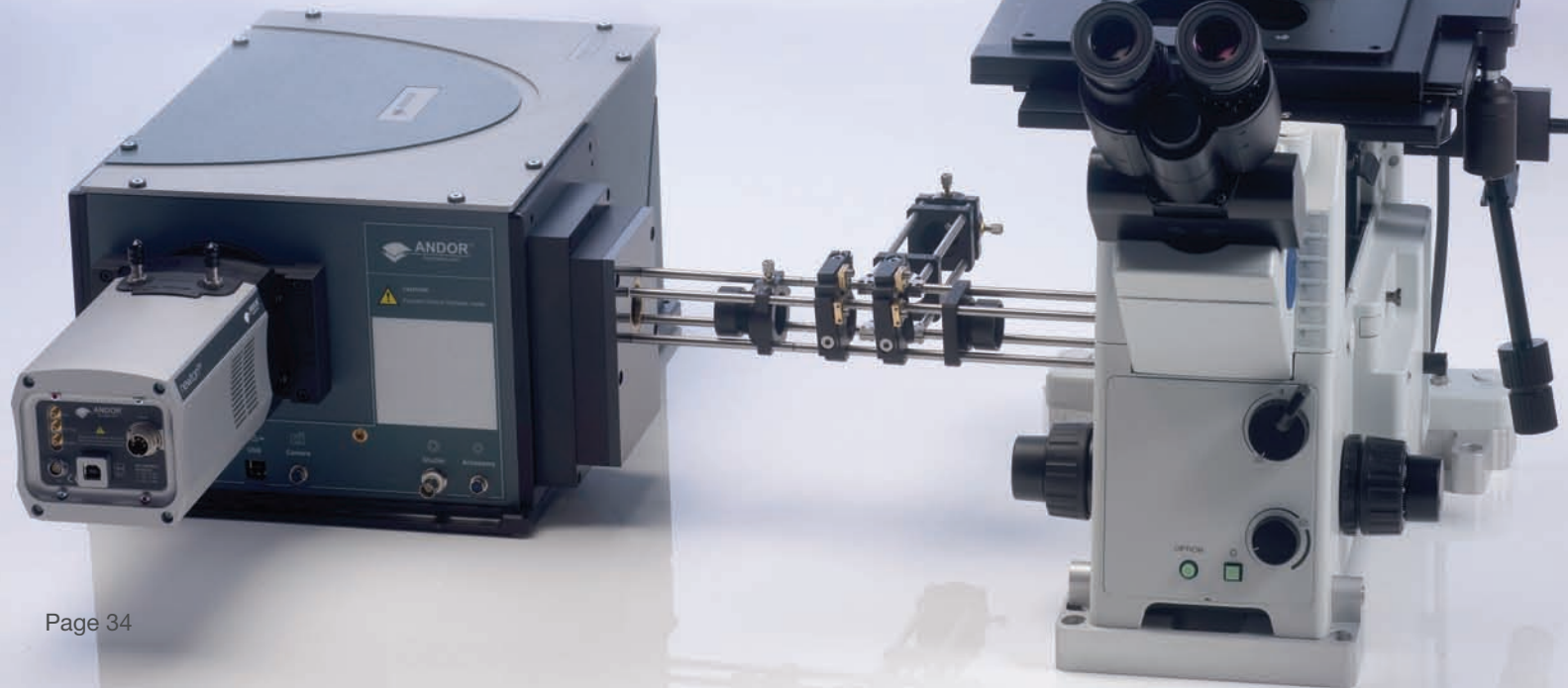
Adding structural and chemical spectral analysis to Microscopy images of bio-samples such as cells and proteins, or materials such as polymers or semi-conductors, is in ever increasing demand amongst the research community. Andor's range of modular interfaces feature cage systems couplers, allowing endlessly configurable connections between Andor Shamrock spectrographs and a wide range of market leading microscopes such as Nikon, Olympus and Zeiss. The Shamrock "wide-aperture" slit opens the door to a single setup with a single detector to image the sample, whilst allowing spectral information collection through the same optical path from the microscope.



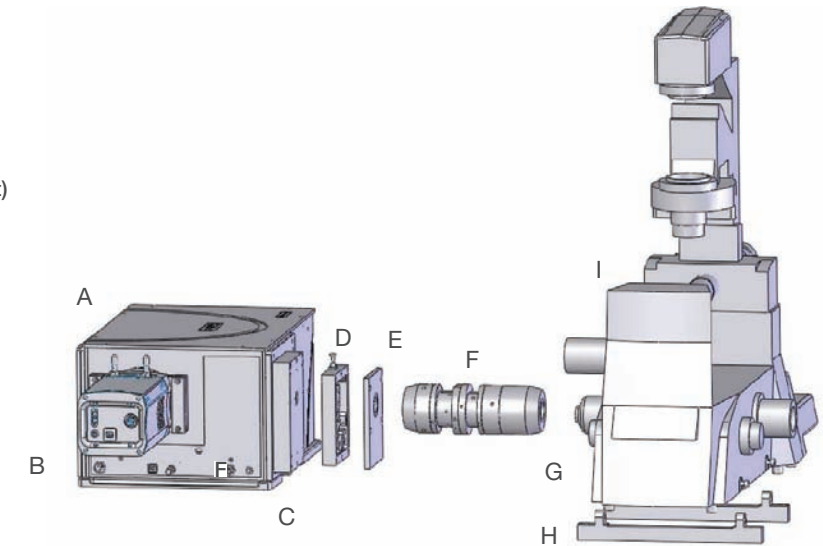
"From sample imaging to analytical information"

### Key applications

- Micro-Raman
- Micro-Fluorescence - Luminescence
- Micro-LIBS



A: Shamrock spectrograph  
 B: CCD or EMCCD detector  
 C: Filter wheel (optional)  
 D: Wide-aperture slit  
 E: C-mount adapter (spectrograph)  
 F: Relay optics (microscope dependant)  
 G: C-mount interface (microscope)  
 H: Feet for optical height matching  
 I: Microscope



Features	Benefits
C-mount interfaces	Seamless integration of Shamrock spectrograph-based systems to market leading upright and inverted microscopes
Microscope feet	Microscope left or right inverted output options – matches precisely Shamrock spectrograph optical height for accurate opto-mechanical coupling
Wide-aperture slit	Up to 12 mm field of view - Andor's imaging-optimised spectrographs allow high quality sample image relay, without compromise in spectral information collection through the same optical channel
Thorlabs or Linos cage systems compatible interfaces	Fully user-configurable optical setups for Micro-Luminescence and Micro-Raman – compatible with 16, 30 and 60 mm versions
EMCCD compatible	Andor Newton <sup>EM</sup> and iXon <sup>EM+</sup> platforms offer a unique combination of single photon sensitivity and high spectral rate & frame rate for challenging low-light Spectroscopy
Software Development Kit	Enables seamless integration with third party hardware and SDK under Labview, C/C++ and Visual Basic

Microscope configuration	Shamrock 303i	Shamrock 500i & 750	Microscope to cage system adapter
<b>Leica DMI4000 / 6000 B</b>			
Left side port	TR-LCDM-MNT-127-LP	TR-LCDM-MNT-146-LP	TR-LCDM-CAGE-ADP
Right side port	TR-LCDM-MNT-127-RP	TR-LCDM-MNT-146-RP	
<b>Nikon Eclipse Ti-E</b>			
Left side port	TR-NKTI-MNT-127-LP	TR-NKTI-MNT-146-LP	TR-NKTI-CAGE-ADP
Right side port	TR-NKTI-MNT-127-RP	TR-NKTI-MNT-146-LP	
<b>Nikon TE-2000</b>			
Left side port	TR-NK2K-MNT-127-LP	TR-NK2K-MNT-146-LP	TR-NK2K-CAGE-ADP
Right side port	TR-NK2K-MNT-127-RP	TR-NK2K-MNT-146-RP	
<b>Olympus IX71/81</b>			
Left side port	TR-OLIX-MNT-127-LP	TR-OLIX-MNT-146-LP	TR-OLIX-CAGE-ADP
<b>Zeiss Axiovert 200</b>			
Left side port	TR-ZSAV-MNT-127-LP	TR-ZSAV-MNT-146-LP	TR-ZSAV-CAGE-ADP
Right side port	TR-ZSAV-MNT-127-RP	TR-ZSAV-MNT-146-RP	
<b>Zeiss Axio Observer</b>			
Left side port	TR-ZAXO-MNT-127-LP	TR-ZAXO-MNT-146-LP	TR-ZAXO-CAGE-ADP
Right side port	TR-ZAXO-MNT-127-RP	TR-ZAXO-MNT-146-RP	

# Scanning Accessories

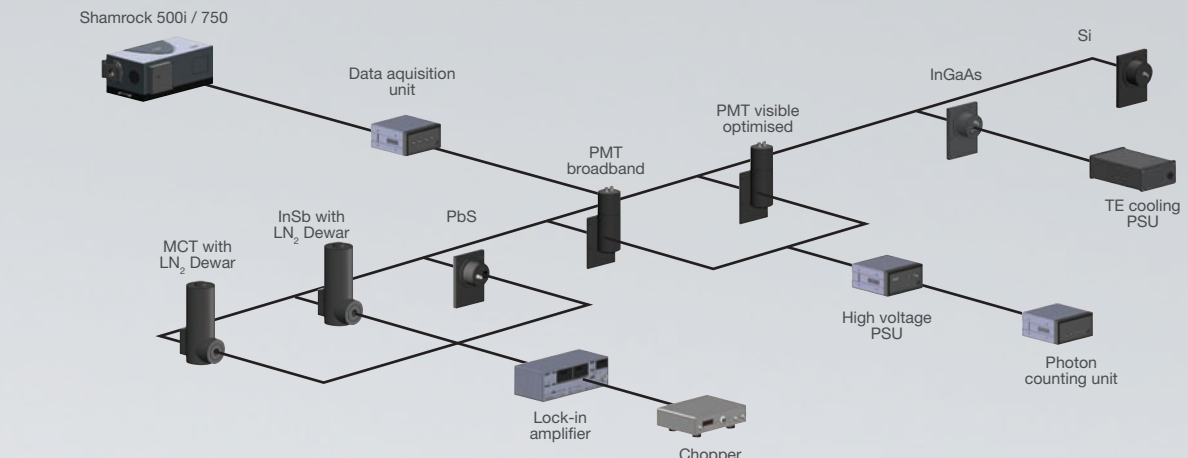
## Perfect complement to Andor's multi-channel detector portfolio

This latest addition to our Spectroscopy portfolio provides a perfect complement to Andor's extensive range of market leading CCD, ICCD, InGaAs and EMCCD detectors. Shamrock spectrograph double detector output configurations allow detection from 180 nm to 12 µm with one single setup. Solis Scanning software platform provides a dedicated single interface for seamless parametrizing and synchronising of single point detectors, spectrographs, data acquisition unit and lock-in amplifiers, with an intuitive interface for complex experiment acquisition sequences.



Click here for specification sheet  
[www.andor.com/Spectroscopy](http://www.andor.com/Spectroscopy)

**NEW!**



### Features

Wide range of single point detectors

Seamless integration with Shamrock spectrographs

Gold/silver optics coating options

Dedicated software interface

3 acquisition modes

USB 2.0 connectivity

### Benefits

Selection of PMTs, silicon photodiode, InGaAs, PbS, InSb and MCT detectors for sensitivity up to 12 µm

All detectors include Shamrock flange for easy opto-mechanical coupling

Ensures monochromator maximum throughput in the infrared region of the spectrum – MCT and InSb detectors include gold-coated focusing optics for maximum detection efficiency

Individual set-up interface for SPD, HV power supplies, photon counting and data acquisition units , lock-in amplifiers and monochromators  
Experiment builder interface for complex experiments involving sequential selection of gratings, filters or monochromators  
Dedicated GUI for data display and manipulation, including mathematical operators and FFT options

Versatile interface for scanning monochromator, time-resolved and photon counting

Plug-and-play data acquisition unit – allows connection to laptops alongside USB-controlled Shamrock monochromators

Part reference	Detector type	Wavelength coverage	Active area (mm)	Cooling
ACC-SR-ASM-0042	MCT *	2-12 µm	1 x 1	LN <sub>2</sub>
ACC-SR-ASM-0043	InSb *	1-5.5 µm	Ø2	LN <sub>2</sub>
ACC-SR-ASM-0045	PbS	0.8-2.9 µm	4 x 5	Room temperature
ACC-SR-ASM-0044	InGaAs	0.8-1.9 µm	Ø3	-40°C TE cooling
ACC-SR-ASM-0046	Si	200-1100 nm	Ø11.28	Room temperature
ACC-SR-ASM-0047	PMT (R928)	185-900 nm	8 x 24	Room temperature
ACC-SR-ASM-0048	PMT (R1527P)	185-680 nm	8 x 24	Room temperature

\* Including gold-focusing mirror for maximum signal collection

Part reference	Function	Features
ACC-SR-ASZ-0053	HV power supply for PMT	0 to 1.5 kV software-controlled range for PMT gain adjustment
ACC-SR-ASZ-0054	Photon counting unit for PMT	Software-selectable discrimination thresholds
ACC-SR-ASZ-0055	Data acquisition unit	USB 2.0 interface, includes 2x SPD acquisition channels, 2x analog outputs for PMT HV power supply control and connections to lock-in amplifiers **

\*\* Recommended models include SRS SR830 with associated SR540 chopper

# Application notes and technical discussions – Andor in action

With over 50,000 users worldwide, Andor products are represented in all the major universities, helping researchers to achieve key advances and discoveries by offering cutting-edge Spectroscopy systems based on the latest technologies available. The result is a great breadth of exciting applications, collaborations and testimonials across researchers' publications which Andor is extremely proud to share with the scientific community.

Innovative techniques and cutting edge research:

- Magneto-Photoluminescence – iXon<sup>EM+</sup> 897 and Shamrock 303i combine for high-speed and high sensitivity silicon nanocrystals study
  - Near-Infrared Photoluminescence – iDus InGaAs 490-1.7 and characterization of single semiconductor quantum wires
  - Raman Flow-Cytometry – Newton<sup>EM</sup> and an innovative approach to rapid cells characterization and sorting
  - Tip-Enhanced Raman Spectroscopy – iDus, Microscopy and AFM combine for label free chemical analysis of biofilms nanostructures
  - Stand-off Laser Induced Breakdown Spectroscopy – iStar 740 and Shamrock 303i in-the-field for remote explosive residue analysis

## Technical discussions – Making sense of sensitivity:

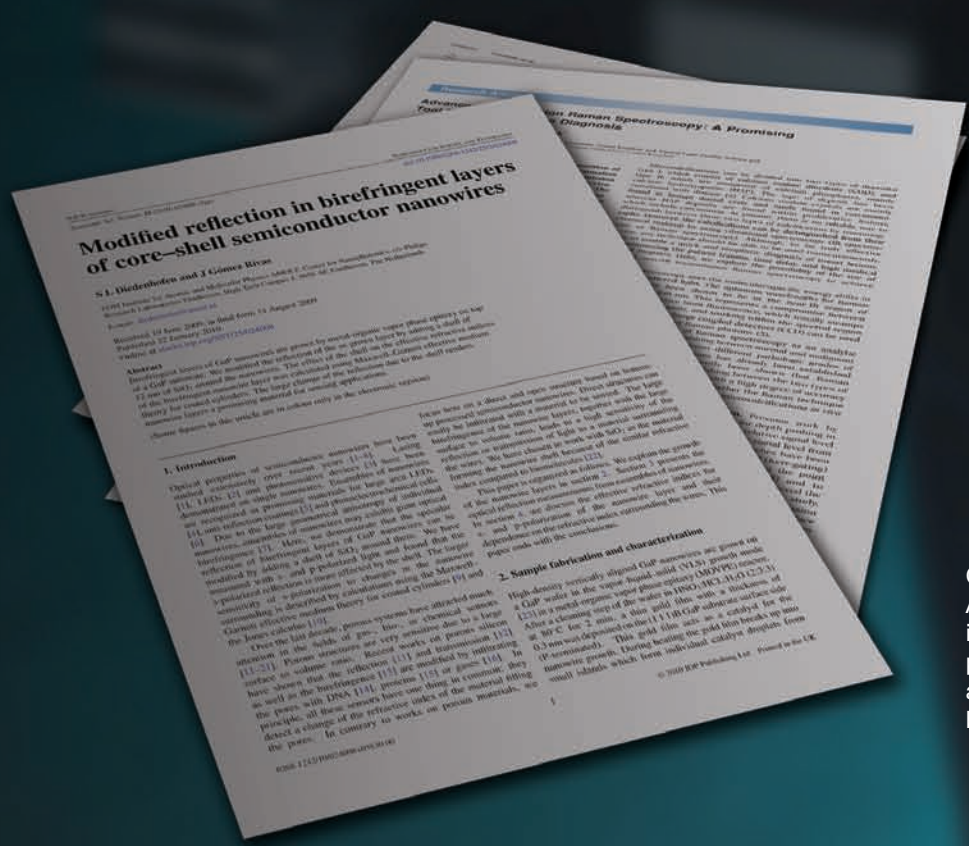
- Detector sensitivity – Key contributing factors and signal-to-noise ratio analysis
  - What is the value of LN<sub>2</sub> versus Thermo-Electric cooling for CCDs and InGaAs?  
Considerations and facts
  - Electron-Multiplying CCD technology for Spectroscopy – how to achieve ultra-fast and ultra-sensitive Spectroscopy detection



Application & learning centre  
[www.andor.com/learning](http://www.andor.com/learning)



Click to view user publications  
[www.andor.com/publications](http://www.andor.com/publications)



Have you found what you are looking for?

Cannot see your publications referenced when your work involved Andor equipment? Are you interested to put forward some of your key innovations and results? Do you have spectacular images, movies or posters you would be keen to share? Interested in collaboration work around a particular application? Our team of application specialists will be eager to discuss your ideas.

## Application Note

### Magneto-PL unveils photoluminescence in Si nanocrystals

Silicon (Si) as a material has dominated the field of microelectronics for quite some time, but when it comes to photonic devices it has had little impact due to its poor light emitting properties. However, nano-structured Si shows a marked increase in light emission efficiency; this was initially observed in porous Si, and more recently in Si nanocrystals.

Explanation of the source of this light emission has been strongly debated over the last two decades, with two possible sources being suggested – a) the influence of localized structural defects and b) the effects of Quantum Confinement (QC) within the nanostructure. Work reported by Dr Manus Hayne and co-workers in *Nature Nanotechnology* [1, 2], has given much insight into the underlying mechanisms. Using an elegant technique based around magneto-photoluminescence (magneto-PL), they were able to distinguish between the two mechanisms by a cycle of measurements on as-crystallized samples. This was followed by passivation of defects with hydrogen, and the subsequent reintroduction of defects by removal of the hydrogen. A key enabler to their work was the ability to measure the very weak PL signals using the high sensitivity detection capability offered by Electron Multiplication (EM) technology.

The quest for silicon-based photonic devices continues unabated with the ultimate goal of seamless integration of photonic devices, such as sensors or light emitters, and the associated digital data-processing electronics. Currently most photonic devices are based on III-V and II-VI semiconductors, whilst all digital electronics are silicon based. This leads to challenges and limitations when it comes to the integration of the different technologies in one system. One example is the use of optical interconnects from chip-to-chip and board-to-board in electronic systems. The emission of light from silicon nanocrystals has given hope to the developments of fully integrated systems based on one material technology. Hayne and co-workers at Lancaster University, Albert Ludwigs University in Freiburg, the Katholieke Universiteit Leuven, and the University of Antwerp set out to understand the fundamental mechanisms underlying this light emission.

A schematic of the experimental set up used by the team is shown in figure 1. The samples consisted of Si nanocrystals – typical diameter of ~3 nm – embedded in  $\text{SiO}_2$ , formed by annealing of  $\text{SiO}/\text{SiO}_2$  layers on Si substrates. Characterization was carried out using high resolution TEM (HR-TEM) imaging, electron spin resonance (ESR) analysis and magneto-PL. PL spectra consisted of broad Gaussian emissions, typically peaked around 1.61 eV (~770 nm with FWHM bandpass of ~130 nm) (see figure 2 inset). Samples were mounted in a cryostatic stage to enable cooling down to 85 K, and a magnetic field, of varying peak field up to 50 T, was applied perpendicular to the plane of the sample (figure 1). Excitation light in the UV was delivered to the sample via optical fibres which included a bandpass filter to reduce background fluorescence from the fibers. The emitted light was collected into a bundle of fibers and delivered to a 0.3 m (Shamrock 303i) spectrograph with an EMCCD camera (iXon DV897-FI). EM gain was set on the camera to enable and optimize measurement of the signal, with a typical exposure time of 5 ms.

In their magneto-PL technique, the application of a high magnetic field is used to manipulate the confinement effects on the free carriers within the nanocrystal [3]. As a consequence of this field-induced ‘squeezing’ of the electrons, a characteristic shift in the wavelength of the light emitted from quantum confinement states should be observed; the higher the field, the higher the PL energy. However, electrons associated with highly localized defects with a characteristic confinement <1 nm should be unaffected by the magnetic field; the light emitted from these sources is expected to exhibit no shift in PL energy. Hence the method has the ability to distinguish between those states confined to a few nanometers and those associated with defects.

The first set of magneto-PL measurements were carried out on an as-crystallized sample; the PL emission was observed to be insensitive to the application of the magnetic field. The sample was then passivated in pure hydrogen at 400°C, which served to de-activate the defect sites. The emission from the passivated sample was then observed to give the expected shift in the emission wavelength with variation in the magnetic field strength; there was a shift of ~1.5 meV with the application of a 50 T field. This is illustrated in figure 2. It was also observed that the overall intensity of the emission increased. A characteristic parabolic shift was observed (figure 2) with field increase, consistent with a wavefunction extent of ~5 nm. This confirmed that the emission was dominated by QC effects in this case. The researchers then went on to reactivate the defects by exposing the sample to intense UV illumination, which removed the ‘passivating’ hydrogen from the defect sites. The PL data again reverted back to showing no sensitivity to the application of the magnetic field, indicative that the emission was again dominated by it due to the localized defects. The results confirmed that when present, defects are the origin of the bulk of the emission within Si nanocrystals, and when there are no defects the emission is dominated by quantum confinement effects within the nanostructure.

EM technology as implemented on the iXon<sup>EM+</sup>, successfully met the major challenges posed by such an experiment, namely the sensitivity to measure extremely weak PL signals, and the speed to allow for averaging over a large number of spectral acquisitions.

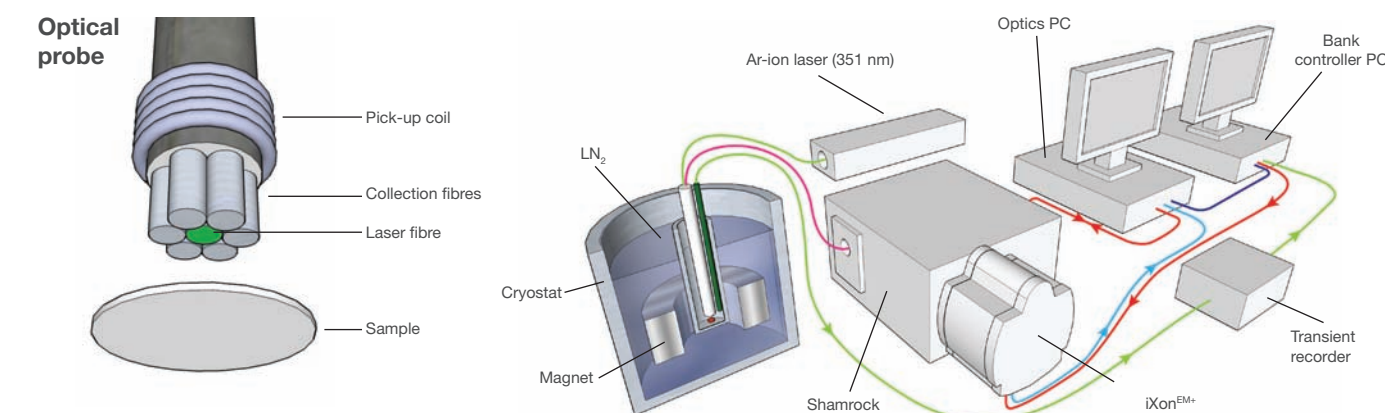


Figure 1: Schematic of experimental set-up at Katholieke Universiteit Leuven, Belgium. The samples were mounted in a cryostat (middle) where they were cooled to 85K. High magnetic fields were applied across the samples as illustrated in the typical characteristic (lower right). The acquisition of the PL signal was timed to coincide with the peak of the applied magnetic field illustrated by the grey bar. The excitation laser was delivered through an optical fiber (top left) and the resultant PL signal was fed via collection fibres into a remotely located Shamrock spectrograph with iXon<sup>EM+</sup> detector.

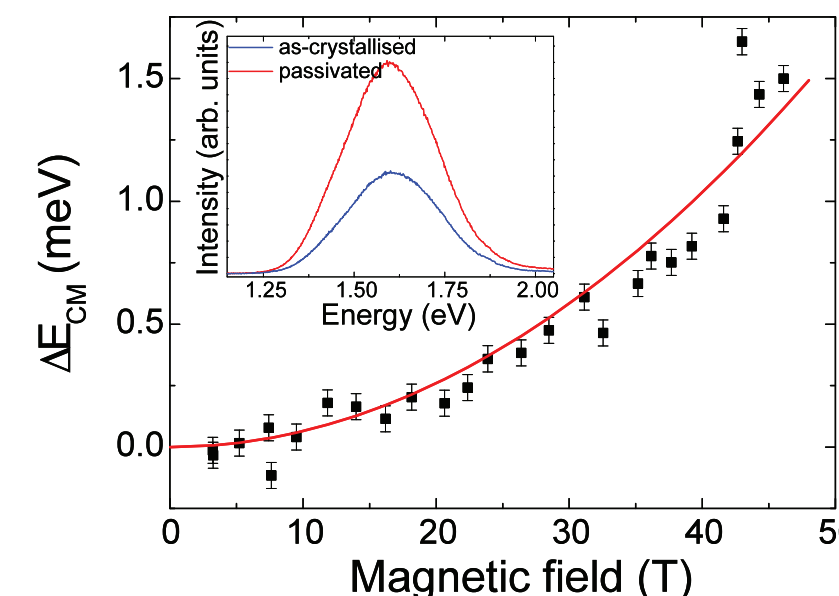
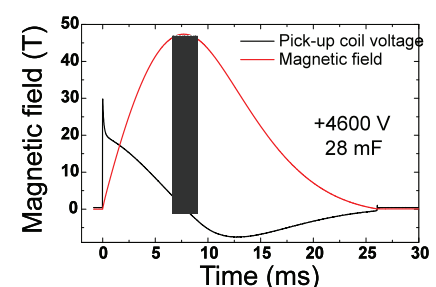


Figure 2: Shift of the photoluminescence (PL) energy for the passivated sample in which there is quantum confinement. The inset shows typical spectrum before (as-crystallized) and after passivation. Note that the PL shift with field is only 1.5 meV and the line width is 300 meV (Courtesy Dr M Hayne, Lancaster University).

Acknowledgement: Graphs courtesy of Dr Manus Hayne, Lancaster University, England.  
Reference material:

- 1) S. Godefroo, M. Hayne, M. Jivanescu, A. Stesmans, M. Zacharias, O. I. Lebedev, G. Van Tendeloo and V. V. Moshchalkov, ‘Classification and control of the origin of photoluminescence from Si nanocrystals’, *Nature Nanotechnology*, Vol. 3, March 2008, 174-178.
- 2) U. Gosele, ‘Shedding new light on silicon’, *Nature Nanotechnology*, Vol. 3, March 2008, p134.
- 3) M. Hayne, J. Maes, S. Bersier, M. Henini, L. Müller-Kirsch, R. Heitz, D. Bimberg and V.V. Moshchalkov, ‘Pulsed magnetic fields as a probe of self-assembled semiconductor nanostructures’, *Physica B*, 346-347 (2004), p421-427.

## Application Note

### NIR micro-photoluminescence characterisation of Single semiconductor Quantum Wires

Nanoscale structures (quantum dots and quantum wires) are being studied extensively with a view to building ever more exotic devices, such as more efficient lasers and LEDs, or quantum information processing components. One type of material under investigation consists of semiconductor quantum wires based on InAs.

These are being explored because of their near-infrared optical properties. Work reported by Dr Benito Alén and co-workers [3] on fundamental studies of isolated InAs nanowires (QWRs) identifies novel behaviour based around the metal-insulator transition in correlated electron systems. They made use of NIR photoluminescence (NIR-PL) to explore the transition dependencies on both excitation power and temperature.

The analysis of the photoluminescence of individual semiconductor quantum wires is an invaluable tool to investigate the role played by attractive and repulsive Coulomb interactions among electrons and holes confined to one dimension. In these systems, the electronic and optical properties change dramatically depending on the number of trapped carriers, but the effect on the emission spectrum can be obscured if many QWRs with different sizes contribute to the emitted light. To ascertain the physics behind and confront the experimental data against existing theories, the photons emitted from just one QWR must be examined using high spatial resolution techniques and high sensitivity light detectors. This approach has been demonstrated for InAs/InP QWRs emitting at  $1.5\text{ }\mu\text{m}$ , by researchers in Spain at the Consejo Superior de Investigaciones Científicas (CSIC) and the Universidad de Valencia.

The prediction of low threshold for laser emission, reduced temperature sensitivity, and slow surface recombination velocity has largely motivated the research on III-V semiconductor QWRs for optoelectronic applications in recent years. Among them, self-assembled InAs/InP QWRs can get their spontaneous emission tuned beyond  $1.6\text{ }\mu\text{m}$  and their areal density reduced down to a few QWRs per square micron [1]. They are therefore ideal candidates for the fabrication of advanced light sources in the telecom spectral region [2], and for the study of novel semiconductor physics. As for the latter, collective phenomena of one-dimensional excitons have been directly investigated in these nanostructures using NIR microphotoluminescence ( $\mu$ -PL) techniques at low temperature, at the Universidad de Valencia and published by B. Alén et al. in Physical Review Letters [3].

The system consisted of a fiber-based confocal microscope arrangement inserted in the exchange gas chamber of an immersion liquid He cryostat. Excitation light from a  $950\text{ nm}$  diode laser was brought into the microscope through a single mode optical fiber whose core acted as the excitation pinhole. The laser light was focused onto the sample through an objective lens ( $\text{NA}=0.55$ ) producing a diffraction limited spot at the excitation wavelength. Light emitted

by the few QWRs present in the excitation spot (see AFM image in figure 1) was collected by the same objective and focused onto a different optical fiber which in turn was connected at its opposite end to a spectrometer equipped with a TE cooled Andor iDus InGaAs (DU490A-1.7) camera. The faint light emitted from the individual QWRs could be detected using exposure times of 10 to 100 seconds thanks to the multichannel detection capabilities of the iDus InGaAs array and low dark current of the cooled array. The samples were made using self-assembly methods of epitaxially growing InAs structures on InP (001) substrates under conditions which preferentially led to the formation of QWRs rather than quantum dots (QDs). Reflection high-energy electron diffraction (RHEED) and Atomic Force Microscopy (AFM) analyses were used to characterize the morphology and aspect ratio of the individual QWRs. These structures were typically  $20\text{ nm}$  wide and  $200\text{ nm}$  long, corresponding to aspect ratios of  $\sim 1:10$ . Experiments were carried out to investigate how the samples behaved with variation in the excitation power, with powers as low as  $8\text{ mW}$  up to  $260\text{ mW}$ . They also investigated the temperature dependence.

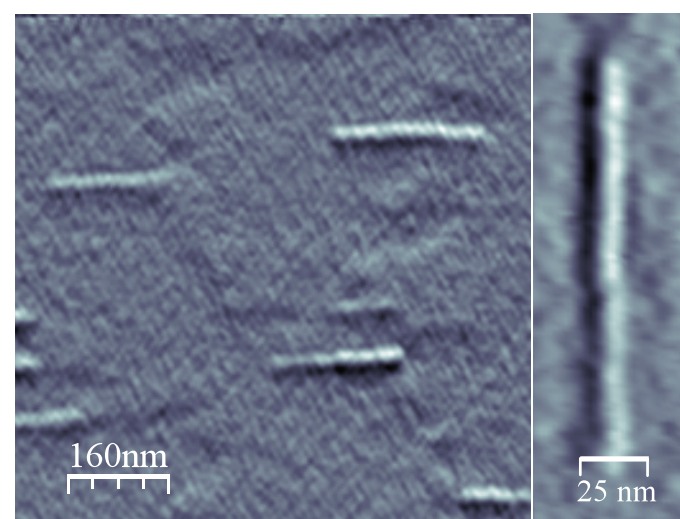


Fig 1: AFM image of the investigated QWRs (Courtesy Dr B Alén, CSIC, Madrid)

Typical examples of  $\mu$ -PL spectra collected on a single QWR as a function of excitation power density are depicted in figure 2. Due to the quantum confinement size effect, the different sized QWRs can emit at different energies, but they show a similar trend with the increasing photo-generated carrier density. The analysis of the lineshape of several spectral features observed at low and high excitation allowed a detailed study of the metal-insulator transition governed by enhanced Coulomb correlations in these systems. At low powers the sharp spectral feature at  $\sim 0.812\text{ eV}$  ( $\sim 1528\text{ nm}$ ) dominated whilst at high powers the broad spectral feature centred at  $\sim 0.807\text{ eV}$  ( $\sim 1538\text{ nm}$ ) dominated. This change in PL emission, induced by changes in carrier density, was indicative of the metal-insulator transition. The spectra show that the insulating excitonic gas (associated with high energy peaks – blue) condenses into a metallic-like electron-hole liquid phase (associated with the low energy band - red), with an increase in carrier density.

Novel behaviour on the metal-insulator transition within a correlated electron system, as realized in single InAs/InP QWRs emitting in the NIR, was clearly demonstrated by Alén and co-workers. They developed techniques based on  $\mu$ -PL, which allowed exploration of the carrier interactions and its dependence on photo-excitation powers and temperature. These fundamental studies will underpin future developments of ever more exotic devices such as high efficiency micro-/nano- lasers and LEDs.

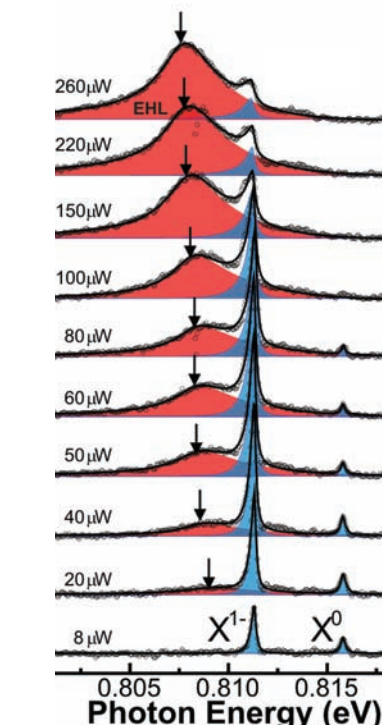


Figure 2. Typical single QWR emission spectra measured at  $5\text{ K}$  with increasing excitation power . (Courtesy Dr B Alén, CSIC, Madrid)

Acknowledgement: Appreciation is gratefully extended to Dr Benito Alén, IMM-CSIC, Madrid and Prof. Juan Martínez Pastor, Universidad de Valencia, Spain.

#### Reference material:

- 1) D. Fuster, B. Alén, L. González, Y. González and J. Martínez-Pastor, "Initial stages of self-assembled InAs/InP(0 0 1) quantum wire formation", Journal of Crystal Growth 301 (2007), 705.
- 2) L. J. Martínez, B. Alén, I. Prieto, D. Fuster, L. González, Y. González, M. L. Dotor, and P. A. Postigo, "Room temperature continuous wave operation in a photonic cristal microcavity laser with a single layer of InAs/InP self-assembled quantum wires", Optics Express 17 (2009), 14993.
- 3) B. Alén, D. Fuster, G. Muñoz-Matutano, J. Martínez-Pastor, Y. González, J. Canet-Ferrer and L. González, "Exciton Gas Compression and Metallic Condensation in a Single Semiconductor Quantum Wire", Phys. Rev. Lett. 101 (2008) 067405.

## Application Note

### Raman Spectral Flow Cytometry

A key and continuing goal in the development of flow cytometry techniques is the ability to measure ever more parameters for each particle under test. Work carried out by Prof John Nolan's group at La Jolla Bioengineering Institute, and reported by Watson et. al. [1] in *Cytometry A*, outlines the development and operation of a Raman Spectral Flow Cytometer (RSFC), which is perhaps the most radical and challenging approach to current efforts in spectral flow cytometry.

In their 'proof of principle' system, Watsons' team bring together Raman Spectroscopy, via Surface Enhanced Raman (SERS), and conventional flow cytometry, by substituting a dispersive-optic spectrograph with multichannel detector (CCD), in place of the traditional mirrors/beam splitters, filters and photomultipliers (PMT) of conventional flow cytometers. They demonstrate a system of sufficient sensitivity to acquire and analyze SERS spectra with good spectral resolution from samples consisting of nanoparticle SERS tags bound to microspheres. The functionality and power of the system is illustrated using two analytical methods, virtual bandpass filtering and principal component analysis (PCA), to distinguish between the different Raman species within their test samples.

A significant motivation for the group's work is to increase the multiplexing capability of cell and particle-based flow cytometry applications. This requires the ability to access more parallel data channels from the same sample at the same time. Conventional systems have been developed to offer higher numbers of simultaneously measurable parameters. Specially configured systems with up to 19 parameters are available (direct scatter, side scatter and multiple fluorescence channels) but this requires multiple PMTs, filters, several lasers, multiple fluorophore labels and wavelength selective mirrors. The problem that arises with trying to extend such systems to more channels, apart from the expense and the operating challenges, is the inherently broad fluorescence characteristics of the fluorophores. As the number of fluorophore fluorescent bands is increased, the more overlapping of bands takes place and it becomes increasingly difficult to distinguish the individual signal channels. This limits the number of possible data channels.

Having a dispersive-optic based system provides a simpler setup configuration and the potential for high resolution Spectroscopy. The La Jolla group has chosen Surface Enhanced Raman Spectroscopy (SERS), with its characteristically information-rich narrow band spectral features, as a route to accessing a higher number of measurable parameters. Two key technologies are being drawn upon in the development of fresh approaches to flow cytometry. The first, a), takes advantage of the ability of silver nanoparticles to enhance the Raman scattering intensity of an active species by many orders of magnitude, or as in other work, the use of fluorescent nanocrystals, with their relatively narrow emission bands, as markers of the species of interest. The second, b), is the development of Electron Multiplication CCD detectors (EMCCD), with their enhanced sensitivity which is advantageous when fast spectral rates and short exposure times are a requirement. Other groups working on spectral flow cytometry are focusing on fluorescence signatures [2] to characterize the sample.

Some of these groups use multianode PMTs or avalanche photodiodes (APD) rather than CCDs for the detectors.

Figure 1 illustrates the flow cell and the interaction region where the laser excites the sample particles or cells. A schematic of the RSFC instrument is shown in figure 2. It shows the main components used: the laser and its delivery into the flow cell (FC) with focusing optics (A); the detection of the Rayleigh side scattered signal, collected by lens optics (C) into an optical fiber (OF) and delivered to a photomultiplier (PMT); the SERS signal collected (B) and coupled into an optical fiber connected to a spectrograph with long pass filter (LP) to eliminate the Rayleigh scatter at the laser wavelength; a Newton EMCCD camera captured the spectral data; the forward scattered data was detected with a photodiode (not shown), which also acted to deliver triggering for acquisitions by the camera.

Their test samples consisted of glass-encapsulated SERS tags (Ag nanoparticles of ~67 nm diameter, with an adsorbed Raman reporter molecule and encapsulated in glass), bound to the surface of polystyrene microspheres (3.3  $\mu\text{m}$  diameter with ~8000 nanoparticles per microsphere). Four different Raman reporters were used in the preparations, each giving its own characteristic Raman signature: each microparticle was tagged with one out of the four Raman reporters. Data was captured for each particle as it passed through the interaction region (figure 1) in the form of a Raman spectrum, typical examples of which are shown in figure 3. Clearly there is potential for a wealth of information from the sharp and highly resolved spectral features of these spectra compared with the broadband data attainable with the traditional filter systems or indeed spectral techniques using fluorescent markers.

Watson et.al. then proceed to demonstrate two powerful methods for analyzing their data to discriminate between the four different types of microparticle. The first approach, referred to as 'virtual bandpass filtering', is analogous to the real-time filtering bandpass techniques of conventional flow cytometry. It offers the possibility to define 'optical filters' to select regions from the SERS spectra to emphasize differences between the four types of particle, leading to the derivation of a new set of parameters for comparison purposes. A particularly nice aspect of this method is the flexibility for optimization, by both readjustment of the virtual bandpass regions and defining the number of new parameters to be used. However, Watson et.al. point out that this approach becomes complex and cumbersome, as the number of SERS tags increases, with their associated density and overlap of spectral features.

The second method they used to distinguish the four SERS tags was that of Principal Component Analysis (PCA). PCA was applied to the first order derivative that was calculated from the smoothed and normalized SERS spectra; the ability to discriminate between different SERS tags, with this advanced and well established analysis technique, was clearly demonstrated.

The use of a spectrograph with spectral deconvolution algorithms has the potential for a more comprehensive and flexible approach to multi-color or multiparameter analysis. The La Jolla group has developed such a system as a new addition to the tools of flow cytometry, the Raman Spectral Flow Cytometer (RSFC). Challenges remain in terms of speed and sensitivity whilst maintaining good resolution. Advances in camera acquisition rates and digital processing speeds will enable faster analysis rates – a key requirement of modern flow cytometry. The coming years will see these challenges being addressed; the potential benefits as regards biological applications is immense.

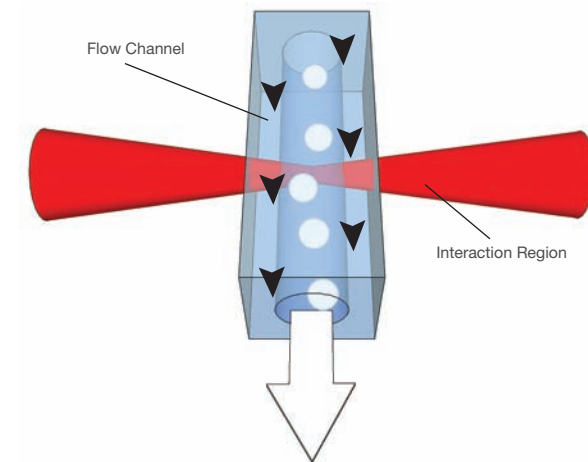


Figure 1: Schematic of the particles in the fluid flow and interaction region of the laser within the flow cell.

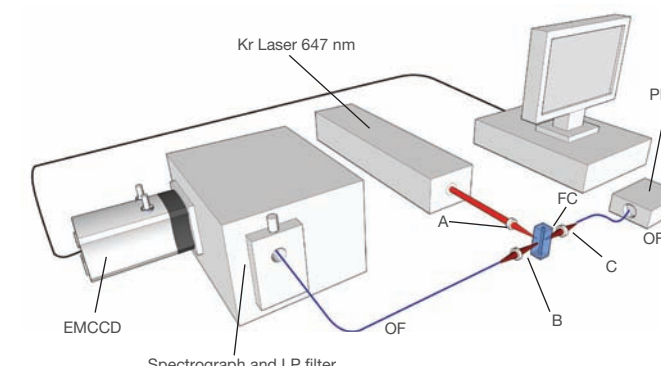


Figure 2: Schematic of RSFC instrument

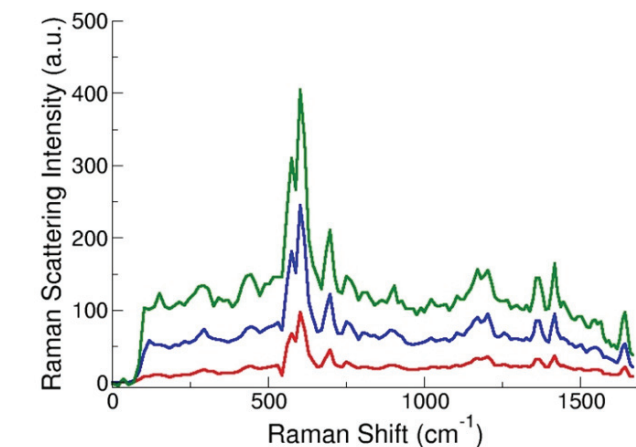


Figure 3: Sample SERS spectra from SERS tag-labelled microparticles. (D. Sebba and J. Nolan, unpublished data)

Acknowledgment: Appreciation is gratefully extended to Prof John Nolan and his group at La Jolla Bioengineering Institute, CA, USA.

#### Reference material:

- 1) Dakota A Watson, Leif O Brown, Danial F Gaskill, Mark Naivar, Steven W Graves, Stephen K Doorn and John P Nolan, 'A Flow Cytometer for the Measurement of Raman Spectra', *Cytometry Part A*, Vol 73A, p119-128, (2008)
- 2) Gregory R Goddard, J P Houston, John C Martin, Steven W Graves, James P Freyer, 'Cellular discrimination based on spectral analysis of intrinsic fluorescence', *Proc. Of SPIE*, Vol. 6859 685908-1, (2008)
- 3) John P Nolan, 'Raman Spectroscopy Meets Flow Cytometry', [www.photonics.com/content/bio/2008/April/bioFeatures](http://www.photonics.com/content/bio/2008/April/bioFeatures)

## Application Note

# TERS – Label-free chemical analysis of nanostructures in biofilms

Tip-Enhanced Raman Spectroscopy (TERS) is developing into a powerful technique for the characterization of bio-molecules at the nanoscale level [1,2,3,4,5]. It facilitates chemical imaging on the scale of single molecules, extending well established techniques such as surface enhanced Raman Spectroscopy (SERS) and Raman mapping.

Work by Dr Thomas Schmid and co-workers from Prof. Renato Zenobi's group at the Dept of Chemistry and Biosciences, ETH Zurich, demonstrates the use of TERS for label-free chemical characterization of nanostructures in biological specimens [1]. The biofilm system chosen for the investigation was based on calcium alginate fibers. TERS provides detailed chemical information at very high spatial resolutions ( $<50$  nm), with one key advantage being label-free characterization. A TERS system essentially brings together scanning probe, microscopy and Spectroscopy technologies.

Prof Zenobi's group set out to test the feasibility of using TERS to carry out label-free chemical characterization of nanostructures within biofilms. Label-free techniques remove the challenges of labeling samples using dyes or tags. Calcium alginate fibers were considered a good representative model for the extracellular polysaccharides of biofilms.

A schematic of the setup used is shown in figure 1. It essentially consisted of three main subsystems – an Atomic Force Microscope - AFM (Veeco Instruments), an inverted confocal laser scanning microscope – CLSM (Fluoview, Olympus), and a Raman Spectroscopy system consisting of a Holospec F/1.8i spectrograph (Kaiser Optical Systems) and an iDus 420 CCD camera (Andor Technology). The excitation laser (532 nm) was delivered via a single mode fiber. The CLSM unit delivered the light into the microscope, where it was focused onto the sample with an oil immersion objective (60x and NA=1.4). The scattered Raman signal was collected by the same objective and passed back through the CLSM unit and a beam splitter to be focused into a multimode fiber, which delivered the signal to the entrance port of the spectrograph. An edge filter placed in front of the spectrograph was used to reject the Rayleigh scattered light from entering the spectrograph. The sample could be scanned in 2D by control of the x-y stage upon which the sample was mounted. A folding mirror in the system allowed for rapid switching between confocal imaging and spectral acquisitions modes.

There are number of key challenges when attempting TERS with such materials. These include:

- the probe tip quality - its shape, size and cleanliness
- carbon contamination - either from ambient or photodecomposition
- heating effects
- oxygen-mediated photobleaching
- the weak Raman activity offered by these particular macro-molecules [3]
- the complexity of the molecules - a large number of functional groups

Generally one is operating in a low light regime when collecting TERS spectra from a sample consisting of a few molecules. By carefully coating the silicon tip with silver, significant enhancements in the Raman signal are possible; typical enhancements of  $\sim 10^4$  can be achieved. This enhancement is attributed to two main mechanisms:

- the excitation of surface plasmon modes between the tip and sample resulting in a multifold increase in the electric field intensity localized at the tip
- chemical enhancement due to the Charge Transfer (CT) mechanism when the molecules' functional groups are in direct contact with the metal tip

Illustrative data is shown in figure 2. An AFM image is on the left and background corrected TERS spectra on the right. The latter were produced when the tip was a few nanometers from the surface (near-field). In contrast, when the tip was the order of microns from the surface (far-field), it had no effect and no spectral signature was evident even with very long exposures (10 mins). Schmid and coworkers identified characteristic marker bands for the macromolecules studied. They observed shifts in the Raman band positions for these complex macromolecules, in contrast to observations for the corresponding bulk samples of the same material which showed no shifts. It also contrasts with less complex molecules where there was no observed shift in the bands for the TERS spectra. They attributed the shifting in large part to the influence of chemical enhancement (CE) processes occurring at the tip interface.

In the first application of TERS on alginates, the group successfully demonstrated the collection of weak Raman spectra at high spatial resolutions from extracellular polymeric substances (EPS) without the need for labeling. Such materials include polysaccharides, nucleic acids and proteins. This work represents a significant step forward in the development of the TERS technique as a reliable, accessible, and robust analytic technique for many applications in the life science, medical and materials fields.

Low photon signals place increased demands on the sensitivity of the detector used and the collection efficiency of the optical system. Only high performance cameras can give the required signal to noise ratios to make such measurements possible. The ideal system will be capable of single photon detection - an area where Electron Multiplying (EM) technology is of a definite benefit. High sensitivity facilitates the use of lower excitation fluences; this minimizes thermal effects and damage to the sample.

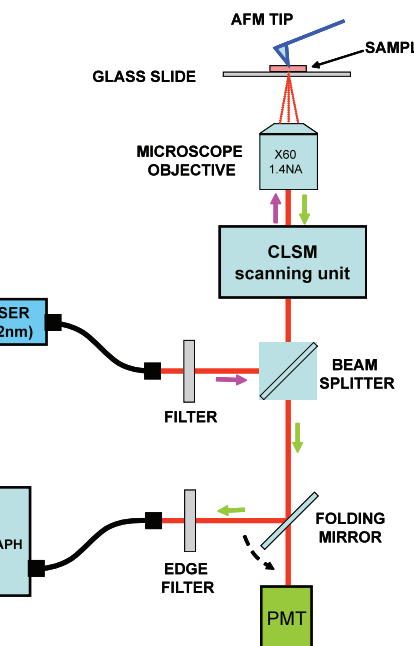


Figure 1: Schematic of the set-up used by Schmid and co-workers for acquisition of TERS spectra.

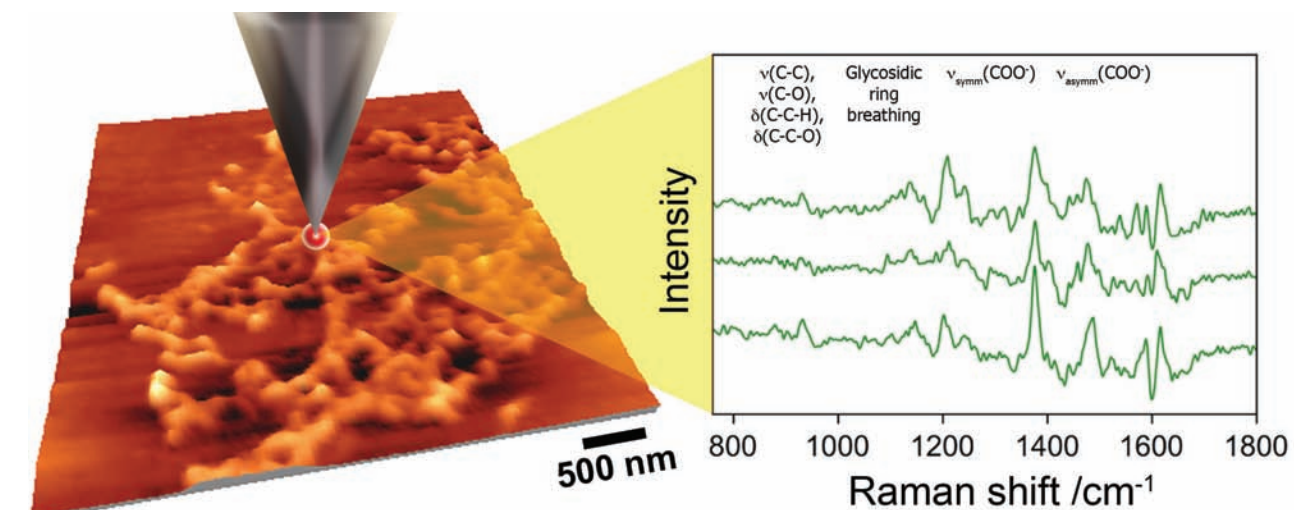


Figure 2: The TERS concept – a metallized tip is used to enhance the Raman response. An AFM image is shown to the left and sample Raman spectra taken from biofilm material is shown to the right. (Courtesy of Prof Zenobi's group, ETH, Zurich)

Acknowledgement: Appreciation is extended to Prof. Zenobi's group, Dept. of Chemistry & Applied Biosciences, ETH Zurich, Switzerland.

### Reference material:

- 1) T Schmid, A Messmer, Boon-Siang Yeo, Weihua Zhang, and R Zenobi. 'Towards chemical analysis of nanostructures in biofilms II: tip-enhanced Raman Spectroscopy of alginates'. *Anal Bioanal Chem*, 391, pp1907–1916 (2008)
- 2) C Vannier, Boon-Siang Yeo, J Melanson, and R Zenobi. 'Multifunctional microscope for far-field and tip-enhanced Raman Spectroscopy'. *Review of Scientific Instruments* 77, 023104(1-5) (2006)
- 3) Boon-Siang Yeo, J Stadler, T Schmid, R Zenobi, and Weihua Zhang. 'Tip-enhanced Raman Spectroscopy – Its status, challenges and future directions'. *Chemical Physics Letters* 472, 1–13 (2009)
- 4) APD Elwick and AR Downes. 'Development of tip-enhanced optical Spectroscopy for biological applications: a review'. *Anal. Bioanal. Chem.* 396, pp45-52 (2010)
- 5) J Steidner and B Pettinger. 'Tip-Enhanced Raman Spectroscopy and Microscopy on Single Dye Molecules with 15nm Resolution'. *Physical Review Letters*, 100, 236101 (2008)

## Application Note

### Stand-off LIBS: a detection technique for explosive residues

Stand-off techniques have received increasing attention as valuable methods for material analysis at remote distances. This is particularly relevant when looking at hazardous contaminants in the environment or residual explosive material, where it is desirable for the analyst to remain at a safe distance from the material being investigated.

Work carried out by Prof JJ Laserna's group at the Dept of Analytical Chemistry in the University of Malaga, reported by González et.al [1], explores the use of stand-off Laser Induced Breakdown Spectroscopy (stand-off LIBS) for the detection of explosive residues in situations simulating 'real environment' scenarios. They looked at the feasibility of detecting the likes of improvised explosive materials (IED) through windows such as those in cars or buildings or within various types of container. A telescopic system was used to focus a high power pulsed laser to a spot on the material to produce a micro-plasma. The same telescope collected the light emission from this plasma which was then analyzed in a spectrograph using the advanced time-gating of an intensified CCD camera.

The ability to detect dangerous contaminants, improvised explosives (IED), home made explosives (HME), or nuclear by-products, has become of increasing importance due to heightened risks in recent decades. In their work, Gonzalez and co-workers set out to test the feasibility of making such measurements with their TELELIBS sensor, and to assess the influences that the barrier position and its composition might have on the quality of those measurements. In allied work the group looked at the influence of atmospheric turbulence on beam propagation to and from the target [2], where they showed that measurements over several tens of meters could be significantly affected by atmospheric turbulence.

A schematic of the typical experimental set up used by the Malaga group is shown in figure 1. It consists of a telescope which takes the light from a laser and focuses it on to a target at a distance of typically 30 m. Two Nd:YAG lasers were used at the fundamental wavelength of 1064 nm, delivering 5 ns long pulses at 10 Hz, and energy of 800 mJ. The two laser outputs were arranged to be overlapped in space and time so that the overall irradiance on target was doubled.

The emission light from the micro-plasma was collected by the same telescope and delivered into a 600 µm core diameter fiber via a dichroic mirror. The excitation source was reflected by the dichroic mirror into the telescope whilst the returning atomic emission light was transmitted through the mirror, where it was then coupled into the optical fiber for delivery to the spectrograph. A Czerny-Turner spectrograph (Shamrock 303i) with an intensified CCD camera (iStar DH740-25F-03) was used to detect the emission. In any LIBS experiment one of the main challenges in attempting to collect discernible atomic emission line spectra is to reject the broad band continuum which occurs during the incidence of the laser pulse and immediately afterwards as the plasma plume evolves. This broad continuum tends to dominate the emission early in time resulting in little or no atomic line data being evident. However, an ICCD allows the acquisition by the camera to be delayed for a time in order to reject this early continuum. In this work a delay of 400 ns was used along

with an exposure or integration time of 9 µs.

Among the substances investigated were sodium chlorate ( $\text{NaClO}_3$ ), dinitrotoluene (DNT), trinitrotoluene (TNT), and some plastic explosives (C2 and H15). A number of barrier materials, including clear glass, some tinted glasses, and colorless PMMA (a polymer material) were placed in the beam path. The team investigated the influence of the target-to-barrier distance on the measured signal to background (S/N) ratios, along with the influence of the optical characteristics of the barrier material, thus accounting for the transmittance of excitation laser light and the returning plasma emission. A suite of chemometric tools were used to analyze the spectral data for the presence or absence of explosive residues.

A number of spectral bands and atomic/ionic emission lines were chosen for fingerprinting and subsequent identification of the explosive substances: examples of such features included the CN band (388.3 nm), the C2 band (471.5 nm, 516.5 nm and 563.5 nm), and the Al (I) line (469.4 nm) among others. The ability to detect a residue was determined by the 'sensitivity' and 'specificity' of the measuring system. Sensitivity is related to the system's ability to identify the presence of an explosive material if it is present i.e. the system flags up the presence of the material when it should. Specificity is related to its ability to identify explosives only if they are present i.e. the system doesn't flag up the presence of explosive when it shouldn't. González and co-workers assessed the capability of their system by measuring the sensitivity for the different residues with the different barrier materials. By increasing the number of laser shots it was possible to increase the detection to 100% sensitivity without impacting on specificity.

Gonzalez and co-workers successfully demonstrated the feasibility of using the stand-off or TELELIBS technique for detection of explosive materials through different types of window or interposed barriers, as long as there was a clear line of sight from the sensor system to the target. They also demonstrated that relatively few laser shots were required to ensure a high level of detection capability and means of distinguishing different residues and that the position of the barrier relative to the target and sensor was unimportant to the analysis. A key enabler for this type of work is the high sensitivity and gating versatility offered by the iStar ICCD camera. Research and validation on stand-off analysis techniques has gained much momentum as demands grow for safe, convenient and quick ways of testing for improvised explosives devices and other hazardous contaminants in the environment.

More recently the group have demonstrated the simultaneous use of both stand-off LIBS/stand-off Raman to analyse such materials [4].

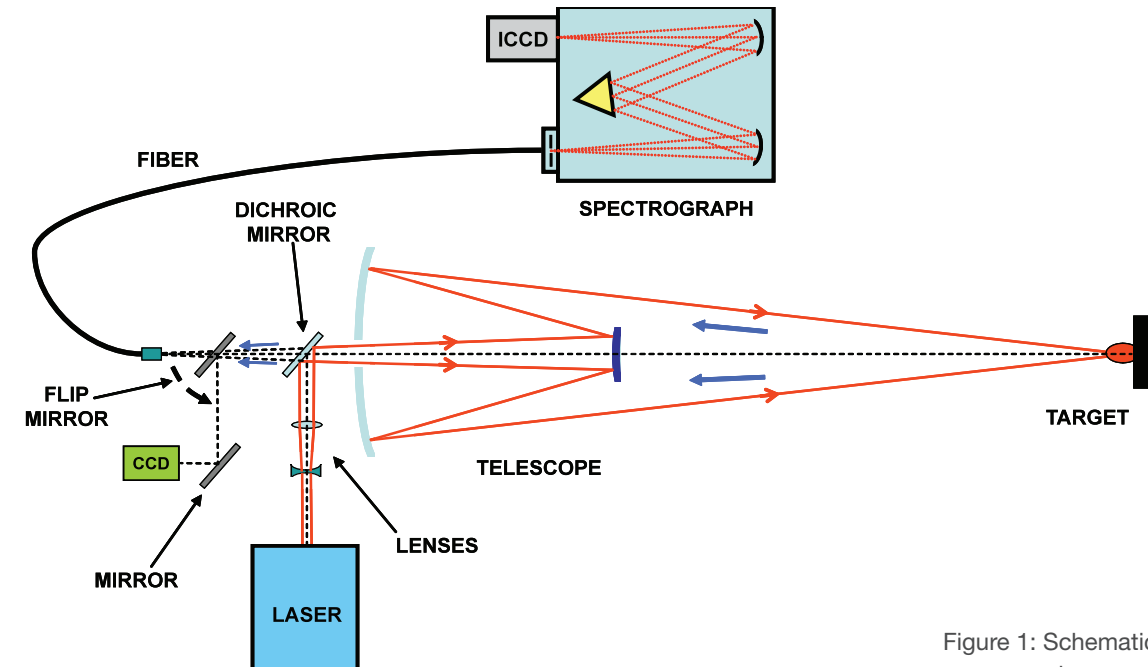


Figure 1: Schematic of the TELELIBS sensor system used in the experiments

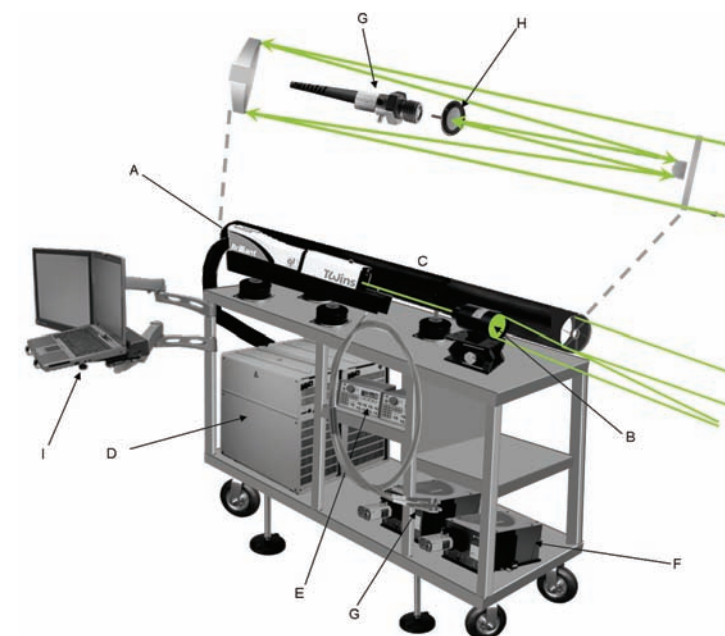


Figure 2: Schematic picture of combined LIBS-Raman system used by the Laserna group.  
A – laser, B – focusing optics, C – telescope, D - power supplies, E – delay generators, F – spectrographs, G – fibers, H – notch filter, I – laptop.

Acknowledgement: Appreciation is gratefully extended to Prof JJ Laserna and his group, University of Malaga, Spain.

#### Reference material:

1. González R, Lucena P, Tobaría LM and Laserna JJ. 'Standoff LIBS detection of explosive residues behind a barrier'. *J. Anal. At. Spectrom.*, 24, 1123–1126 (2009)
2. Laserna JJ, Fernández Reyes R, González R, Tobaría L, and Lucena P. 'Study on the effect of beam propagation through atmospheric turbulence on standoff nanosecond laser induced breakdown Spectroscopy measurements'. *Optics Express*, 17, No. 12, pp 10265–10276 (2009)
3. Luis Alonso Alvarez-Trujillo, Alejandro Ferrero and J. Javier Laserna. 'Preliminary studies on stand-off laser induced breakdown Spectroscopy detection of aerosols'. *J. Anal. At. Spectrom.*, 23, pp 885–888 (2008)
4. J Moros, JA Lorenzo, P Lucena, LM Tobaría, and JJ Laserna. 'Simultaneous Raman Spectroscopy-Laser-Induced Breakdown Spectroscopy for Instant Standoff Analysis of Explosives Using a Mobile Integrated Sensor Platform'. *Analytical Chemistry*, 82 (4), pp 1389–1400, (2010)

## Techical Note

### Sensitivity of CCD cameras – some key factors to consider

Sensitivity is a key performance feature of any detection system. When assessing the sensitivity of any CCD sensor, it is the achievable Signal-to-Noise Ratio (SNR) which is of key importance. This encapsulates the capacity to have the signal stand out from the surrounding noise.

The approach to ensure the best possible SNR ratio is to a) develop a sensor with the highest possible quantum efficiency and b) reduce the various sources of noise to a minimum. Quantum Efficiency (QE) is related to the ability of the sensor to respond to the incoming photon signal and the conversion of it to a measurable electron signal. Clearly the greater the number of photoelectrons produced for a given photon signal the higher the QE. QE is usually expressed as a probability – typically given in percentage format – where for example a QE of 0.6 or 60% indicates a 60% chance that a photoelectron will be released for each incident photon. QE is a wavelength or photon energy dependent function, and a sensor is generally chosen which has the highest QE in the wavelength region of interest. Various means have been employed to improve the quantum efficiency of CCD sensors. These include:

- Back Illumination – where the sensor is back-thinned and the light is delivered through the back making it easier for the incident photons to reach and be absorbed in the active layer of the sensor
- Anti-reflection coatings – optimised for the particular wavelength region of interest
- Deep-depletion – where the active layer is increased in extent to increase probability of absorption of photons in the near-infrared (NIR) part of the spectrum
- Lumogen coatings – to enhance the sensitivity in the UV region by the absorption and conversion of UV photons to visible photons which are more readily detected by the CCD
- Micro-lenses – more relevant to imaging sensors than Spectroscopy – allows more light to be collected into the sensitive area of the sensor leading to an increase in the fill-factor

The next key challenge is reducing the overall noise to its minimum (the latter is often referred to as the noise floor). Shot noise within the photon generated (electronic) signal ( $S$ ) is an intrinsic contribution to the overall noise and is related to fundamental quantum physics; it will always be part of any signal. If the number of photons in the incident signal is denoted by  $P$  and the quantum efficiency by QE, the photoelectron signal generated will be given by  $S = (QE.P)$ .

Next to consider is the system or camera noise which has three main contributors, the dark current (DC) of the sensor, spurious charge such as clock induced charge (CIC), and the readout noise from the output electronics (pre-amp and A/D node). The sources of noise and the means of dealing with them are summarized below:

- Signal Shot Noise ( $N_{SN}$ ) – fundamentally intrinsic to any signal  $N_{SN} = \sqrt{S} = \sqrt{(QE.P)}$
- Dark noise ( $N_{DN}$ ) – associated with the thermally generated dark current  $N_{DN} = \sqrt{(DC.t)}$  – where 't' corresponds to the exposure time: dark current (DC) is reduced by cooling of sensor
- Clock Induced Charge Noise ( $N_{CIC}$ ) – spurious noise generated during the clocking of the pixels when moving the charge out of the sensor; this is minimised by implementation of fine tuned and well controlled clocking voltages, in particular fine control over clocking edges down to nanosecond resolutions

- Readout Noise ( $N_{RN}$ ) – this arises in the readout electronics before the digitized signal is sent to the PC and may be reduced by using lower readout rates and clean clocking pulses

Usually a high performance camera is operated at certain temperatures and clocking speeds such that the detection limit is determined by the readout noise. The various sources of noise may be added in quadrature to give the overall system or camera noise which may be expressed as:

$$\text{System\_Noise} = \sqrt{N_{RN}^2 + N_{DN}^2 + N_{CIC}^2}$$

The system noise characteristics for a typical iDus – BRDD CCD camera are shown in figure 1. Clearly the dark noise will rise with increase in exposure times such that for long exposures the overall system noise (and consequently the detection limit) will become dominated by the dark noise contribution. With cooling, the dark noise contribution is reduced significantly and with sufficient cooling can be reduced to an insignificant level. This shows up as the plateau region where the system noise is now readout-noise limited. The advantage of cooling is evident when extremely long exposure times ( $>10^3$ s, if not  $10^4$ 's of seconds) are required in a given experiment. However, if short exposure times are being used, then it is clear that there is little benefit in using ultra deep cooling. As an illustration, consider exposure times less than 1000 seconds (a long exposure time). There is little or no advantage cooling the sensor below -75°C, where the system is operating on the low plateau corresponding to the read out noise limited regime. Similarly, if exposures less than 10s are being used, there is little or no benefit to be gained by cooling below -50°C. When the temperature dependence of the QE is considered then one has to be careful when choosing the best operating point or temperature for optimum performance particularly if working in the NIR region (see Technical note page 52-53).

The overall signal to noise (SNR) for a given CCD system may be expressed in the form:

$$SNR = \frac{QE.P}{\sqrt{N_{RN}^2 + N_{DN}^2 + N_{CIC}^2 + N_{SN}^2}}$$

This function enables the performance of any conventional CCD to be assessed given the values for the key parameters – usually contained in the specification or performance sheets.

A number of points worth noting are,

- the QE has some temperature dependence which has particular implications when working in the NIR region – simply cooling a sensor to the lowest possible temperature does not necessarily ensure optimum performance of the camera
- the demands on cooling are somewhat reduced when using short exposure times (<1 s)
- deep-cooling is required for longer exposures (>10 s)

Advanced detectors have been developed to extend sensitivity to the level of detecting a single photon. These systems amplify the initially detected signal using a multiplication process leading to an enhanced S/N at the read out of the CCD. The two main technologies are:

- ICCD – intensified charge couple devices where an intensifier tube is added in front of a standard CCD camera; the intensifier uses a Micro-Channel Plate (MCP) to provide the amplification of the signal before detection on the CCD
- EMCCD – Electron Multiplication (EM) charge coupled device which uses a sensor with a special read out register; the EM register amplifies the electronic signal using a process known as ion impact ionisation

The degree by which a basic signal is amplified or multiplied is referred to as the gain factor. This can be selected through the software and leads to alteration of the voltages across the MCP in the case of the ICCD and the clocking voltages applied in the EM read out register of the EMCCD.

When an EMCCD or ICCD is being used an additional source of noise must be taken into account which is associated with the amplification process itself; this variation is intrinsic to any multiplication process. This is quantified by what is termed the Noise Factor (F). For EMCCD cameras the noise factor is  $\sqrt{2}$  or ~1.41. The noise factor in ICCDs depends on the type and quality of intensifier tube used: these can have values from ~1.6 to ~3.5. Taking the noise factor (F) and the actual or real gain (G) into account, the total noise for systems

offering gain may be expressed as:

$$\text{Noise}(EM, ICCD) = \sqrt{N_{RN}^2 + G^2.F^2.(N_{DN}^2 + N_{CIC}^2 + N_{SN}^2)}$$

The SNR ratio for an EMCCD or ICCD may be written as:

$$SNR = \frac{QE.P}{\sqrt{\left(\frac{N_{RN}}{G}\right)^2 + F^2.(N_{DN}^2 + N_{CIC}^2 + N_{SN}^2)}}$$

When high performance systems are operated in a deep cooled low-noise regime, where dark and spurious noise are negligible compared with the read out noise, this expression for the SNR may be simplified to:

$$SNR = \frac{QE.P}{\sqrt{\left(\frac{N_{RN}}{G}\right)^2 + F^2.(N_{SN}^2)}}$$

It can be seen here that by increasing the gain G, the term involving the read-out noise,  $N_{RN}$ , becomes insignificant compared with the intrinsic shot noise of the signal, leading to ultra-sensitive detection capability. EMCCD and ICCD systems operated with appropriate configurations with sufficiently high gain can be used for single photon counting type experiments.

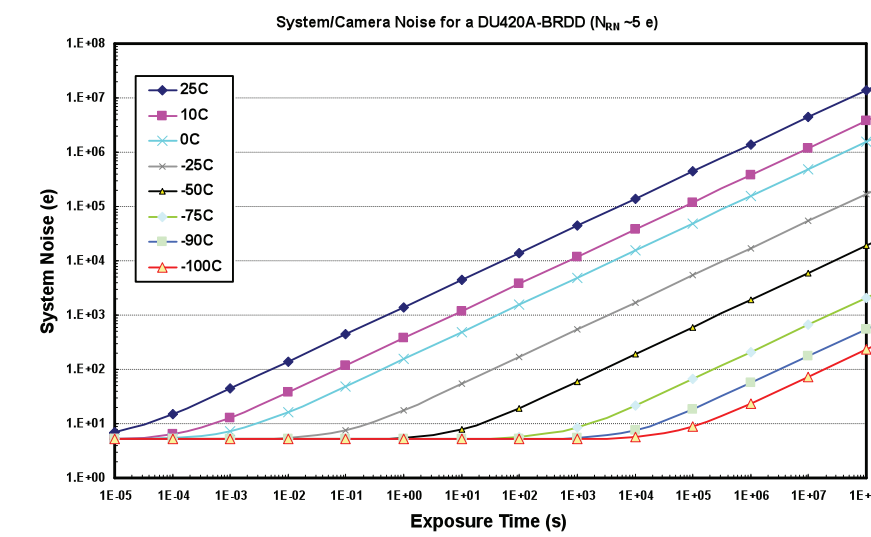


Figure 1: The detection limit as a function of exposure time for single pixel (imaging mode) which are read out at 33 kHz with readout noise of 4.6 electrons.

## Technical Note

### **LN<sub>2</sub> versus TE cooling for BRDD and InGaAs sensors**

A widely made assumption when looking for the best performance from a CCD detector is the ‘cooler the better’. An intrinsic source of noise within all CCD detectors is that associated with thermally generated ‘dark current’. Cooling is clearly the means of reducing this particular noise source.

However, it is also very important to remember than the quantum efficiency (QE) has a temperature dependence, and in this case the QE actually gets worse with cooling. This is a very important consideration for some detectors when operated in certain spectral regions, where extending the deep cooling to ever lower temperatures can lead to non-optimised operation of the system; that it to say there exists some temperature beyond which further cooling can be a disadvantage. One such case is a back-illuminated deep-depletion (BRDD) sensor used in the NIR region from 750 nm to 1000 nm.

The sensitivity of the fall-off in QE with cooling is depicted in figure 1 for a BRDD sensor. As can be seen the fall-off is quite dramatic and at the illustrated wavelength of 950 nm, the QE falls in relative terms by ~40%. This clearly arises a question around the trade-off between cooling to minimize dark noise and the desire to have QE as large as possible. To assess if there is an optimum temperature region for a given set of experimental conditions and what that temperature might be, it is useful to assess the SNR ratio possible at different temperatures of the sensor. The SNR ratio is the key parameter in any discussion on sensitivity.

If we consider the system or camera noise as summarized in the equation below and illustrated for a typical BRDD sensor in figure 1 on page 51, then it is desirable to be operating at the noise floor (plateau at base of curves). But if we are working with exposures <1 s, as an illustrative example, we could work at a range of temperatures between -50°C and -100°C and still be operating at the detection limit.

$$\text{System Noise} = \sqrt{N_{RN}^2 + N_{DN}^2 + N_{CIC}^2}$$

However, when the QE is considered, it will be found that a better SNR will be possible for these exposures when operating at temperatures towards the upper end of this range i.e. around -50°C.

The SNR is shown in figure 2 for a low level photon flux of 10 photons/pixel/second at wavelengths around 950 nm falling on a BRDD sensor. Generally as the sensor is cooled the SNR improves but interestingly at the lower temperatures the SNR is better at -75°C than at -90°C. This is indicative of the influence in the fall in QE and consistent with a transition point in the region of -70°C to -90°C where further cooling is disadvantageous to the overall sensitivity.

The SNR characteristic is shown for this particular sensor being read out at the slowest rate of 33 kHz but the same trends apply for the characteristics if operating with the higher readout speed of 100 kHz with readout noise of ~16 e<sup>-</sup>. It is also important to note that even with longer exposure times the same trend is maintained and at no

point does the deeper-cooled SNR exceed that at -75°C. In addition, when dealing with stronger photon fluxes the SNR characteristics will be even more favourable to that of -75°C compared with -100°C. The inset in figure 2 shows in greater detail the SNR curves for short exposure times.

From this example of working in the NIR region the degree of cooling must be considered carefully to ensure optimum performance in terms of SNR. In the case of the silicon-based BRDD sensor, ultra deep cooling as provided by liquid nitrogen can be a clear disadvantage when compared with deep-cooling in the -70°C to -90°C region. Thermo Electric (TE) cooling not only satisfies these requirements in a well controlled manner, but also avoids the inconvenience, cost and safety implications of working with liquid nitrogen systems.

#### Deep cooling InGaAs sensors – important implications

Just as ultra deep cooling does not guarantee optimum performance for a conventional silicon based CCD sensor, there are analogous implications for the ultra deep cooling of InGaAs sensors. As InGaAs sensors tend to be thermally noisier than their silicon counterparts, deep cooling, as supplied by TE and LN<sub>2</sub> cooling systems, is of more critical importance. However, there are two key factors which are often overlooked when deciding on the requirements for the optimum performance of an InGaAs system. These are:

- a) influence of the background ambient blackbody radiation
- b) shift in the bandgap edge with cooling

Figure 3 shows dark signal characteristics for the cooling of an iDus InGaAs (DU490A-1.7) array. These curves show the expected decrease in dark signal as the sensor gets cooler but they tend to flatten out into a plateau region beyond which further cooling of the sensor produces little or no improvement in the dark signal. A TE Peltier cooler is used to cool the sensor for the reduction of the thermally generated dark signal and a liquid coolant flowing through a copper block is used to remove heat from the warm end of the Peltier cycle. Consequently for these test measurements, the coolant determines the ambient temperature i.e. the temperature of the camera housing (including window) surrounding the sensor. The characteristic curves for different coolant temperatures show that the dark charge becomes limited by the ambient blackbody radiation from the surroundings. In practice the blackbody radiation which can enter directly through the window from the surroundings will also be added to the overall background radiation.

There is a limit to which the camera body and window can be cooled. It has to remain above the dew point, otherwise moisture will condense on the window and camera electronics. The dew point is typically between 10°C and 15°C (depends on climate/lab conditions) and as can be seen from the characteristic for coolant at 10°C, the

sensor needs cooled to just below -70°C to enter the plateau region; this is well within the capacity of TE cooling. To ensure optimum performance from these InGaAs cameras, it is strongly recommended that liquid coolant is used to enable operation just above the dew point.

Secondly, one has to be careful when measuring signals near the upper cut-off wavelength. As for silicon, cooling causes a shift in the energy of the bandgap edge; this leads to a shift in the cut-off wavelength. In InGaAs, increased cooling causes a striking shift of this cut-off towards shorter wavelengths. Figure 4 shows relative QE curves at several temperatures for the InGaAs sensor as used in the iDus DU490A-1.7 camera. This effect results in a shift dependence of ~0.6 nm/K that leads to a shift of ~70 nm to shorter wavelengths when cooling down to -100°C. This effect is of extreme importance if one is

working in the wavelength region around 1.6 μm.

As with BRDD sensors working in the NIR region, one must consider carefully the degree of deep-cooling and the ability to control it, when ensuring optimum performance of an InGaAs system in terms of SNR. If using short to medium exposure times then TE cooling is more than adequate as long as the system is operating in a regime where the background dark signal is ‘ambient-blackbody-radiation’ limited. The latter is ensured with liquid coolant such that the camera is operated just above the dew point. If working at the upper end of the sensor’s wavelength sensitivity, e.g. around 1.6 μm, the accurate controllability of temperature will be a distinct advantage for optimization of sensitivity.

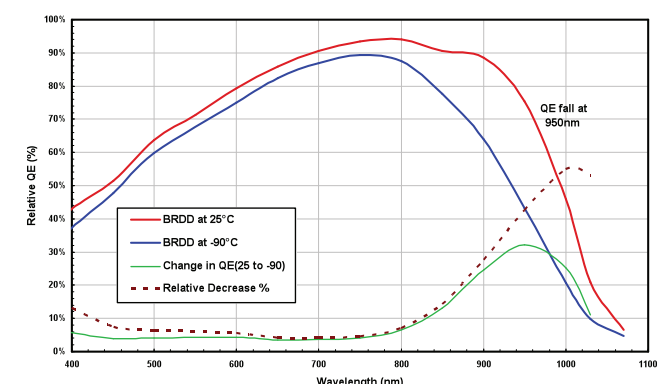


Figure 1: The relative change in QE for the BRDD sensor between 25°C and -90°C.

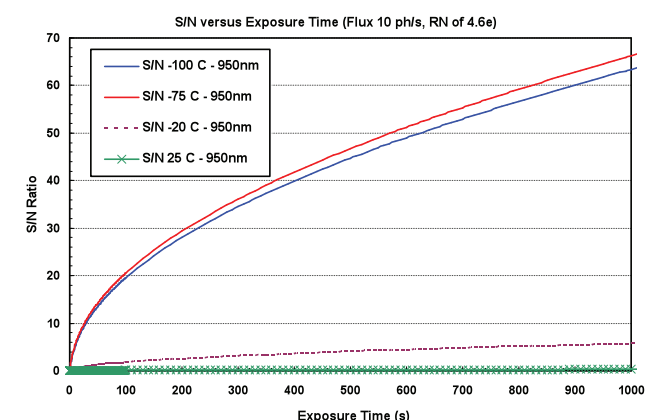


Figure 2: SNR versus exposure time for a low light photon flux of 10 ph/pix/s (950 nm) incident on the pixels of a BRDD sensor. The readout noise corresponds to the slowest rate of 33 kHz with a readout noise of 4.6 e<sup>-</sup>.

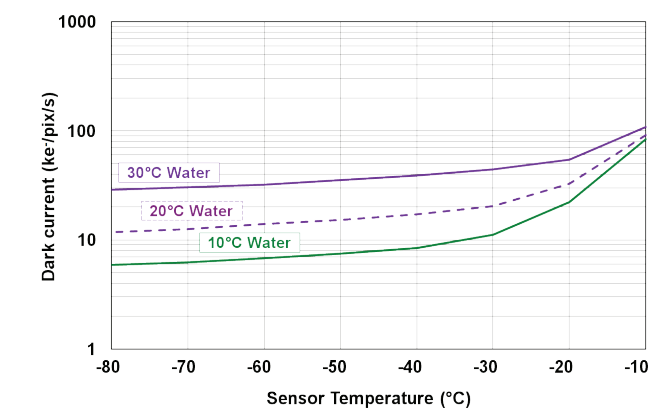


Figure 3: Dark signal characteristics for an InGaAs iDus camera where the dark signal depends on both the sensor temperature and the ambient blackbody radiation. The dark signal of the sensor is plotted at different temperatures for different ambient temperatures i.e. temperatures of the front end of the surrounding camera housing. The flat plateau regions correspond to background blackbody radiation limited detection.

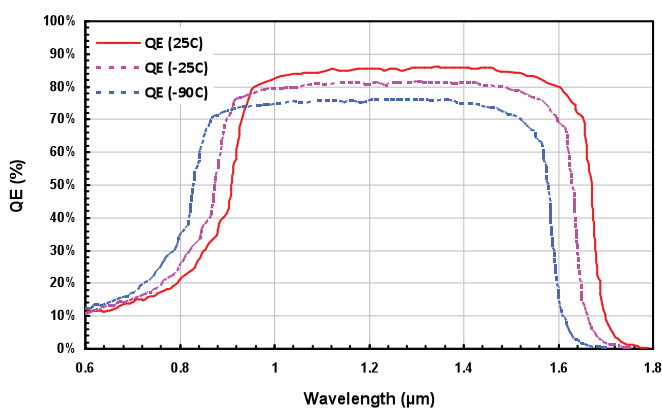


Figure 4: Variation of the relative QE of an InGaAs sensor with cooling. The solid curve is experimentally measured data at ambient (25°C). The broken curves are modelled data based on both experimental measurements and theory, which indicated a shift in the band edge towards higher energies of ~0.75 nm/K and a drop in peak QE of the order of 0.1 %/K, with fall in temperature.

## Technical Note

### EMCCD technology for Spectroscopy

Electron Multiplication (EM) technology has been one of the most important developments in light detection over the last decade. It has revolutionized the whole area of low-light Spectroscopy and imaging, enabling research that hitherto would not have been possible. EM on the CCD chip allows for the amplification of the captured electron signal before it is ever read out through the camera electronics resulting in reduction of the effective readout noise to sub-electron levels.

Sensors implementing EM amplification offer ultra-sensitive detection down to the single photon level. The first and most powerful EMCCD camera for Spectroscopy – the Newton<sup>EM</sup> – was introduced by Andor in 2005.

Other Andor cameras which implement EM sensors are the iXon<sup>EM+</sup> and Luca<sup>EM</sup> families which are used primarily for imaging applications though some are being used for Spectroscopy particularly where fast spectral rates are a prime requirement. The Newton<sup>EM</sup> has the added versatility and flexibility of being usable as both a conventional CCD and as an EMCCD; it is effectively ‘two-cameras-in-one’ with one simple click in the software to switch between them.

EM technology comes into its own when operating in a low-light regime (typically <100 photon per pixel), where the added sensitivity offers obvious benefits. Such scenarios may arise when dealing with an intrinsically weak signal, when fast spectral rates are required with minimal exposure times, or in situations where the excitation energy has to be kept low to avoid damage to the sample under investigation. Figure 1 illustrates a comparison of a conventional CCD with an EMCCD where the spectral intensity has been deliberately delivered in a low photon regime with the use of neutral density filters. The experimental conditions were exactly the same apart from the application of EM gain. Increasing the gain pulls the spectral features out of the noise to be clearly visible (figure 1. bottom), features that would otherwise have remained buried in the noise floor of the conventional system (figure 1. top).

EM technology is implemented on the CCD sensor with the inclusion of a special readout register which takes the rows of pixel charge packets from the active area of the sensor and delivers them to the readout node electronics, whilst in the process causing the charge packets to be amplified i.e. the numbers of signal electrons is multiplied. The readout node consists of the pre-amplifier (Pre-Amp) and analog-to-digital (A/D) electronics which converts the analog signal to the digital representation in ‘counts’. This digitized signal can then be sent to the computer for analysis. It is this readout node which gives rise to one of the most important sources of noise in the overall system – the readout noise ( $N_{RN}$ ) – and in the highest performance detection systems often determines the ultimate detection limit or sensitivity of the camera. It is the effective overcoming of this readout noise where EM gain delivers its benefit.

The basic principle of EM technology is illustrated in figure 2. The sensor has two readout registers, a normal or conventional register and the EM register. The clocking voltages used on the EM register are higher than for conventional clocking. These higher voltages cause the electrons to acquire sufficient energy such that extra electrons are released by a process known as impact ionization; the increased

charge package is stored in the next pixel along the chain. There is a small probability of this process actually creating additional electrons within the packet but with multiple elements or stages within the readout register significant overall gains are possible. Gains in the number of electrons up to factors of x1000 are possible – hence the term Electron Multiplication (EM).

The key advantage of on-chip-amplification before the readout node is to ensure the signal is not readout noise limited. Gain raises the signal well above the noise floor; the latter is largely determined by the readout noise of the system. An alternative way to think of this effect is in terms of the ‘effective’ readout noise. With increasing gain the effective readout noise can be decreased to the sub-electron level. Reduction in the overall noise is reflected in improved signal-to-noise (SNR) ratios and enhanced sensitivity. It is worth noting that further increase of the gain above the point where the effective readout noise is at its minimum level (< 1 electron), produces no improvement in the sensitivity. Indeed with very high gains it may serve to decrease the dynamic range of the system. The application of different gains is easily implemented through the software and results in fine adjustments of the clocking voltages in the readout register – higher voltages resulting in higher gain.

The SNR ratio is the key parameter in determining when EM gain will offer its advantages over the conventional CCD. There are four types of noise to be considered when considering the optimum SNR performance of any camera, those associated with the camera – dark current ( $N_{DN}$ ), spurious or CIC ( $N_{CIC}$ ) and readout noise ( $N_{RN}$ ), and that associated with the signal itself – namely the signal shot noise ( $N_{SN}$ ). An additional noise source must be taken into account when dealing with any multiplication or gain system such as with the EMCCD. This is encapsulated within what is called the noise factor (F) and for the EMCCD has a value of ~1.4, a value that is consistent with both theory and experimental observation. Denoting the EM gain by G, the quantum efficiency of the sensor by QE, the photon flux per pixel by P, and taking into account the noise factor, F, the SNR for the EMCCD can be expressed as:

$$SNR = \frac{QE \cdot P}{\sqrt{\left(\frac{N_{RN}}{G}\right)^2 + F^2 \left(N_{DN}^2 + N_{CIC}^2 + N_{SN}^2\right)}}$$

This reduces to the basic SNR equation for the conventional sensor with the gain G=1 and the noise factor F=1. Figure 3 shows SNR curves for the Newton<sup>EM</sup> with low photon signals. The ideal curve corresponds to the ultimate noise limit of the signal shot noise. Several curves for different gains are included which show that increasing the

gain is beneficial for the lower photon signals. The characteristic for the conventional CCD crosses over that of the EMCCD – with gain x 100 - at a signal of ~53 photons per pixel. This means that weaker signals below this transition point will benefit from EM gain, whereas for stronger signals above this level there is a better SNR with the conventional system. When the systems are operated at the fastest readout speed of 3 MHz, the readout noise is greater and the benefits of EM gain would be seen for even stronger photon signals up to just under 100 photons/pixel. It will be noted that as the photon signal increases, the SNR ratio for the conventional CCD approaches that of the ideal curve i.e. the noise becomes limited by the intrinsic shot noise of the signal. However, in the case of the EMCCD the SNR ratio approaches the ideal but will always have a systematic offset towards lower SNR; this offset is associated with the noise factor (F) of the gain register.

#### Application areas which benefit from EM technology

- Raman Spectroscopy
- Micro-Spectroscopy
- Multi-spectral Imaging
- Hyper-spectral Imaging
- Fast reaction processes
- FRET
- Single molecule Spectroscopy
- Transient (Pump-Probe) Spectroscopy
- Nano-dot Photoluminescence
- Organic Luminescence
- Atomic emission Spectroscopy
- Flow cytometry
- Electroluminescence

When operated with very high gain and signals with ultra-low levels, an EMCCD can be used in ‘photon counting mode’. This is a special mode of detection where the camera can count single photon events and build up a spectrum over time based on the discrete counting of these events. It is this ultra-high sensitivity and extremely fast spectral readout rates, along with a full featured, versatile and easy-to-use configuration platform that make the Newton<sup>EM</sup> the ideal choice for the most challenging Spectroscopy applications.

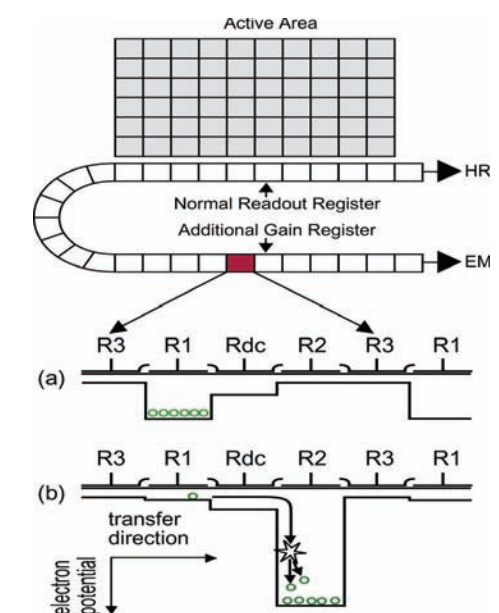


Figure 2: Signal amplification by electron impact ionization – EM gain. Schematic shows charge being clocked through the EM register and being amplified in the process.

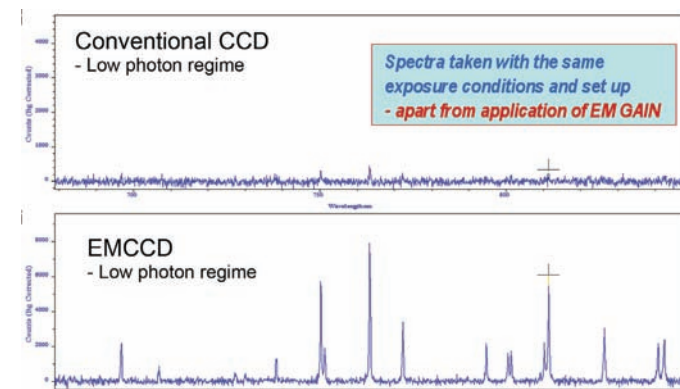


Figure 1: Comparison of the EMCCD with the conventional CCD for low light levels. Even the weakest spectral features can be observed with the application of EM gain which would otherwise remain obscured in the background noise of the conventional CCD. Both spectra taken under the same conditions apart from the application of gain. Data captured for a Newton DU971N-BV camera on a Shamrock 500i spectrograph using single scans with Full Vertical Binning (FVB).

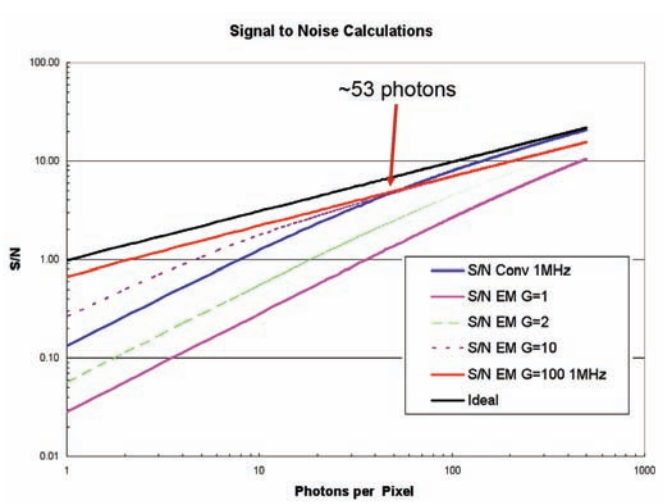


Figure 3: Signal to Noise ratios (SNR) for the EM and conventional CCDs operating in the low photon regime. SNR ratios here are based on a Newton<sup>EM</sup> (DU970N) EMCCD operating at 1 MHz readout rate. The conventional, ideal and curves for several values of gain are included.

# Part Numbers

## Accessories

### Fibre optics assemblies

ME-OPT-8004	1 way fiber, single 50um core, UV/VIS, SMA-SMA, 2 m
SR-OPT-8002	1 way fiber bundle, 100 um core, LOH-VIS/NIR, 2 m
SR-OPT-8007	2 way fiber bundle, 100 um core, LOH-VIS/NIR, 2 m
SR-OPT-8008	4 way fiber bundle, 100 um core, LOH-VIS/NIR, 2 m
SR-OPT-8009	5 way fiber bundle, 100 um core, LOH-VIS/NIR, 2 m
SR-OPT-8013	3 way fiber bundle, 100 um core, LOH-VIS/NIR, 2 m
SR-OPT-8014	1 way fiber bundle, 100 um core, HOH-UV/VIS, 2 m
SR-OPT-8015	2 way fiber bundle, 100 um core, HOH-UV/VIS, 2 m
SR-OPT-8016	3 way fiber bundle, 100 um core, HOH-UV/VIS, 2 m
SR-OPT-8017	4 way fiber bundle, 100 um core, HOH-UV/VIS, 2 m

### Filters Neutral Density

TN-0300-001-#UV	ND 0.3, UV-Vis
TN-0300-001-NIR	ND 0.3, Vis Nir
TN-0400-001-#UV	ND 0.4, UV-Vis
TN-0500-001-#UV	ND 0.5, UV-Vis
TN-0600-001-#UV	ND 0.6, UV-Vis
TN-0600-001-NIR	ND 0.6, Vis Nir
TN-0700-001-#UV	ND 0.7, UV-Vis
TN-0800-001-#UV	ND 0.8, UV-Vis

### Filters Long & Short pass

TL-0400-001	400 nm cut-on, 400-2000 nm trans., Ø25.4 mm
TL-0450-001	450 nm cut-on, 450-2000 nm trans., Ø25.4 mm
TL-0500-001	500 nm cut-on, 500-2000 nm trans., Ø25.4 mm
TL-0550-001	550 nm cut-on, 550-2000 nm trans., Ø25.4 mm
TL-0600-001	600 nm cut-on, 600-2000 nm trans., Ø25.4 mm
TL-0650-001	650 nm cut-on, 650-2000 nm trans., Ø25.4 mm
TL-0700-001	700 nm cut-on, 700-2000 nm trans., Ø25.4 mm
TL-0750-001	750 nm cut-on, 750-2000 nm trans., Ø25.4 mm
TL-0800-001	800 nm cut-on, 800-2000 nm trans., Ø25.4 mm
TL-0850-001	850 nm cut-on, 850-2000 nm trans., Ø25.4 mm
TL-0900-001	900 nm cut-on, 900-2000 nm trans., Ø25.4 mm
TL-0950-001	950 nm cut-on, 950-2000 nm trans., Ø25.4 mm
TL-1000-001	1000 nm cut-on, 1000-2000 nm trans., Ø25.4 mm

SR-OPT-8018	5 way fiber bundle, 100 um core, HOH-UV/VIS, 2 m
SR-OPT-8019	1 way fiber bundle, 200 um core, LOH-VIS/NIR, 2 m
SR-OPT-8020	2 way fiber bundle, 200 um core, LOH-VIS/NIR, 2 m
SR-OPT-8021	3 way fiber bundle, 200 um core, LOH-VIS/NIR, 2 m
SR-OPT-8022	4 way fiber bundle, 200 um core, LOH-VIS/NIR, 2 m
SR-OPT-8024	1 way fiber bundle, 200 um core, HOH-UV/VIS, 2 m
SR-OPT-8025	2 way fiber bundle, 200 um core, HOH-UV/VIS, 2 m
SR-OPT-8026	3 way fiber bundle, 200 um core, HOH-UV/VIS, 2 m
SR-OPT-8027	4 way fiber bundle, 200 um core, HOH-UV/VIS, 2 m

TN-0900-001-#UV	ND 0.9, UV-Vis
TN-1000-001-#UV	ND 1.0, UV-Vis
TN-1000-001-NIR	ND 1.0, Vis Nir
TN-1500-001-#UV	ND 1.5, UV-Vis
TN-2000-001-#UV	ND 2.0, UV-Vis
TN-2000-001-NIR	ND 2.0, Vis Nir
TN-3000-001-#UV	ND 3.0, UV-Vis
TN-3000-001-NIR	ND 3.0, Vis Nir

TS-0400-001	400 nm cut-on, 240-400 nm trans., Ø25.4 mm
TS-0450-001	450 nm cut-on, 270-450 nm trans., Ø25.4mm
TS-0500-001	500 nm cut-on, 300-500 nm trans., Ø25.4 mm
TS-0550-001	550 nm cut-on, 330-550 nm trans., Ø25.4 mm
TS-0600-001	600 nm cut-on, 360-600 nm trans., Ø25.4 mm
TS-0650-001	650 nm cut-on, 390-650 nm trans., Ø25.4 mm
TS-0700-001	700 nm cut-on, 420-700 nm trans., Ø25.4 mm
TS-0750-001	750 nm cut-on, 450-750 nm trans., Ø25.4 mm
TS-0800-001	800 nm cut-on, 480-800 nm trans., Ø25.4 mm
TS-0850-001	850 nm cut-on, 510-850 nm trans., Ø25.4 mm
TS-0900-001	900 nm cut-on, 540-900 nm trans., Ø25.4 mm
TS-0950-001	950 nm cut-on, 570-950 nm trans., Ø25.4 mm
TS-1000-001	1000 nm cut-on, 600-1000 nm trans., Ø25.4 mm

## Accessories cont.

### Light sources

ACC-OCE-HG-1	Hg-Ar calibration lamp and power supply
LK-##AR-PEN	Ar pen ray calibration lamp
LK-##KR-PEN	Kr pen ray calibration lamp
LK-##NE-PEN	Ne pen ray calibration lamp
LK-##XE-PEN	Xe pen ray calibration lamp
LK-DHRD-OCE	Deuterium-Halogen lamp, radiometrically calibrated
LK-HGAR-PEN	Hg-Ar pen ray calibration lamp
LK-HGNE-PEN	Hg-Ne pen ray calibration lamp

### Single point detectors & Scanning accessories

ACC-SR-ASM-0042	MCT detector with LN <sub>2</sub> Dewar and Au focusing mirror
ACC-SR-ASM-0043	InSb detector with LN <sub>2</sub> Dewar and Au focusing mirror
ACC-SR-ASM-0044	InGaAs detector + TE cooler and power supply
ACC-SR-ASM-0045	PbS with built-in amplifier
ACC-SR-ASM-0046	Si photodiode, UV-enhanced

### Microscope accessories

TR-LCDM-CAGE-ADP	Cage system adapter to Leica DMI4000/6000B
TR-LCDM-MNT-127-LP	Feet set for Leica DMI4000/6000B left port, SR303i
TR-LCDM-MNT-127-RP	Feet set for Leica DMI4000/6000B right port, SR303i
TR-LCDM-MNT-146-LP	Feet set for Leica DMI4000/6000B left port, SR500i/750
TR-LCDM-MNT-146-RP	Feet set for Leica DMI4000/6000B right port, SR500i/750
TR-NKTI-CAGE-ADP	Cage system adapter to Nikon Eclipse Ti-E
TR-NKTI-MNT-127-LP	Feet set for Nikon Eclipse Ti-E left port, SR303i
TR-NKTI-MNT-127-RP	Feet set for Nikon Eclipse Ti-E right port, SR303i
TR-NKTI-MNT-146-LP	Feet set for Nikon Eclipse Ti-E left port, SR500i/750
TR-NKTI-MNT-146-RP	Feet set for Nikon Eclipse Ti-E right port, SR500i/750
TR-NK2K-CAGE-ADP	Cage system adapter to Nikon TE2000
TR-NK2K-MNT-127-LP	Feet set for Nikon TE2000 left port, SR303i
TR-NK2K-MNT-127-RP	Feet set for Nikon TE2000 right port, SR303i
TR-NK2K-MNT-146-LP	Feet set for Nikon TE2000 left port, SR500i/750
TR-NK2K-MNT-146-RP	Feet set for Nikon TE2000 right port, SR500i/750
TR-ZAXO-CAG-ADP	Cage system adapter to Zeiss Axio Observer
TR-ZAXO-MNT-127-LP	Feet set for Zeiss Axio Observer left port, SR303i
TR-ZAXO-MNT-127-RP	Feet set for Zeiss Axio Observer right port, SR303i
TR-ZAXO-MNT-146-LP	Feet set for Zeiss Axio Observer left port, SR500i/750
TR-ZAXO-MNT-146-RP	Feet set for Zeiss Axio Observer right port, SR500i/750

## Cameras

### Accessories

ACC-XW-CHIL-160	Oasis 160 ultra compact chiller unit with hose
CCI-010	PCI card MHz for ICCD
CCI-23	PCI card iXon <sup>EM+</sup>
IO-160	Input/Output and synchronization box
OPTION-C1-AR1	AR coated window (400-900 nm) for Spectroscopy CCD
OPTION-C1-MGF2	MgF <sub>2</sub> window for Spectroscopy CCD

### iDus & iDus InGaAs

DU401A-BR-DD	1024x128, 26 µm, BI Deep Depletion, 100 kHz, -100°C
DU401A-BV	1024x127, 26 µm, BI + Vis AR coating, 100 kHz, -100°C
DU401A-FI	1024x127, 26 µm, Front-Illuminated, 100 kHz, -100°C
DU420A-BR-DD	1024x256, 26 µm, BI Deep Depletion, 100 kHz, -100°C
DU420A-BU	1024x255, 26 µm, BI 350 nm-optimized, 100 kHz, -100°C
DU420A-BU2	1024x255, 26 µm, BI 250 nm-optimized, 100 kHz, -100°C
DU420A-BV	1024x255, 26 µm, BI + Vis AR coating, 100 kHz, -100°C
DU420A-OE	1024x255, 26 µm, Open Electrode, 100 kHz, -100°C
DU490A-1.7	512x1, 25x500 µm, InGaAs 1.7 µm cutoff, 100 kHz, -85°C
DU490A-2.2	512x1, 25x250 µm, InGaAs 2.2 µm cutoff, 100 kHz, -85°C

PS150	ICCD power supply for deep cooling
P25 Shutter	Prontor 25 mm standalone shutter
PS25	CCD power supply for deep cooling
SD-166	P25 Prontor 25 mm shutter control
XU-RECR/TRANS	USB 2.0 fiber optic extender - emitter and receiver
XW-RECR	Koolance Exos II recirculator with mains power supply

### iStar

DH720-18F-03	1024x256 CCD, Ø18 mm, Gen 2 Broad, 5 ns
DH720I-18F-03	1024x256 CCD, Ø18 mm, Gen 2 Broad, 5 ns, Intelligate
DH720-18U-03	1024x256 CCD, Ø18 mm, Gen 2 Broad, 2 ns
DH720I-18U-03	1024x256 CCD, Ø18 mm, Gen 2 Broad, 2 ns, Intelligate
DH720-18F-04	1024x256 CCD, Ø18 mm, Gen 2 Broad, 5 ns, P46
DH720-18U-04	1024x256 CCD, Ø18 mm, Gen 2 Broad, 2 ns, P46
DH720-18F-05	1024x256 CCD, Ø18 mm, Gen 2 Broad, 10 ns, MgF <sub>2</sub>
DH720I-18F-05	1024x256 CCD, Ø18 mm, Gen 2 Broad, 10 ns, MgF <sub>2</sub> , Intelligate
DH720-18U-05	1024x256 CCD, Ø18 mm, Gen 2 Broad, 5 ns, MgF <sub>2</sub>
DH720I-18U-05	1024x256 CCD, Ø18 mm, Gen 2 Broad, 5 ns, MgF <sub>2</sub> , Intelligate
DH720-18H-13	1024x1024 CCD, Ø18 mm, Gen 2 Red, 50ns
DH720-18F-63	1024x1024 CCD, Ø18 mm, Gen 3 Vis, 5 ns
DH720-18U-63	1024x1024 CCD, Ø18 mm, Gen 3 Vis, 2 ns
DH720-18F-73	1024x1024 CCD, Ø18 mm, Gen 3 Nir, 5 ns
DH720-18U-73	1024x1024 CCD, Ø18 mm, Gen 3 Nir, 2 ns
DH720-18H-83	1024x1024 CCD, Ø18 mm, Gen 2 UV, 100 ns
DH720I-18H-83	1024x1024 CCD, Ø18 mm, Gen 2 UV, 100 ns, Intelligate
DH720-18F-93	1024x1024 CCD, Ø18 mm, Gen 3 InGaAs, 5 ns
DH720-18U-93	1024x1024 CCD, Ø18 mm, Gen 3 InGaAs, 2 ns
DH720I-18F-A3	1024x1024 CCD, Ø18 mm, Gen 3 Vis-Nir, 5 ns
DH720-18U-A3	1024x1024 CCD, Ø18 mm, Gen 3 Vis-Nir, 2 ns
DH720-18U-A3	1024x1024 CCD, Ø18 mm, Gen 3 Vis-Nir, 2 ns
DH720-18F-C3	1024x1024 CCD, Ø18 mm, Gen 3 Nir + UV coating, 5 ns
DH720-18U-C3	1024x1024 CCD, Ø18 mm, Gen 3 Nir + UV coating, 2 ns
DH720-18F-E3	1024x1024 CCD, Ø18 mm, Gen 2 UV, 5 ns
DH720I-18F-E3	1024x1024 CCD, Ø18 mm, Gen 2 UV, 5 ns, Intelligate
DH720-18U-E3	1024x1024 CCD, Ø18 mm, Gen 2 UV, 2 ns
DH720I-18U-E3	1024x1024 CCD, Ø18 mm, Gen 2 UV, 2 ns, Intelligate
DH720-25F-03	1024x512 CCD, Ø25 mm, Gen 2 Broad, 3 ns
DH720I-25F-03	1024x512 CCD, Ø25 mm, Gen 2 Broad, 3 ns, Intelligate
DH720-25U-03	1024x512 CCD, Ø25 mm, Gen 2 Broad, 7 ns
DH720I-25U-03	1024x512 CCD, Ø25 mm, Gen 2 Broad, 7 ns, Intelligate
DH740-18F-03	2048x512 CCD, Ø18 mm, Gen 2 Broad, 5 ns
DH740I-18F-03	2048x512 CCD, Ø18 mm, Gen 2 Broad, 5 ns, Intelligate
DH740-18U-03	2048x512 CCD, Ø18 mm, Gen 2 Broad, 2 ns
DH740I-18U-03	2048x512 CCD, Ø18 mm, Gen 2 Broad, 2 ns, Intelligate
DH740-18F-04	2048x512 CCD, Ø18 mm, Gen 2 Broad, 5 ns, P46
DH740I-18F-04	2048x512 CCD, Ø18 mm, Gen 2 Broad, 2 ns, P46
DH740-18U-04	2048x512 CCD, Ø18 mm, Gen 2 Broad, 5 ns, P46
DH740I-18U-04	2048x512 CCD, Ø18 mm, Gen 2 Broad, 2 ns, P46
DH740-18F-05	2048x512 CCD, Ø18 mm, Gen 2 Broad, 10 ns, MgF <sub>2</sub>
DH740I-18F-05	2048x512 CCD, Ø18 mm, Gen 2 Broad, 10 ns, MgF <sub>2</sub> , Intelligate
DH740-18U-05	2048x512 CCD, Ø18 mm, Gen 2 Broad, 5 ns, MgF <sub>2</sub>
DH740I-18U-05	2048x512 CCD, Ø18 mm, Gen 2 Broad, 5 ns, MgF <sub>2</sub> , Intelligate
DH740-18H-13	2048x512 CCD, Ø18 mm, Gen 2 Red, 50ns
DH740-18F-63	2048x512 CCD, Ø18 mm, Gen 3 Vis, 5 ns
DH740-18U-63	2048x512 CCD, Ø18 mm, Gen 3 Vis, 2 ns
DH740-18F-73	2048x512 CCD, Ø18 mm, Gen 3 Nir, 5 ns
DH740-18U-73	2048x512 CCD, Ø18 mm, Gen 3 Nir, 2 ns
DH740-18H-83	2048x512 CCD, Ø18 mm, Gen 2 UV, 2 ns
DH740I-18H-83	2048x512 CCD, Ø18 mm, Gen 2 UV, 100 ns, Intelligate
DH740-18F-93	2048x512 CCD, Ø18 mm, Gen 3 InGaAs, 5 ns
DH740-18U-93	2048x512 CCD, Ø18 mm, Gen 3 InGaAs, 2 ns
DH740I-18F-A3	2048x512 CCD, Ø18 mm, Gen 3 Vis-Nir, 5 ns
DH740-18U-A3	2048x512 CCD, Ø18 mm, Gen 3 Vis-Nir, 2 ns
DH740-18U-A3	2048x512 CCD, Ø18 mm, Gen 3 Vis-Nir, 2 ns
DH740-18F-C3	2048x512 CCD, Ø18 mm, Gen 3 Nir + UV coating, 5 ns
DH740-18U-C3	2048x512 CCD, Ø18 mm, Gen 3 Nir + UV coating, 2 ns
DH740-18U-C3	2048x512 CCD, Ø18 mm, Gen 3 Vis-Nir + UV coating, 2 ns
DH740-18F-E3	2048x512 CCD, Ø18 mm, Gen 2 UV, 5 ns
DH740I-18F-E3	2048x512 CCD, Ø18 mm, Gen 2 UV, 5 ns, Intelligate
DH740-18U-E3	2048x512 CCD, Ø18 mm, Gen 2 UV, 2 ns
DH740I-18U-E3	2048x512 CCD, Ø18 mm, Gen 2 UV, 2 ns, Intelligate
DH740-25F-03	2048x512 CCD, Ø25 mm, Gen 2 Broad, 3 ns
DH740I-25F-03	2048x512 CCD, Ø25 mm, Gen 2 Broad, 3 ns, Intelligate
DH740-25U-03	2048x512 CCD, Ø25 mm, Gen 2 Broad, 7 ns
DH740I-25U-03	2048x512 CCD, Ø25 mm, Gen 2 Broad, 7 ns, Intelligate

## Cameras cont.

DH720-18F-E3	1024x256 CCD, Ø18 mm, Gen 2 UV, 5 ns
DH720I-18F-E3	1024x256 CCD, Ø18 mm, Gen 2 UV, 5 ns, Intelligate
DH720-18U-E3	1024x256 CCD, Ø18 mm, Gen 2 UV, 2 ns
DH720I-18U-E3	1024x256 CCD, Ø18 mm, Gen 2 UV, 2 ns, Intelligate
DH720-25F-03	1024x256 CCD, Ø25 mm, Gen 2 Broad, 3 ns
DH720I-25F-03	1024x256 CCD, Ø25 mm, Gen 2 Broad, 3 ns, Intelligate
DH720-25U-03	1024x256 CCD, Ø25 mm, Gen 2 Broad, 7 ns
DH720I-25U-03	1024x256 CCD, Ø25 mm, Gen 2 Broad, 7 ns, Intelligate
DH740-18F-03	2048x512 CCD, Ø18 mm, Gen 2 Broad, 5 ns
DH740I-18F-03	2048x512 CCD, Ø18 mm, Gen 2 Broad, 5 ns, Intelligate
DH740-18U-03	2048x512 CCD, Ø18 mm, Gen 2 Broad, 2 ns
DH740I-18U-03	2048x512 CCD, Ø18 mm, Gen 2 Broad, 2 ns, Intelligate
DH740-18F-04	2048x512 CCD, Ø18 mm, Gen 2 Broad, 5 ns, P46
DH740I-18F-04	2048x512 CCD, Ø18 mm, Gen 2 Broad, 2 ns, P46
DH740-18U-04	2048x512 CCD, Ø18 mm, Gen 2 Broad, 5 ns, P46
DH740I-18U-04	2048x512 CCD, Ø18 mm, Gen 2 Broad, 2 ns, P46
DH740-18F-05	2048x512 CCD, Ø18 mm, Gen 2 Broad, 10 ns, MgF <sub>2</sub>
DH740I-18F-05	2048x512 CCD, Ø18 mm, Gen 2 Broad, 10 ns, MgF <sub>2</sub> , Intelligate
DH740-18U-05	2048x512 CCD, Ø18 mm, Gen 2 Broad, 5 ns, MgF <sub>2</sub>
DH740I-18U-05	2048x512 CCD, Ø18 mm, Gen 2 Broad, 5 ns, MgF <sub>2</sub> , Intelligate
DH740-18H-13	2048x512 CCD, Ø18 mm, Gen 2 Red, 50ns
DH740-18F-63	2048x512 CCD, Ø18 mm, Gen 3 Vis, 5 ns
DH740-18U-63	2048x512 CCD, Ø18 mm, Gen 3 Vis, 2 ns
DH740-18F-73	2048x512 CCD, Ø18 mm, Gen 3 Nir, 5 ns
DH740-18U-73	2048x512 CCD, Ø18 mm, Gen 3 Nir, 2 ns
DH740-18H-83	2048x512 CCD, Ø18 mm, Gen 2 UV, 100 ns
DH740I-18H-83	2048x512 CCD, Ø18 mm, Gen 2 UV, 100 ns, Intelligate
DH740-18F-93	2048x512 CCD, Ø18 mm, Gen 3 InGaAs, 5 ns
DH740-18U-93	2048x512 CCD, Ø18 mm, Gen 3 InGaAs, 2 ns
DH740I-18F-A3	2048x512 CCD, Ø18 mm, Gen 3 Vis-Nir, 5 ns
DH740-18U-A3	2048x512 CCD, Ø18 mm, Gen 3 Vis-Nir, 2 ns
DH740-18U-A3	2048x512 CCD, Ø18 mm, Gen 3 Vis-Nir, 2 ns
DH740-18F-C3	2048x512 CCD, Ø18 mm, Gen 3 Nir + UV coating, 5 ns
DH740-18U-C3	2048x512 CCD, Ø18 mm, Gen 3 Nir + UV coating, 2 ns
DH740-18F-E3	2048x512 CCD, Ø18 mm, Gen 2 UV, 5 ns
DH740I-18F-E3	2048x512 CCD, Ø18 mm, Gen 2 UV, 5 ns, Intelligate
DH740-18U-E3	2048x512 CCD

## Cameras cont.

iXon <sup>EM+</sup>	
DU-885K-C00-#VP	EM, 1004x1002, 8 µm, Virtual Phase, 35 MHz, -95°C
DU-888E-C00-#BV	EM, 1024x1024, 13 µm, BI + Vis AR coating, 10 MHz, -100°C
DU-888E-C00-UVB	EM, 1024x1024, 13 µm, BI + UV coating, 10 MHz, -100°C

DU-897E-C00-#BV EM, 512x512, 16 µm, BI + Vis AR coating, 10 MHz, -100°C

---

DU-897E-C00-UVB EM, 512x512, 16 µm, BI + UV coating, 10 MHz, -100°C

Newton & Newton<sup>EM</sup>

DU920P-BR-DD	1024x256, 26 µm, BI Deep Depletion, 3 MHz, -100°C
DU920P-BU	1024x255, 26 µm, BI 350 nm-optimized, 3 MHz, -100°C
DU920P-BU2	1024x255, 26 µm, BI 250 nm-optimized, 3 MHz, -100°C
DU920P-BV	1024x255, 26 µm, BI + Vis AR coating, 3 MHz, -100°C
DU920P-OE	1024x255, 26 µm, Open Electrode, 3 MHz, -100°C
DU920P-UVB	1024x255, 26 µm, BI + UV coating, 3 MHz, -100°C
DU940P-BU	2048x512, 13.5 µm, BI 350 nm-optimized, 3 MHz, -100°C
DU940P-BU2	2048x512, 13.5 µm, BI 250 nm-optimized, 3 MHz, -100°C
DU940P-BV	2048x512, 13.5 µm, BI + Vis AR coating, 3 MHz, -100°C
DU940P-FI	2048x512, 13.5 µm, Front-Illuminated, 3 MHz, -100°C

DU940P-UV	2048x512, 13.5 µm, FI + UV coating, 3 MHz, -100°C
DU970P-BV	EM, 1600x200, 16 µm, BI + Vis-AR coating, 3 MHz, -100°C
DU970P-FI	EM, 1600x200, 16 µm, Front-Illuminated, 3 MHz, -100°C
DU970P-UV	EM, 1600x200, 16 µm, FI + UV coating, 3 MHz, -100°C
DU970P-UVB	EM, 1600x200, 16 µm, BI + UV coating, 3 MHz, -100°C
DU971P-BV	EM, 1600x400, 16 µm, BI + Vis AR coating, 3 MHz, -100°C
DU971P-FI	EM, 1600x400, 16 µm, Front-Illuminated, 3 MHz, -100°C
DU971P-UV	EM, 1600x400, 16 µm, FI + UV coating, 3 MHz, -100°C
DU971P-UVB	EM, 1600x400, 16 µm, BI + UV coating, 3 MHz, -100°C

# Spectrographs

#### **Mechelle & specific accessories**

ME5000	Mechelle 5000 unit
ME-OPT-0007	UV-VIS-NIR collector-collimator
ME-SHT-9002	Shutter assembly
ME-SLT-10*50	10x50 $\mu\text{m}$ slit
ME-SLT-100*50	100x50 $\mu\text{m}$ slit

ME-SLT-200*50	200x50 µm slit
ME-SLT-25*25	25x25 µm slit
ME-SLT-25*50	25x50 µm slit
ME-SLT-50*25	50x25 µm slit
ME-SLT-50*50	50x50 µm slit

#### **Shamrock 163 & specific accessories**

SR-163	Shamrock 163 base unit
SR1-ASM-0020	Manual adjustable input slit, 3 mm high
SR1-ASM-0020-EQ	Manual adjustable input slit, 6 mm high
SR1-ASM-0023	C-mount input adapter
SR1-ASM-7003	Ø1" filter holder
SR1-ASM-7004	Rectangular 1" filter holder
SR1-ASM-8032	Fixed ferrule adapter
SR1-ASM-8035	Fixed SMA input adapter
SR1-ASM-8036	Fiber ferrule adapter (adjustable slit & shutter)

SR1-ASM-8038	Fixed slit holder
SR1-ASZ-8033	Fixed SMA input adapter (correction lens)
SR1-ASZ-8034	Fixed slit input adapter (correction lens)
SR1-ASZ-8044	InGaAs flange (correction lens)
SR1-GRT-0085-0130	Grating 85 l/mm, 130 nm blaze
SR1-GRT-0100-1600	Grating 100 l/mm, 1600 nm blaze
SR1-GRT-0150-0300	Grating 150 l/mm, 300 nm blaze
SR1-GRT-0150-0500	Grating 150 l/mm, 500 nm blaze
SR1-GRT-0150-0800	Grating 150 l/mm, 800 nm blaze

## Spectrographs cont.

SR1-GRT-0150-1250	Grating 150 l/mm, 1250 nm blaze	SR1-GRT-1200-0500	Grating 1200 l/mm, 500 nm blaze
SR1-GRT-0150-2000	Grating 150 l/mm, 2000 nm blaze	SR1-GRT-1200-0750	Grating 1200 l/mm, 750 nm blaze
SR1-GRT-0200-0750	Grating 200 l/mm, 750 nm blaze	SR1-GRT-1200-1080	Grating 1200 l/mm, 1080 nm blaze
SR1-GRT-0200-1700	Grating 200 l/mm, 1700 nm blaze	SR1-GRT-1200-EH	Grating 1200 l/mm, Holographic, 400-1200 nm
SR1-GRT-0235-0750	Grating 200 l/mm, 1700 nm blaze	SR1-GRT-1500-0250	Grating 1500 l/mm, 250 nm blaze
SR1-GRT-0300-0300	Grating 300 l/mm, 300 nm blaze	SR1-GRT-1800-0400	Grating 1800 l/mm, 400 nm blaze
SR1-GRT-0300-0422	Grating 200 l/mm, 1700 nm blaze	SR1-GRT-1800-0500	Grating 1800 l/mm, 500 nm blaze
SR1-GRT-0300-0500	Grating 300 l/mm, 500 nm blaze	SR1-GRT-1800-DH	Grating 1800 l/mm, Holographic, 190-900 nm
SR1-GRT-0300-0760	Grating 300 l/mm, 760 nm blaze	SR1-GRT-1800-FH	Grating 1800 l/mm, Holographic, 350-900 nm
SR1-GRT-0300-0860	Grating 300 l/mm, 860 nm blaze	SR1-GRT-2400-0300	Grating 2400 l/mm, 300 nm blaze
SR1-GRT-0300-1000	Grating 300 l/mm, 1000 nm blaze	SR1-GRT-2400-BH	Grating 2400 l/mm, Holographic, 190-800 nm
SR1-GRT-0300-1200	Grating 300 l/mm, 1200 nm blaze	SR1-GRT-2400-GH	Grating 2400 l/mm, Holographic, 250-600 nm
SR1-GRT-0300-1700	Grating 300 l/mm, 1700 nm blaze	SR1-SLT-9003	Shutter assembly (PCI)
SR1-GRT-0400-0400	Grating 400 l/mm, 400 nm blaze	SR1-SLT-9004	Shutter assembly (I <sup>2</sup> C)
SR1-GRT-0400-0550	Grating 400 l/mm, 550 nm blaze	SR1-SLH-0010-3	10 um x 3 mm slit for shutter
SR1-GRT-0500-0330	Grating 500 l/mm, 330nm blaze	SR1-SLH-0025-3	25 um x 3 mm slit for shutter
SR1-GRT-0500-0560	Grating 500 l/mm, 560nm blaze	SR1-SLH-0050-3	50 um x 3 mm slit for shutter
SR1-GRT-0600-0300	Grating 600 l/mm, 300 nm blaze	SR1-SLH-0075-3	75 um x 3 mm slit for shutter
SR1-GRT-0600-0500	Grating 600 l/mm, 500 nm blaze	SR1-SLH-0100-3	100um x 3 mm slit for shutter
SR1-GRT-0600-0650	Grating 600 l/mm, 650 nm blaze	SR1-SLH-0200-3	200 um x 3 mm slit for shutter
SR1-GRT-0600-0750	Grating 600 l/mm, 750 nm blaze	SR1-SLT-0010-3	10 um x 3 mm slit
SR1-GRT-0600-1000	Grating 600 l/mm, 1000 nm blaze	SR1-SLT-0025-3	25 um x 3 mm slit
SR1-GRT-0600-1200	Grating 600 l/mm, 1200 nm blaze	SR1-SLT-0050-3	50 um x 3 mm slit
SR1-GRT-0600-1600	Grating 600 l/mm, 1600 nm blaze	SR1-SLT-0075-3	75 um x 3 mm slit
SR1-GRT-0600-1900	Grating 600 l/mm, 1900nm blaze	SR1-SLT-0100-3	100 um x 3 mm slit
SR1-GRT-1200-0300	Grating 1200 l/mm, 300 nm blaze	SR1-SLT-0200-3	200 um x 3 mm slit
SR1-GRT-1200-0400	Grating 1200 l/mm, 400 nm blaze		

## **Shamrock 303i & specific accessories**

SR-303I-A	Shamrock 303i base unit, single output port	SR3-GRT-0050-0600	Grating 50 l/mm, 600 nm blaze
SR-303I-B	Shamrock 303i base unit, double output port	SR3-GRT-0060-0750	Grating 60 l/mm, 750 nm blaze
MFL-SR303I-888	iXon mounting flange kit DU888	SR3-GRT-0120-0330	Grating 120 l/mm, 330nm blaze
MFL-SR303I-INTER	Intermediate plane CCD mounting flange (Imaging)	SR3-GRT-0150-0300	Grating 150 l/mm, 300 nm blaze
MFL-SR303I-IXON	iXon mounting flange kit (Not 888)	SR3-GRT-0150-0500	Grating 150 l/mm, 500 nm blaze
SR-ASM-0003	Additionnal blank grating turret	SR3-GRT-0150-0800	Grating 150 l/mm, 800nm blaze
SR-ASM-0022	Adjustable feet set (4off)	SR3-GRT-0150-1250	Grating 150 l/mm, 1250 nm blaze
SR-ASZ-0005	Slit assembly for second exit port	SR3-GRT-0150-2000	Grating 150 l/mm, 2000 nm blaze
SR-ASZ-0034	Wide-aperture entrance slit	SR3-GRT-0235-0750	Grating 235 l/mm, 750 nm blaze
SR-SHT-9001	Entrance shutter for SR-303i	SR3-GRT-0300-0300	Grating 300 l/mm, 300 nm blaze

## Spectrographs cont.

SR3-GRT-0300-0500	Grating 300 l/mm, 500 nm blaze
SR3-GRT-0300-0760	Grating 300 l/mm, 760 nm blaze
SR3-GRT-0300-1000	Grating 300 l/mm, 1000 nm blaze
SR3-GRT-0300-1200	Grating 300 l/mm, 1200 nm blaze
SR3-GRT-0300-1700	Grating 300 l/mm, 1700 nm blaze
SR3-GRT-0300-2000	Grating 300 l/mm, 2000 nm blaze
SR3-GRT-0300-3000	Grating 300 l/mm, 3000 nm blaze
SR3-GRT-0400-0850	Grating 400 l/mm, 850 nm blaze
SR3-GRT-0500-0230	Grating 500 l/mm, 230 nm blaze
SR3-GRT-0600-0300	Grating 600 l/mm, 300 nm blaze
SR3-GRT-0600-0400	Grating 600 l/mm, 400 nm blaze
SR3-GRT-0600-0500	Grating 600 l/mm, 500 nm blaze
SR3-GRT-0600-0650	Grating 600 l/mm, 650 nm blaze
SR3-GRT-0600-0750	Grating 600 l/mm, 750 nm blaze
SR3-GRT-1200-0300	Grating 1200 l/mm, 300 nm blaze
SR3-GRT-1200-0400	Grating 1200 l/mm, 400 nm blaze
SR3-GRT-1200-0500	Grating 1200 l/mm, 500 nm blaze
SR3-GRT-1200-0600	Grating 1200 l/mm, 600 nm blaze
SR3-GRT-1200-0750	Grating 1200 l/mm, 750 nm blaze
SR3-GRT-1200-1000	Grating 1200 l/mm, 1000 nm blaze
SR3-GRT-1200-1100	Grating 1200 l/mm, 1100 nm blaze
SR3-GRT-1200-EH	Grating 1200 l/mm, Holographic, 400-1200 nm
SR3-GRT-1800-0500	Grating 1800 l/mm, 500 nm blaze
SR3-GRT-1800-DH	Grating 1800 l/mm, Holographic, 190-900 nm
SR3-GRT-1800-FH	Grating 1800 l/mm, Holographic, 350-900 nm
SR3-GRT-2400-0300	Grating 2400 l/mm, 300 nm blaze
SR3-GRT-2400-BH	Grating 2400 l/mm, Holographic, 190-800 nm
SR3-GRT-2400-GH	Grating 2400 l/mm, Holographic, 250-600 nm
SR3-GRT-MR-AL+MGF2	Shamrock SR-303i flat mirror for grating turret, Al+MgF <sub>2</sub> coating
SR3-GRT-1000-0250	Grating 1000 l/mm, 250 nm blaze

### Shamrock 500i/750 & specific accessories

SR-500I-A	SR500i base, single entrance slit, CCD exit port
SR-500I-B1	SR500i base, single entrance and exit slit, CCD exit port
SR-500I-B2	SR500i base, single entrance slit, dual CCD exit ports
SR-500I-C	SR500i base, double entrance slit, CCD exit port
SR-500I-D1	SR500i base, double entrance slit, CCD exit port and exit slit
SR-500I-D2	SR500i base, double entrance slit, dual CCD exit port
SR-750-A	SR750 base, single entrance slit, CCD exit port
SR-750-B1	SR750 base, single entrance and exit slit, CCD exit port
SR-750-B2	SR750 base, single entrance slit, dual CCD exit ports
SR-750-C	SR750 base, double entrance slit, CCD exit port
SR-750-D1	SR750 base, double entrance slit, CCD exit port and exit slit
SR-750-D2	SR750 base, double entrance slit, dual CCD exit port
MFL-SR500	CCD mounting flange kit
MFL-SR500-IXON	iXon mounting flange kit
SR-ASM-0025	Manual slit assembly baffle, 6W x 4H
SR-ASM-0026	Manual slit assembly baffle, 6W x 6H
SR-ASM-0027	Manual slit assembly baffle, 6W x 8H
SR-ASM-0028	Manual slit assembly baffle, 6W x 10H
SR-ASM-0029	Manual slit assembly baffle, 6W x 14H
SR-ASM-0059	Additionnal blank grating turret
SR-ASM-0062	Exit port slit adapter for CCD flange
SR-ASZ-0030	Manual exit port slit
SR-ASZ-0032	Motorized entrance slit (front port)
SR-ASZ-0033	SR750 InGaAs camera flange
SR-ASZ-0035	Motorized entrance slit (side port)
SR-ASZ-0036	Motorized slit for second exit port
SR-ASZ-7005	Motorised filter wheel
SR-SHT-9002	Shutter for entrance ports
SR5-GRT-0075-12000	Grating, 75 l/mm blazed at 12000 nm
SR5-GRT-0085-1350	Grating, 85 l/mm blazed at 1350 nm
SR5-GRT-0150-0300	Grating, 150 l/mm blazed at 300 nm
SR5-GRT-0150-0500	Grating, 150 l/mm blazed at 500 nm
SR5-GRT-0150-0800	Grating, 150 l/mm blazed at 800 nm
SR5-GRT-0150-1250	Grating, 150 l/mm blazed at 1250 nm
SR5-GRT-0150-2000	Grating, 150 l/mm blazed at 2000 nm
SR5-GRT-0150-8000	Grating, 150 l/mm blazed at 8000 nm
SR5-GRT-0300-0300	Grating, 300 l/mm blazed at 300 nm

## Spectrographs cont.

SR5-GRT-0300-0500	Grating, 300 l/mm blazed at 500 nm
SR5-GRT-0300-0760	Grating, 300 l/mm blazed at 760 nm
SR5-GRT-0300-1000	Grating, 300 l/mm blazed at 1000 nm
SR5-GRT-0300-1200	Grating, 300 l/mm blazed at 1200 nm
SR5-GRT-0300-1700	Grating, 300 l/mm blazed at 1700 nm
SR5-GRT-0300-2000	Grating, 300 l/mm blazed at 2000 nm
SR5-GRT-0300-3000	Grating, 300 l/mm blazed at 3000 nm
SR5-GRT-0300-4800	Grating, 300 l/mm blazed at 4800 nm
SR5-GRT-0600-0300	Grating, 600 l/mm blazed at 300 nm
SR5-GRT-0600-0500	Grating, 600 l/mm blazed at 500 nm
SR5-GRT-0600-0750	Grating, 600 l/mm blazed at 750 nm
SR5-GRT-0600-1000	Grating, 600 l/mm blazed at 1000 nm
SR5-GRT-0600-1200	Grating, 600 l/mm blazed at 1200 nm
SR5-GRT-0600-1600	Grating, 600 l/mm blazed at 1600 nm
SR5-GRT-0600-1900	Grating, 600 l/mm blazed at 1900 nm
SR5-GRT-0600-2500	Grating, 600 l/mm blazed at 2500 nm
SR5-GRT-0720-2000	Grating, 720 l/mm blazed at 2000 nm
SR5-GRT-0830-1200	Grating, 830 l/mm blazed at 1200 nm
SR5-GRT-0900-0550	Grating, 900 l/mm blazed at 550 nm
SR5-GRT-1000-1310	Grating, 1000 l/mm blazed at 1310 nm
SR5-GRT-1200-0300	Grating, 1200 l/mm blazed at 300 nm
SR5-GRT-1200-0500	Grating, 1200 l/mm blazed at 500 nm
SR5-GRT-1200-0750	Grating, 1200 l/mm blazed at 750 nm
SR5-GRT-1200-1000	Grating, 1200 l/mm blazed at 1000 nm
SR5-GRT-1200-EH	Grating 1200 l/mm, Holographic, 400-1200 nm
SR5-GRT-1800-0500	Grating, 1800 l/mm blazed at 500 nm
SR5-GRT-1800-DH	Grating 1800 l/mm, Holographic, 190-900 nm
SR5-GRT-1800-FH	Grating 1800 l/mm, Holographic, 350-900 nm
SR5-GRT-2400-0240	Grating, 2400 l/mm blazed at 240 nm
SR5-GRT-2400-0300	Grating, 2400 l/mm blazed at 300 nm
SR5-GRT-2400-BH	Grating 2400 l/mm, Holographic, 190-800 nm
SR5-GRT-2400-GH	Grating 2400 l/mm, Holographic, 250-600 nm

### Shamrock 303i, 500i and 750 generic accessories

ACC-SR-ASZ-0056	Sample chamber
SR-ASM-0002	Oriel 1.5" flange adapter
SR-ASM-0010	Motorised slit baffle - 6x8 mm (WxH)
SR-ASM-0011	Motorised slit baffle - 6x14 mm (WxH)
SR-ASM-0013	Nikon lens F-mount input adapter
SR-ASM-0014	Pen ray lamp mount for entrance slit
SR-ASM-0015	Motorised slit baffle - Ø15 mm
SR-ASM-0016	Motorised slit baffle - 6x4 mm (WxH)
SR-ASM-0017	Motorised slit baffle - 6x6 mm (WxH)
SR-ASM-0021	C-mount input adapter
SR-ASM-0038	F/Matcher for SR-303i, 11 mm ferrule input
SR-ASM-0039	F/Matcher for 500i, ferrule input
SR-ASM-0040	F/Matcher for 750, ferrule input
SR-ASM-0041	SMA adaptor for F/matcher
SR-ASM-0065	Cage system adapter
SR-ASM-8006	X-adjustable fibre ferrule adapter
SR-ASM-8010	XY adjustable fibre ferrule adapter
SR-ASM-8040	Purge plug for Shamrock

## Software

ANDOR-SDK-CCD	Software Development Kit - CCD and EMCCD
ANDOR-SDK-ICCD	Software Development Kit - ICCD
ANDOR-SR-STANDALONE	Shamrock standalone GUI interface
SOLIS (S)	Solis Spectroscopy Software
SOLIS (SC)	Solis Scanning monochromator Software

# Andor Customer Support

Andor products are regularly used in critical applications and we can provide a variety of customer support services to maximise the return on your investment and ensure that your product continues to operate at its optimum performance.

Andor has customer support teams located across North America, Asia and Europe, allowing us to provide local technical assistance and advice. Requests for support can be made at any time by contacting our technical support team at [www.andor.com/customersupport](http://www.andor.com/customersupport).

Andor offers a variety of support under the following format:

- On-site product specialists can assist you with the installation and commissioning of your chosen product
- Training services can be provided on-site or remotely via the Internet
- A testing service to confirm the integrity and optimise the performance of existing equipment in the field is also available on request.

A range of extended warranty packages are available for Andor products giving you the flexibility to choose one appropriate for your needs. These warranties allow you to obtain additional levels of service and include both on-site and remote support options, and may be purchased on a multi-year basis allowing users to fix their support costs over the operating lifecycle of the products.

## Head Office

7 Millennium Way  
Springvale Business Park  
Belfast BT12 7AL  
Northern Ireland  
Tel: +44 (28) 9023 7126  
Fax: +44 (28) 9031 0792

## North America

425 Sullivan Avenue  
Suite 3  
South Windsor, CT 06074  
USA  
Tel: +1 (860) 290 9211  
Fax: +1 (860) 290 9566

## Japan

4F NE Sarugakucho Building  
2-7-6 Sarugaku-Cho  
Chiyoda-Ku  
Tokyo 101-0064  
Japan  
Tel: +81 (3) 3518 6488  
Fax: +81 (3) 3518 6489

## China

Room 502 Yu Yang Zhi Ye Building  
A 2 Xiao Guan Bei Li  
An Wai, Chaoyang District  
Beijing 100029  
China  
Tel: +86 (10) 5129 4977  
Fax: +86 (10) 6445 5401

